Towards Paleoclimate Reanalysis via Ensemble Kalman Filtering, Proxy Forward Modeling and Fuzzy Logic

A Dissertation

submitted in Fulfillment of the Requirements for the Degree of

Doctor rerum naturalium (Dr. rer. nat.)

to the Department of Earth Sciences

of the Freie Universität Berlin

by

John Walter Acevedo Valencia

Berlin, February 2015

Supervisors:

Prof. Dr. Ulrich CUBASCH
Institute of Meteorology
Freie Universität Berlin

Prof. Dr. Sebastian REICH
Institute of Mathematics
Universität Potsdam

Date of the viva voce/defence: 8th June, 2015

Declaration of Authorship

I, John Walter ACEVEDO VALENCIA, declare that this thesis titled, “Towards Paleoclimate Reanalysis via Ensemble Kalman Filtering, Proxy Forward Modeling and Fuzzy Logic” and the work presented in it are my own. I confirm that:

- This work was done wholly or mainly while in candidature for a research degree at this University.
- Where any part of this thesis has previously been submitted for a degree or any other qualification at this University or any other institution, this has been clearly stated.
- Where I have consulted the published work of others, this is always clearly attributed.
- Where I have quoted from the work of others, the source is always given. With the exception of such quotations, this thesis is entirely my own work.
- I have acknowledged all main sources of help.
- Where the thesis is based on work done by myself jointly with others, I have made clear exactly what was done by others and what I have contributed myself.

Signed: _____

Date: _____

Towards Paleoclimate Reanalysis via Ensemble Kalman Filtering, Proxy Forward Modeling and Fuzzy Logic

by John Walter ACEVEDO VALENCIA

Abstract

This thesis investigates several aspects of the assimilation of climate proxy records with the purpose of eventually generating retrospective paleo-climate analyses, namely a paleo-reanalysis.

Firstly, the problem of estimating the Time-Averaged (TA) state of a system out of TA observations using Ensemble Kalman Filter (EnKF) is revisited under strongly nonlinear coupled conditions. A comparison is performed for the two previously used updating algorithms as well as for a newly introduced one. We find that for our experimental setting these updating strategies exhibit significantly different performances depending on the length of the time averaging, which complements the prior knowledge on TA estimation via EnKF. Furthermore, our proposed approach appears as a very promising option for the regime of short averaging periods.

Secondly, the process-based Tree-Ring-Width (TRW) model Vaganov-Shashkin-Lite (VSL) is analyzed in terms of Fuzzy Logic (FL) theory. Based on the Principle of Limiting Factors (PLF), VSL combines temperature and moisture time series in a nonlinear fashion to obtain simulated TRW chronologies. We show that the entire model formulation can be embedded into the FL framework and that the traditional mathematical formulation of the PLF corresponds to a particular representation of a fuzzy intersection operation. Accordingly, this reinterpretation suggest several natural modifications to VSL's modeling approach and fosters new interpretations of tree-ring-growth limitation processes. The impact of several FL-based formulation changes on VSL's forward modeling performance is assessed for a global network of TRW chronologies, finding a remarkable insensitivity to the particular representation of the PLF.

Finally, the assimilation of TRW chronologies is investigated within a perfect model Data Assimilation (DA) setting using VSL as observation operator and a EnKF-based TA state estimation strategy. VSL's formulation implies three compounding, challenging features when used as observation operator: (i) time averaging, (ii) "switching recording" of 2 variables and (iii) bounded response windows leading to "thresholded response". DA experiments involving pseudo-TRW observations are performed first for a chaotic 2-scale dynamical system, used as a cartoon of the atmosphere-land system, and then for an Atmospheric General Circulation Model (A-GCM). Results reveal that VSL's non-linearities may considerable deteriorate the performance of EnKF for TA estimation, as compared to the utilization of a TA linear observation operator. Moreover, this assimilation skill loss appears to be strongly linked to the lack of smoothness of the growth rate function. Consequently, VSL's performance as observation operator can be enhanced by resorting to smoother FL representations of the principle of limiting factors. Additionally, our results suggests that the efficiency of a TRW chronology at reducing analysis errors is limited by the yearly internal variability strength at the chronology site. This finding can in principle be profitably used to guide and optimize future proxy record sampling campaigns.

Acknowledgements

I want to express my gratitude to all the people and institutions that in one way or another contributed to the successful end of my PhD studies. I feel indebted to Helmholtz-Gemeinschaft, Freie Universität Berlin and Deutsche Forschungsgemeinschaft for their generous funding. This research work was produced within the Helmholtz graduate research school GEOSIM.

I greatly thank Prof. Ulrich Cubasch for all the trust he have had in my work since the beginning of the application process to GEOSIM. It was a privilege to be in contact with such an insightful scientist. I am deeply grateful to Prof. Sebastian Reich for all the knowledge and motivation he shared with me. It was really inspiring to be closely advised by such a committed researcher and humble person.

Many scientist has provided me very valuable feedback regarding my research work. In particular, I want to thank Isabel Dorado for her great support concerning dendroclimatology. I acknowledge Suz Tolwinski-Ward, Michael Evans, Christian Reick, Gerd Helle, Petra Breitenmosser and Jörg Franke for very insightful discussions regarding tree ring growth modeling. Jeffrey Anderson, Kayo Ide, Georg Gottwald and Katja Matthes gave me truly helpful advise concerning the assimilation of proxy records into climate models.

During my stay in Berlin, I have had the opportunity to develop several valuable friendships. First of all, I want to show my strong appreciation to my dear pals Bijan, Nico, Emmanuele and Edoardo for making so enjoyable my PhD life. I sincerely thank Jana,

Nawinda, Lara, Kay and Yuang for all the lively discussions within the Numerical Mathematics working group of Potsdam University. I'm grateful to Thomas, Kerstin, Tim, Daniel, Christopher, Stefan and Ingo for all the help I received from them in the meteorology institute. Karen Leever, Sahar Sodoudi and Forough Sodoudi sincerely supported me at very intense moments of my PhD, thanks a lot for that.

Last but not least, I want to show my appreciation to Berlin for its amazing vibe, and to Germany for its progressive culture. It has certainly been a time full of rewarding experiences and learning. Danke für Alles!!

Dedicated to my family core. To my parents, Maria Bertilda and Luis Eduardo, whose great efforts in life made this possible. To my sister Emilse, for her unconditional support. To my wife Camila, for all the good times we had together . . .

“A tu escuela llegue sin entender porque llegaba
en tus salones encuentro mil caminos y encrucijadas
y aprendo mucho y no aprendo nada
maestra vida camará, te da y te quita, y te quita y te da”

“me encontré frente a la muerte y en sus ojos vi el sentido
y con el miedo conmigo así yo aprendí a quererte
y hoy se que nada es seguro ya que todo es pasajero
la muerte es el mensajero que con la ultima ahora viene
y el tiempo no se detiene ni con amor ni dinero”

Maestra Vida, Ruben Blades

Contents

CHAPTER 1

Introduction

1.1 The Paleo-Reanalysis Idea

Global prediction centers deliver every six hours high quality estimates of the atmospheric state by merging model predictions and observations in a process called Data Assimilation (DA)[1] [Talagrand, 1997]. These estimates, denoted as analysis in the DA jargon, can in principle be gathered so as to create archives of the weather state that can be employed in climate studies. Such collections of analyses, nonetheless, would necessarily exhibit numerous discontinuities due to frequent updates of an operational prediction system, and as a consequence their usability would be rather limited.

A strategy to enhance the homogeneity of analysis datasets was proposed in the late 1980s [Trenberth and Olson, 1988; Bengtsson and Shukla, 1988] under the name of

[1] The DA terminology have started to be used for methods that estimate the optimal parameters of model given certain observational information. Along this monograph, these techniques will be referred to as model optimization methods while the DA term will be reserved for state estimation approaches.

retrospective climate analysis, or simply “reanalysis”. An unchanging combination of prediction model and DA scheme can be rerun during a recent climate period, assimilating historical instrumental records. Furthermore, due to the absence of operational time constrains many new off-line observations can be used. The first atmospheric reanalysis was accomplished in the early 1990s by a collaboration between NCEP and NCAR [Kalnay et al., 1996] and since then an ever growing number of reanalysis projects has taken place, covering several components of the earth system e.g., atmosphere, hydrosphere and terrestrial biosphere [Bosilovich et al., 2013].

Nowadays, reanalyses constitute one of the most important information sources in climate research [Rood and Bosilovich, 2010]. They assimilate big amounts of observations and provide fields with consistent spatial and temporal resolutions for all model variables. Nevertheless, it should be borne in mind that reanalyses still present several important drawbacks e.g., (i) the evolving nature of observational systems tends to introduce spurious variability and trends, (ii) observational constrains are strongly dependent on variable, location and time, and (iii) invariant physical quantities such as water content may not be strictly preserved [Dee et al., 2013].

Current reanalysis development efforts are mainly focused on two directions: (i) effectively assimilating the wealth of observation available for recent decades, particularly satellite data, and (ii) extending the length of the datasets as much as possible. Following the later, the 20th Century Reanalysis (20CR) [Compo et al., 2011] has already achieved an atmospheric reanalysis starting in 1871 by assimilating only surface pressures [Compo et al., 2006]. Despite the sparsity of the assimilated observations, 20CR quality for the extratropical Northern Hemisphere is comparable to present three-day operational weather predictions. Moreover, the employed ensemble DA technique directly provides uncertainty estimates, which do not exist for most of the reanalysis datasets.

Given the great success of the reanalysis concept into climate science, since the early 2000s the paleoclimate community have started investigating the possibility of assimilating paleoclimate records into climate models, with the purpose of generating paleo-reanalysis datasets stretching beyond the instrumental period [Hughes and Ammann, 2009; Guiot et al., 2009; Brönnimann, 2011], very much in the in the spirit of 20CR.

Paleo-reanalysis appear as a very promising approach to paleoclimate reconstruction, as the states obtained in this way are in principle consistent both with historic records and the physics of the climate system as represented by the model equations. In practice, however, there are numerous stumbling blocks arising from the challenging features of paleoclimate data as well as from the sheer complexity of the climate system.

1.2 Paleoclimate Proxy Data

Spatially extended meteorological networks date back to the middle of the 19th century, accordingly, climate conditions previous to this time can only be inferred from natural archives such as tree trunks, coral reefs, glacials and sediments. These archives have been long sampled by the paleoclimate research community in order to create the so-called proxy records [Jones and Mann, 2004]. Currently, there is an impressive variety of proxy data types and their records are systematically developed and stored in worldwide databanks. Some proxy records are able to resolve annual or seasonal features and accordingly they are classified as high-resolution ones, e.g., tree rings, coral data, speleothems, high accumulation ice cores and laminated sediment cores. The rest of the proxy types present lower temporal resolutions ranging from decades to millennia [Jones et al., 2009].

The formation of a proxy record involves biological, physical, and/or chemical mechanisms, driven by multiple environmental factors including climate and human activities. As a consequence, there exist several challenging features that distinguish proxy data from standard instrumental observations, most notably, low time resolution, pronounced spatial sparseness, high noise levels and potentially nonlinear relationship with climate variables [Evans et al., 2013]. Additionally, the climatic signal recorded in a proxy record typically corresponds to Time-Averaged (TA) climate quantities, rather than instantaneous ones.

This thesis will pay special attention to the proxy record type with the longest tradition: Tree-Ring-Width (TRW) chronologies [Fritts, 1976]. This terrestrial proxy presents the

largest and densest spatial coverage among all proxies currently available (albeit strongly biased towards the Northern hemisphere). Additionally, together with coral data, TRW chronologies present a highly stable yearly resolution. Besides the width of the ring, there are several other numerical quantities that can be retrieved from tree rings e.g., wood density and isotopic composition. Oxygen and carbon isotope ratios have shown very strong climatic signals even for the tropical zones where TRW is typically weakly connected to climate [McCarroll and Loader, 2004]. On the other hand, isotopic analysis is a rather expensive procedure. As a result, the availability of isotope chronologies is still quite limited.

1.3 Statistical Climate Reconstructions

Proxy records have been traditionally inverted into climate quantities by means of statistical approach, consisting of two steps:

1. Calibration of a statistical model between proxy records and instrumental records of a target climate quantity during their overlapping time period.
2. Reconstruction of the targeted climate variable by applying the calibrated model to the non-overlapping section of the proxy records.

The employed statistical models have been largely dominated by multivariate linear regression techniques, the paleo-data used have been either mono- or multi-proxy networks, and the climate targets have been either broad indices, e.g., global mean surface temperature and El Niño Southern Oscillation (ENSO), or 2-dimensional fields, e.g., surface temperature and Palmer Drought Severity Index (PDSI) [Mann et al., 2008; Cook et al., 1999].

Statistical inversion has been profusely used to reconstruct paleoclimate quantities at local, regional and global scales [Jones et al., 2009]. However, since recent years there has been an increasing awareness of the caveats of statistical reconstructions. Accordingly, many papers have been devoted to the analysis of the performance of climate

reconstruction methodologies under simplified conditions using the idea of Pseudo-Proxy Experiment (PPE) [Smerdon, 2012]. Within these methodological studies, a trajectory of a climate model is selected as the "true" climate evolution and from it, artificial proxy records are generated, typically by adding noise to a time-averaged climate variable. Afterwards, pseudo-proxies are used as input data for a reconstruction method and the reconstructed climate quantities are compared to the "real" ones, which are known in this simplified setting.

PPEs have revealed that even assuming a linear climate-proxy relationship, climate fields reconstructed through linear regression are not physically consistent in general, and are prone to show variance losses and spatially variable mean biases [Smerdon et al., 2011]. In reality, proxy formation comprises complex processes that can easily introduce nonlinear dependencies [Hughes et al., 2010; Evans et al., 2013]. Moreover, different proxy data kinds react in distinctive ways to specific sets of climate variables. Therefore, the validity of combining different proxy types into a multi-proxy reconstruction is currently discussed [Evans et al., 2013].

1.4 Process-based Proxy Forward Modeling

Given the high complexity of the climate-proxy relationship, since recent years the paleoclimate community has been interested in adopting more realistic methodologies, that take into account the different processes by which climate conditions get imprinted into proxy records. One of the most promising approaches in this direction is "Proxy Forward Modeling" [Hughes et al., 2010; Evans et al., 2013], which take climate forcing as input data and generate artificial proxy records that can be directly compared to actual proxy records. This strategy is diametrically opposed to the traditional inverse approach where climate conditions are directly inverted from proxy data.

Proxy forward models can be used for different purposes such as model-paleodata comparison in the proxy space [Evans et al., 2013] and the prediction of the future evolution or proxy archives [Vaganov et al., 2006]. Despite its forth direction, forward models

can also be used for reconstruction by resorting to probabilistic inversion strategies, such as Bayesian hierarchical modeling [Tolwinski-Ward et al., 2014], Markov Chain Monte Carlo (MCMC) [Boucher et al., 2014] and DA [Hughes et al., 2010].

Nowadays, there exist process-based forward models for many different proxy types, most notably TRW chronologies [Vaganov et al., 2006; Evans et al., 2006; Tolwinski-Ward et al., 2011], tree-ring isotopes [Roden et al., 2000; Danis et al., 2012; Evans, 2007], coral isotopes [Thompson et al., 2011], ocean sediments [Heinze, 2001; Schmidt, 1999] and stalagmite isotopes [Baker et al., 2012]. There are also initiatives to model the transport of isotopes within the atmosphere [Sturm et al., 2010]. Depending on the particular application and the availability of data, proxy forward models assume different complexity levels which go from the minimalistic linear pseudo-proxies, introduced in section 1.3, to comprehensive models that simulate the proxy generation process as realistically as possible.

1.4.1 Tree ring growth forward models

Tree ring growth has been studied during several decades, mostly from the point of view of ecological disciplines. As a result there exist several eco-physiological models, most notably TREERING 2000 [Fritts et al., 1999], MAIDEN [Danis et al., 2012; Misson et al., 2004] and the Vaganov-Shashkin (VS) model [Vaganov et al., 2006; Evans et al., 2006], which simulate many complicated phenomena such as photosynthesis, carbon allocation and cellular wood formation processes. All these comprehensive tree growth models have shown remarkable skill for local studies in data-rich areas. However, because of their high complexity, ecophysiological models are very demanding in terms of data quantity and quality, and consequently their applicability for global studies is rather limited. Additionally, their high number of parameters make very costly, or even prohibitively expensive, the usage of systematic tuning procedures.

With the purpose of developing a process-based forward model for TRW chronologies which could be applied to global climate studies, a simplified version the VS model, called Vaganov-Shashkin-Lite (VSL), was recently introduced by Tolwinski-Ward et al. [2011].

This model has been shown to skilfully simulate the climate-driven tree-ring growth for very diverse species and climate regimes, both at regional [Tolwinski-Ward et al., 2011; Acevedo et al., 2013] and global scales [Breitenmoser et al., 2014], based solely on 3 external factors - temperature, soil moisture and solar radiation - and 4 tunable parameters. Moreover, thanks to its small number of parameters, VSL can be systematically calibrated using for example a MCMC scheme [Tolwinski-Ward et al., 2013]. With that VSL presents itself as a perfect candidate for a TRW observation operator within a paleo-DA setting.

1.5 Paleo-Reanalysis Studies

1.5.1 Data assimilation techniques for paleoclimate

To date, several very diverse paleo-DA schemes have been proposed, all of them with advantages ($\oplus$) and disadvantages ($\ominus$) (see [Hughes and Ammann, 2009; Widmann et al., 2010] as reference material):

Pattern Nudging [von Storch et al., 2000] and **Forcing Singular Vectors** [Barkmeijer et al., 2003; van der Schrier and Barkmeijer, 2005] techniques were designed to curb the atmospheric circulation towards a target pattern by means of an artificial term added to the model dynamics. $\oplus$: useful to test hypothesis regarding paleoclimate circulation anomalies. $\ominus$: no probabilistic basis; proxy records cannot be directly assimilated.

4-Dimensional Variational Analysis (4D-Var) methodology has been used to assimilate pseudo-proxies into an ocean model [Paul and Schäfer-Neth, 2005; Kurahashi-Nakamura et al., 2014]. $\oplus$: time dependent statistics; high robustness to observational sparsity [Whitaker et al., 2009]. $\ominus$: Gaussian statistics assumed; very demanding implementation due to the need of the adjoint operator, which is not available for current coupled climate models.

Ensemble Kalman Filter (EnKF) was adapted to time-averaged observations [Dirren and Hakim, 2005] and tested in an hierarchy of atmospheric models [Huntley and

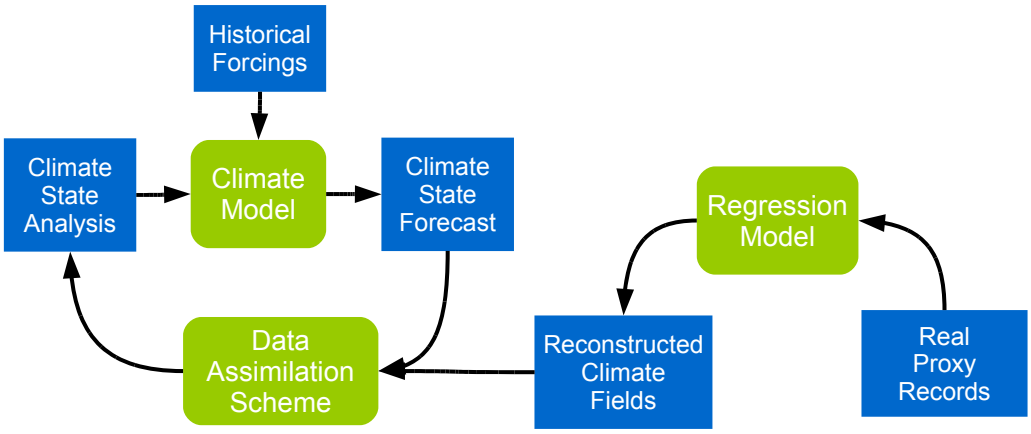

(a) Assimilating climate reconstructions.

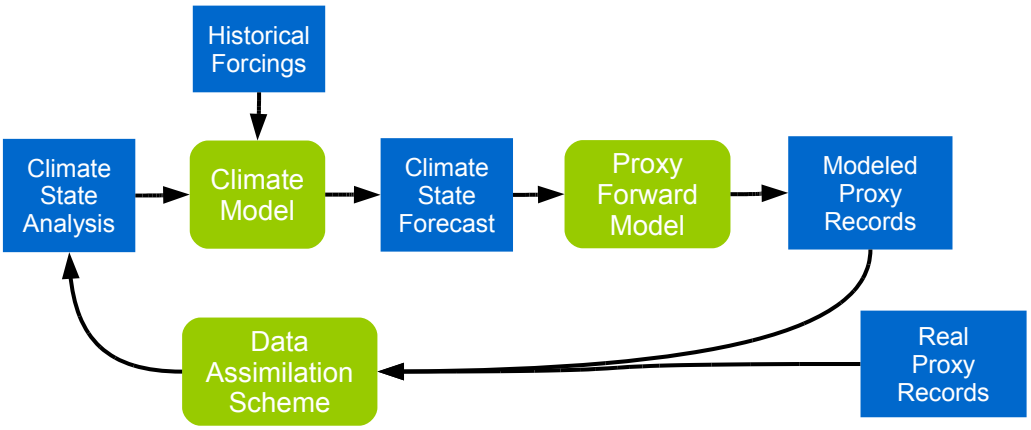

(b) Assimilating proxy records.

FIGURE 1.1: Schematic of paleoclimate data assimilation approaches. Sharp (rounded) cornered boxes represent data (processes).

Hakim, 2010; Bhend et al., 2012; Pendergrass et al., 2012; Steiger et al., 2014]. ⊕: time dependent statistics; very robust to very sparse observation networks; straightforward to implement; provides uncertainty estimates. ⊖: Gaussian statistics assumed; Accuracy depends on ensemble size.

Particle filter has been tested with a Earth system model of intermediate complexity [Annan and Hargreaves, 2012; Dubinkina and Goosse, 2013; Mathiot et al., 2013]. ⊕: time dependent statistics; no Gaussian statistical assumptions. ⊖: very large

ensembles needed; tendency to collapse for small ensembles [Annan and Hargreaves, 2012].

Among all this techniques, EnKF offers an appealing trade-off between accuracy, implementation easiness and computational expense. EnKF works robustly for very sparse observation networks and moderate number of ensemble members [Whitaker et al., 2009]. Its implementation does not require adjoint model and uncertainty estimates can be directly obtained from the ensemble spread [Hamill, 2006].

The main disadvantage of EnKF within a paleoclimate setting is its inability to handle strongly non-Gaussian Probability Density Functions (PDFs), which can result from the nonlinearities of climate models and observation operators. Nonetheless, it is very difficult to remove this limitation, given that strictly non-Gaussian DA techniques have been so far prohibitively expensive to run for high dimensional systems. In particular, particle filters are known to be strongly liable to the "curse of dimensionality": accurate estimation requires ensembles whose size grows exponentially with the system dimension [Bengtsson et al., 2008; Annan and Hargreaves, 2012]. Recent improvements to the sampling strategies of particle filters have enhanced significantly their scaling properties [van Leeuwen, 2010; Dubinkina and Goosse, 2013], however it is still unclear whether particle filters will reach the robustness of traditional Gaussian DA techniques at an affordable computational price.

1.5.2 Link between climate forcing and proxy records

Regarding the relationship between climate state and climate-driven proxy signals, all the studies considered in this section have assumed a linear dependency. Few works have assimilated statistical climate reconstructions coming from actual proxy records [van der Schrier and Barkmeijer, 2005; Goosse et al., 2010; Mathiot et al., 2013], whereas most of the studies have assimilated linear pseudo-proxies.

Given the high complexity of the real climate-proxy relationship (see section 1.2), a natural step to increase the realism of paleo-DA experiments would be the use of process-based proxy forward models to directly link climate model output with proxy records (see figure 1.1(b)). This approach offers in principle several potential advantages over the assimilation of climate reconstructions (see figure 1.1(a)), e.g., (i) the dependency on statistical stationarity must be weaker due to the process-knowledge contained into the forward model, (ii) the limitations of statistical reconstructions would not be directly inherited by paleo-reanalyses and (iii) the extraction of the proxy climate signal would be more consistent with the proxy recording mechanisms. An important complication of using forward models into paleo-DA setting is the necessity of an specific forward model for each proxy data type. In this research work I focus on the modelling and assimilation of TRW chronologies via VS-Lite model.

1.6 Thesis Outline

This manuscript investigates several aspects of the problem of assimilating proxy records into climate models using EnKF techniques and process-based proxy forward models. First of all, chapter 2 briefly reviews the general concepts of DA and EnKF, so as to set the context for the TA filtering techniques, which are described in detail at the end of the chapter. Chapter 3 presents a new comparison of the different filtering strategies to estimate TA states, this time under strongly nonlinear coupling conditions. Chapter 4 is devoted to the reinterpretation of VSL in terms of Fuzzy Logic (FL) theory, which reveals several natural modifications to the model equations. The sensitivity of the model performance to this FL-based formulation changes is assessed for a global network of TRW chronologies. Chapter 5 studies the applicability of VSL as forward operator into a simplified DA setting, paying special to the influence of the FL-based model modifications on the DA skill. Chapter 6 presents a set of DA experiments analogous to the ones studied in chapter 5, this time utilizing an Atmospheric General Circulation Model (A-GCM) Finally, a summary of the results as well as an outlook are provided in chapter 7.

CHAPTER 2

Filtering Time-Averaged Observations

2.1 Data Assimilation Basics

The term Data Assimilation (DA) was initially used to designate the process of estimating the state of a system using observations and the physical laws governing the evolution of the system as represented in a numerical model [Talagrand, 1997]. DA is typically performed in the shape of an analysis cycle comprising two phases:

Analysis step: the state of a system is estimated at a given time by combining probabilistically available observations and the prior knowledge of state. This estimate is normally referred to as analysis or posterior.

Forecast step: a numerical model of the system is used predict the future state of the system, using as starting point the analysis. The obtained prediction is used in turn as prior information for the next analysis step.

The period of the analysis cycle is determined by several factors such as availability of observations, computational resources and the time scales of the modeled system. Within operational atmosphere prediction settings, the typical periods of global and regional analysis cycles are 6 hours and 1 hour respectively [Kalnay, 2003]. DA methods have evolved from very empirical approaches, such as Newtonian relaxation, to probabilistic ones that estimate the state Probability Density Function (PDF) conditional to the observations. (see Kalnay [2003] Lahoz et al. [2010] for comprehensive accounts of DA methods for geophysical applications).

2.1.1 Kalman Filter

Given a model with state $\mathbf{x}(t) \in \mathbb{R}^n$, the Kalman Filter (KF)[Kalman, 1960] assumes that the forecast state PDF is given by a Gaussian function with mean $\mathbf{x}^f$ and covariance $\mathbf{P}^f \in \mathbb{R}^{n\times n}$:

$$p(\mathbf{x}) \propto \exp(-\frac{1}{2}(\mathbf{x}-\mathbf{x}^f)^T(\mathbf{P}^f)^{-1}(\mathbf{x}-\mathbf{x}^f)). \tag{2.1}$$

Observations $\mathbf{y}(t_j) \in \mathbb{R}^k$ are assumed to have Gaussian distributed measurement errors and therefore the conditional probability of the observation vector $\mathbf{y}$ given the state $\mathbf{x}$ follows the expression:

$$p(\mathbf{y} \mid \mathbf{x}) \propto \exp(-\frac{1}{2}(\mathbf{y}-\widehat{\mathrm{H}}\mathbf{x}^f)^T\mathbf{R}^{-1}(\mathbf{y}-\widehat{\mathrm{H}}\mathbf{x}^f)), \tag{2.2}$$

where $\widehat{\mathrm{H}}$ denotes the observation operator and $\mathbf{R} \in \mathbb{R}^{k\times k}$ is the observation covariance matrix. By virtue of Bayes theorem, the conditional probability of the state given the observations, i.e., the analysis PDF, takes the form:

$$p(\mathbf{x} \mid \mathbf{y}) \propto \exp(-\frac{1}{2}(\mathbf{x}-\mathbf{x}^f)^T(\mathbf{P}^f)^{-1}(\mathbf{x}-\mathbf{x}^f) - \frac{1}{2}(\mathbf{y}-\widehat{\mathrm{H}}\mathbf{x}^f)^T\mathbf{R}^{-1}(\mathbf{y}-\widehat{\mathrm{H}}\mathbf{x}^f)). \tag{2.3}$$

Given the Gaussianity of functions 2.1 and 2.2, function 2.3 is again a Gaussian PDF whose mean and covariance can be calculated, provided that $\widehat{\mathrm{H}}$ is linear, yielding the

so-called Kalman update equations (see [Lorenc, 1986] for details):

$$\mathbf{x}^a = \mathbf{x}^f + \mathbf{K}(\mathbf{y} - \widehat{\mathrm{H}}\mathbf{x}^f), \tag{2.4}$$

$$\mathbf{P}^a = (\mathbf{I} - \mathbf{K}\widehat{\mathrm{H}})\mathbf{P}^f; \tag{2.5}$$

where the Kalman gain matrix $\mathbf{K}$ is given by the expression:

$$\mathbf{K} = \mathbf{P}^f\widehat{\mathrm{H}}^\dagger(\widehat{\mathrm{H}}\mathbf{P}^f\widehat{\mathrm{H}}^\dagger + \mathbf{R})^{-1}. \tag{2.6}$$

2.1.2 Ensemble Kalman Filter (EnKF)

For geophysical systems, the model state size can be of the order millions and hence the calculation of covariance matrices becomes prohibitively expensive. In order to overcome this limitation, Evensen [1994] proposed to approximate the KF equations by way of an ensemble of model states $\mathbf{X}(t) = (\mathbf{x}_1, \ldots, \mathbf{x}_m)$, that represents the model state PDF. This approach constitutes a Monte Carlo approximation, where the best estimate and its uncertainty are given by the ensemble mean and spread, respectively. This latter characteristic of the ensemble is typically quantified by means of the standard deviation of the ensemble around its mean.Within EnKF the aforementioned DA cycle steps take the following form:

Forecast step: an initial ensemble members are simultaneously propagated in time using the model dynamics, so as to generate a forecast ensemble.

Analysis step: the empirical mean and covariance of the forecast ensemble are calculated and used as approximations of the corresponding quantities in the KF equations:

$$\langle \mathbf{X}_f \rangle = \frac{1}{m}\sum_{i=1}^{m}\mathbf{x}_i^f, \quad \mathbf{P}^f = \frac{1}{m-1}\mathbf{X}_f{}'(\mathbf{X}_f{}')^T. \tag{2.7}$$

Here $\mathbf{X}_f{}' \in \mathbb{R}^{n\times m}$ denotes the forecast ensemble deviation matrix:

$$\mathbf{X}_f{}' = \mathbf{X}_f - \langle \mathbf{X}_f \rangle \mathbf{e}^T. \tag{2.8}$$

where $\mathbf{e} = (1, \ldots, 1) \in \mathbb{R}^m$. In order to start a new forecast step, it is necessary to generate an analysis ensemble whose covariance satisfies equation 2.5. This can be achieved in many different ways, giving rise to two main families of Ensemble Kalman Filters: Stochastic and Deterministic filters (see [Hamill, 2006] for a detailed account of available updating algorithms). For the stochastic EnKF [Burgers et al., 1998], an observational ensemble $\mathbf{Y}$ is created by adding a set of realization of the observational noise to the observation vector $\mathbf{y}$, and the analysis ensemble is generated via the following update equations:

$$\mathbf{X}_a = \mathbf{X}_f + \mathbf{K}\left(\mathbf{Y} - \widehat{\mathrm{H}}\mathbf{X}_f\right). \tag{2.9}$$

Notice that the use of random noise introduces sampling error, which can be significant for small ensemble sizes. This additional error source is not present for deterministic updating algorithms, given that they avoid the generation of an observational ensemble. Instead, they calculate the analysis mean $\overline{\mathbf{X}_a}$ and deviations $\mathbf{X}_a{}'$ using different update formulae (see Tippett et al. [2003] for a description of the most representative deterministic updating approaches).

EnKF converges to KF in the limit of infinite number of ensemble members. In practice, however, the spread of the ensemble is typically too low due to the finite ensemble size, and therefore the forecast uncertainty is underestimated. In these circumstances, the filter is overconfident on the prediction and after some assimilation cycles the observations become completely ignored. This phenomenon, known as filter divergence, is pragmatically counteracted by increasing the spread of the ensemble. This procedure is known as covariance inflation and is typically achieved by multiplying the ensemble deviations by a constant greater than one. A different situation where the filter operation can diverge has been observed for sparse observational grids with small observational noise [Gottwald and Majda, 2013]. In these conditions the update step can produce analysis states which are not consistent with the true dynamics. Subsequently, this analysis states are very strongly pushed towards the attractor by the model dynamics, and doing so the integrator my generate machine infinity values. When this happens the model crashes and the filter is said to experience a catastrophic divergence.

Another undesired consequence of the finite ensemble size is that an observation will typically present significant spurious correlations with distant grid points. This side effect, which can be very detrimental for the filter performance, is normally prevented by another pragmatic remedy called "covariance localization". There are two main localization methodologies:

B-localization [Hamill et al., 2001]: the elements of the background covariance matrix are multiplied by a function that decreases monotonically with distance, so that large-range correlations are discarded. The most traditional function utilized for B-localization is the one introduced by Gaspari and Cohn [1999].

R-localization [Hunt et al., 2007]: the elements of the observation error covariance matrix are multiplied by a function that increases exponentially with distance, in such a way that far away observations appear as having infinite error and accordingly are not taken into account for the analysis.

The EnKF forecast step allows model nonlinearity given that the whole model, potentially nonlinear, is utilized to evolve the ensemble. The analysis step, in turn, is linear due to the Gaussian assumption and then its performance might be deteriorated by nonlinear effects coming from the model or the observation operators. Notice that there exist fully nonlinear DA methods, however for high-dimensional applications they are currently unwieldy and appear to remain that way in the foreseeable future. Consequently, there is an strong interest in adapting Gaussian DA techniques to work into nonlinear settings.

2.1.3 Observation System Simulation Experiments

Given a prediction system comprising a dynamical model and a DA scheme, forecast and analysis errors arise from many different sources, e.g. model imperfections, inadequacy of the DA strategy and insufficiency of observational information, which interact with each other in practice. In order to disentangle the effects of these error sources, a DA scheme is typically tested under simplified conditions by means of numerical experiments, currently known as OSSEs, whose realism level is gradually increased.

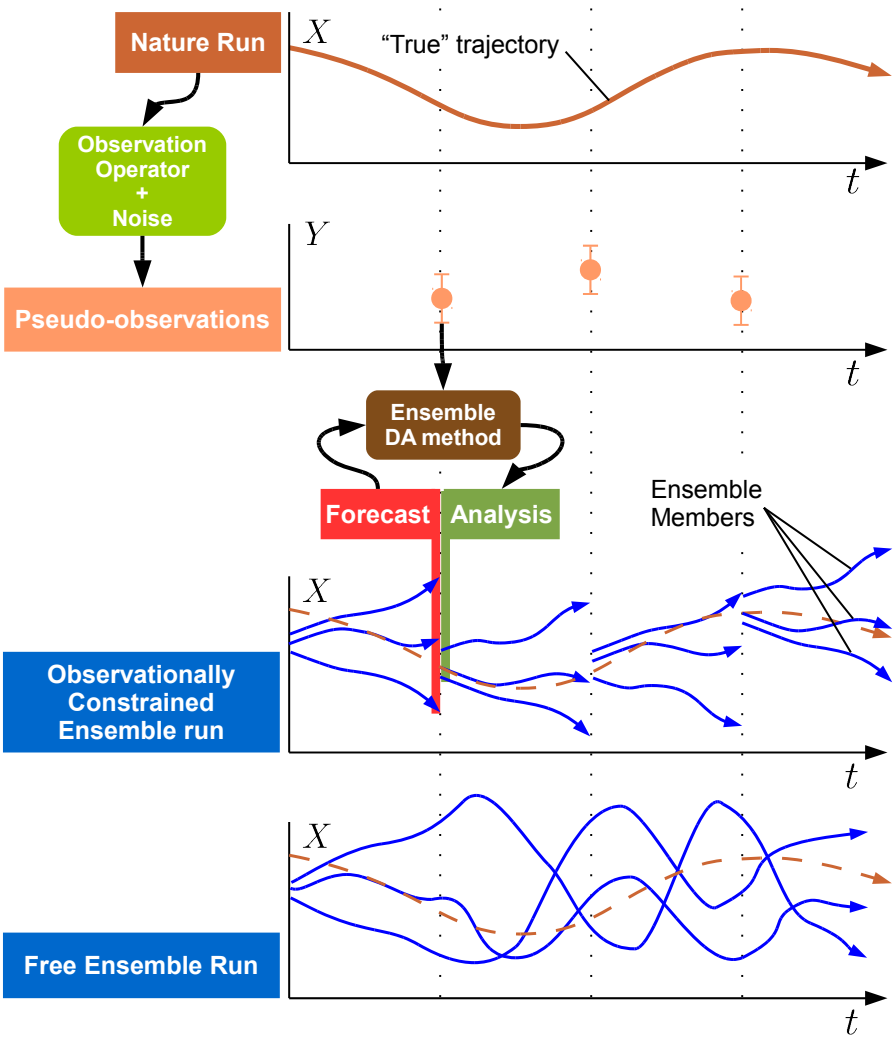

FIGURE 2.1: Schematic of a typical Observation System Simulation Experiment (OSSE) with an ensemble DA method. t designates the time axis and $X(Y)$ denotes the model state (observation) space. Sharp (rounded) cornered boxes represent data (processes).

An OSSE consists of (i) a single model trajectory $\mathbf{x}^{\text{NATURE}}$, typically referred to as "true" run or "nature" run, that is used as prediction target, (ii) pseudo-observations created by applying the observation operator to $\mathbf{x}^{\text{NATURE}}$ and adding simulated observational noise, and (iii) an observationally constrained run $\mathbf{X}^{\text{DA}}$, obtained by performing a sequence of analysis cycles where the pseudo-observations are assimilated (see figure 2.1). Notice that an OSSE follows essentially the same rationale as the Pseudo-Proxy Experiment (PPE) introduced in section 1.3.

The nature run is normally generated by running the dynamical model starting from

a random sample of the model climatology. Notice that thanks to the availability of the truth model evolution for an OSSE, the forecast and analysis skill of the observationally constrained run can be directly assessed, using for example the Root Mean Square Error (**RMSE**) of the ensemble mean:

$$\textbf{RMSE}(\langle \mathbf{X}^{\text{DA}} \rangle) = \left(\overline{(\mathbf{x}^{\text{NATURE}} - \langle \mathbf{X}^{\text{DA}} \rangle)^2} \right)^{\frac{1}{2}}, \tag{2.10}$$

where $\overline{}$ and $\langle\ \rangle$ denote the time and ensemble mean operators, respectively.

An additional run frequently performed for OSSEs involving ensemble DA methods, is a free ensemble run $\mathbf{X}^{\text{FREE}}$, where no observations are assimilated and then the ensemble just freely evolved under the action of the model dynamics (see figure 2.1). $\mathbf{X}^{\text{FREE}}$ is intended to provide a benchmark of performance, against which it is possible to asses the the added value of the DA scheme, using for example the error reduction regarding the free run, $\mathcal{E}^{\text{FREE}}_{\text{REDUCTION}}$, given by the following expression:

$$\mathcal{E}^{\text{FREE}}_{\text{REDUCTION}}(\mathbf{X}^{\text{DA}}) = 100\% \cdot \left(1 - \frac{\textbf{RMSE}(\mathbf{X}^{\text{DA}})}{\textbf{RMSE}(\mathbf{X}^{\text{FREE}})} \right). \tag{2.11}$$

As mentioned before, the development and evaluation of a DA setting should be carried out gradually, by way of a hierarchy of increasingly realistic OSSEs. A typical first step is to create $\mathbf{x}^{\text{NATURE}}$, $\mathbf{X}^{\text{FREE}}$ and $\mathbf{X}^{\text{DA}}$ using the same model, which leads to the so-called "perfect model" OSSEs. In a real-world setting the dynamical model is always an imperfect representation of reality, then a natural next step is a "imperfect model" OSSE, where $\mathbf{X}^{\text{FREE}}$ and $\mathbf{X}^{\text{DA}}$ are performed using for example a simplified version of the model utilized to create $\mathbf{x}^{\text{NATURE}}$.

2.2 Assimilating Time-Averaged Observations through EnKF

Measuring the instantaneous value of a quantity is not possible, strictly speaking, due to the finite response time of every sensor. However, in practice it is common that the time scales of the system under study are much longer that the response time, and hence the

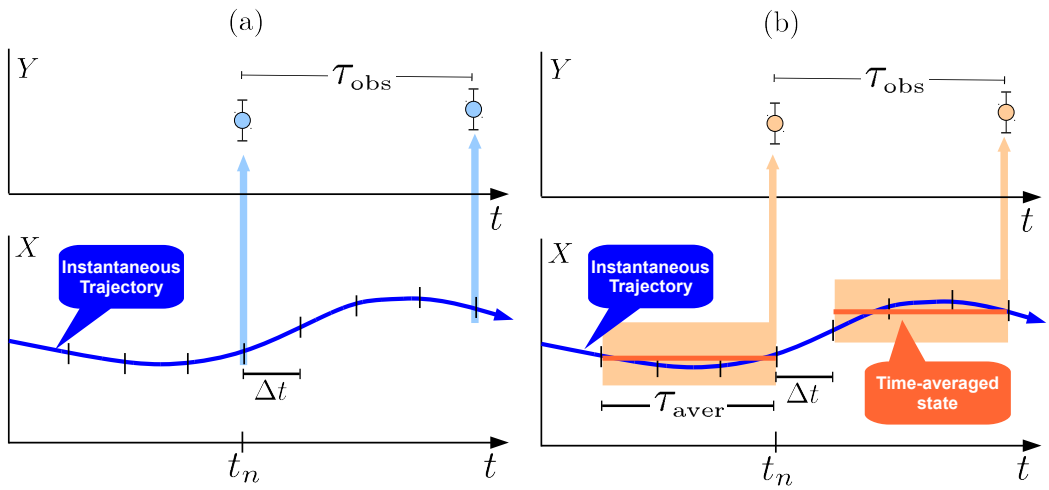

FIGURE 2.2: Schematic of the state-observation relationship for instantaneous (a) and Time-Averaged observations (b). t designates the time axis and $X(Y)$ denotes the model state (observation) space. τ_{obs} (τ_{aver}) stands for the observational (averaging) period.

observations can be assumed instantaneous. There are, nonetheless, situations where this assumption does not hold and the Time-Averaged (TA) nature of the observations ought to be taken into account, e.g., rain gauges, wind meters and climate proxy records.

Observational time averaging periods range from hours, in the case of precipitation or wind measurements, to years or even decades, in the case of proxies. In general, the time averaging period does not coincide with the observation period, and can be even longer as is the case of Tree-Ring-Width (TRW) records where a ring typically carries information of a time period longer than one year, as a result of biological and/or ecological persistence [Wu et al., 2013].

The problem of assimilating TA observations differs in several respects from the traditional assimilation of instantaneous quantities. One TA observation conveys information of a segment of the model state trajectory, as opposed to an instantaneous observation whose signal relates only to an instant of the model evolution (see figure 2.2). Moreover, due to the low pass filter action of time averaging, high frequencies are smoothed out and do not get recorded into the TA observations. Consequently, a new estimation target is pursued: the TA state.

Along this thesis the symbol $\overline{}^{\tau_{\text{aver}}}$ is used to represent the following time averaging operator:

$$\overline{*(t)}^{\tau_{\text{aver}}} = \frac{1}{\tau_{\text{aver}}} \int_{t_n - \tau_{\text{aver}}}^{t_n} *(t)\, dt, \tag{2.12}$$

where $*$ represents an arbitrary time dependent quantity, τ_{aver} is the length of the averaging period and t_n is the instant at which the observations becomes available (see figure 2.2). Using this notation, a TA observation $\overline{\mathbf{y}}^{\tau_{\text{aver}}}$ can be written as

$$\overline{\mathbf{y}}^{\tau_{\text{aver}}}(t_n, \tau_{\text{aver}}) = \overline{\widehat{\mathrm{H}}(\mathbf{x}(t))}^{\tau_{\text{aver}}} + \text{noise}, \tag{2.13}$$

where $\widehat{\mathrm{H}}$ designates the instantaneous observation operator.

2.2.1 Updating approaches for Time-Averaged state estimation

Given TA observations of a system, the estimation of its TA state can be pursued using EnKF by altering the structure of the traditional analysis step. This modifications of the analysis algorithm give rises to different updating approaches.

2.2.1.1 Time-Augmented Update (TAug-Up) strategy

All the instantaneous states belonging to the averaging interval are updated [Huntley and Hakim, 2010]. This can be conveniently expressed in mathematical terms making use of the state augmentation concept [Nichols, 2010], which essentially attaches additional variables to the estimated state, typically with the purpose of estimating model parameters. In the present case, the instantaneous state corresponding to the observation arrival time is augmented with all the previous states contributing to the observation, giving rise to a higher dimensional control vector called the Time-Augmented state:

$$\mathbb{x}(t_n, \tau_{\text{aver}}) = [\mathbf{x}(t_i)], \quad t_n - \tau_{\text{aver}} > t_i > t_n. \tag{2.14}$$

An equivalent procedure can be applied to the ensemble in order to create the Time-Augmented (TAUG) ensemble:

$$\mathbb{X}(t_n, \tau_{\text{aver}}) = [\mathbf{X}(t_i)], \quad t_n - \tau_{\text{aver}} > t_i > t_n, \tag{2.15}$$

over which the EnKF update equations are applied (see figure 2.4(a) for an schematic view of the updating scheme and appendix A.1 for details of the algorithm).

2.2.1.2 Time-Averaged Update (TA-Up) strategy

Only the TA part of the system dynamics is constrained by updating the TA component of the TAUG state [Dirren and Hakim, 2005]. This can be achieved by performing at assimilation time the following TA decomposition:

$$\mathbb{X}_f = \overline{\mathbb{X}_f}^{\tau_{\text{aver}}} + \widetilde{\mathbb{X}_f}. \tag{2.16}$$

where $\widetilde{\mathbb{X}_f}$ designates the TA deviations. Subsequently, a EnKF update is applied over $\overline{\mathbb{X}_f}^{\tau_{\text{aver}}}$ to obtain the TA analysis, which is finally added to the unaltered TA deviations providing the instantaneous analysis states (see figure 2.4(a) for an schematic view of the updating scheme and appendix A.2 for details of the algorithm). The rationale of this approach is that TA linear observations can only contain TA information. This comes from the commutation of the TA operator and a linear observation operator:

$$\overline{\mathbf{y}}^{\tau_{\text{aver}}}(t_n, \tau_{\text{aver}}) = \overline{\widehat{\mathrm{H}}(\mathbf{x})}^{\tau_{\text{aver}}} + \text{noise} = \widehat{\mathrm{H}}(\overline{\mathbf{x}}^{\tau_{\text{aver}}}) + \text{noise}. \tag{2.17}$$

2.2.2 Comparison of updating strategies

In the limit $\tau_{\text{aver}} = 0$, the two aforementioned updating approaches reduce to the standard instantaneous updating strategy, while for $\tau_{\text{aver}} > 0$ they present significant differences in several respects:

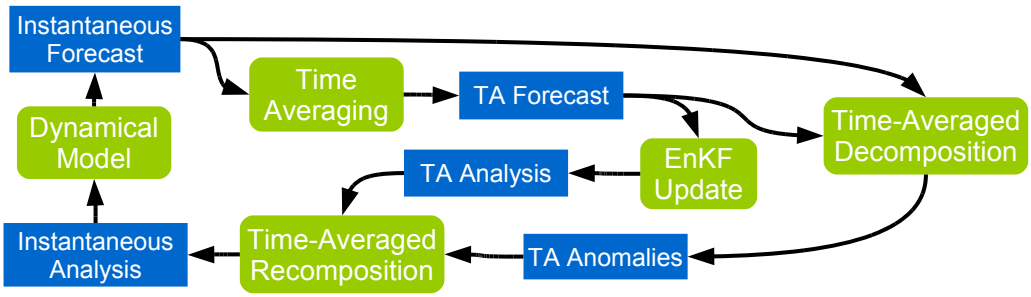

(a) Time-Averaged Update (TA-Up)

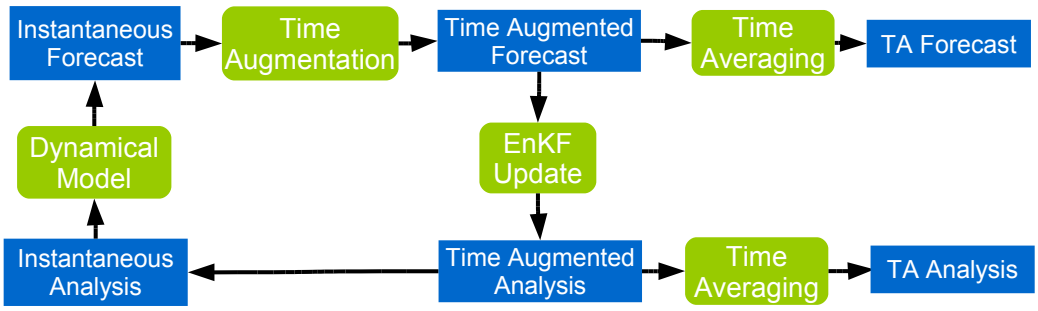

(b) Time-Augmented Update (TAug-Up)

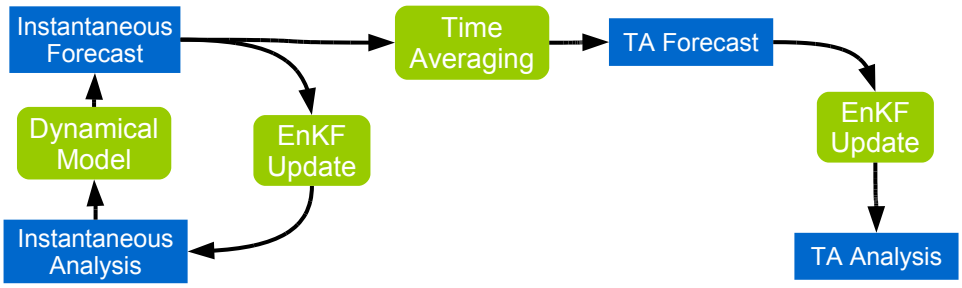

(c) Time-Averaged + Instantaneous Update (TAI-Up)

FIGURE 2.3: Schematic of updating strategies for Time-Averaged state estimation. Sharp (rounded) cornered boxes represent data (processes).

- Estimation skill: to the present, TA-Up and TAug-Up strategies have only been compared once for the assimilation of surface and tropopause TA linear observations into a quasi-geostrophic atmospheric model [Huntley and Hakim, 2010]. This research work reported equivalent numerical error levels in the TA quantities for both updating strategies, while for the instantaneous quantities, TAug-Up presented slightly better performance but only for short averaging periods. This numerical

evidence was supported by an analytical proof showing that TAug-Up reduces to TA-Up one provided (i) a linear observation operator and (ii) negligible covariances between TA ensemble observations and the TA ensemble deviations (see appendix A.3 for details of the proof).

- Computational expense: For the TAug-Up, each instantaneous state within the averaging period should be updated using the EnKF equations. Therefore, the computational cost of the analysis step increases linearly with the length of the averaging interval. On the other hand, the TA-Up demands only the update of the TA ensemble. There are some additional costs arising from the accumulation of the ensemble state during the forecast step, as well as the TA decomposition and recomposition of the ensemble at analysis time. These latter expenses are, nonetheless, small compared to the multiple instantaneous updates needed for the TAug-Up.

In these state of affairs, the convenience of using a particular updating approach clearly depends on the time averaging length. In the regime of long averaging periods, TAug-Up strategy becomes highly –or even prohibitively– expensive, hence TA-Up methodology clearly appears as the only cost-effective option. Moreover, given that a τ_{aver} increment involves a size increase for the TAUG state $\mathbb{X}$ but no more observational information, TAug-Up is expected to be more liable to statistical noise coming from the finite ensemble size, especially for large values of τ_{aver} [Huntley and Hakim, 2010]. On the other hand, in the regime of long averaging periods TAug-Up offers better estimation capabilities. Notice, however, that even for low τ_{aver} values this technique can become unaffordable in practice due to the very high dimensionality of geophysical models. This strong downside of the TAug-Up approach motivates us to propose in the following section a new hybrid updating strategy hereafter referred to as the TAI-Up methodology.

Finally, it is important to notice that the comparison conducted by Huntley and Hakim [2010] is considerably limited. The mid latitude atmospheric model utilized does present multi-scale phenomena, however it lacks the strong inter-component interactions present in the global climate system, e.g., the tropical atmosphere-ocean coupling responsible for El Niño Southern Oscillation (ENSO). Accordingly, in the next chapter a new comparison study is perform under strongly multi-scale coupling conditions.

2.2.2.1 Time-Averaged + Instantaneous Update (TAI-Up) strategy

Instantaneous and TA states are estimated independently, each one by means of its own EnKF analysis step (see figure 2.4(c)). This can be expressed in mathematical terms as a normal EnKF update performed over the following augmented vector:

$$\mathbb{X}_{\text{TAI}}(t_n, \tau_{\text{aver}}) = [\overline{\mathbb{X}_f}^{\tau_{\text{aver}}}, \mathbf{X}(t_n)], \tag{2.18}$$

which comprises the TA state and last instantaneous state within the observation interval. Notice that compared to TA-Up, TAI-Up involves only an additional instantaneous EnKF update. Hence their computational costs are comparable.

The TAI-Up methodology proposal is motivated on two aspects of the TAug-Up strategy: (i) the TA state is estimated in a very costly way by updating all the instantaneous forecast states contributing to the observation and, subsequently averaging the corresponding instantaneous analyses, (ii) the forecast solely depends on the last instantaneous analysis state within the observation interval. Accordingly, we hypothesize that the estimation of the TA state can be achieved in a more effective way by updating directly the TA ensemble state, while keeping the instantaneous estimation unaltered. It is our hope then that our hybrid updating strategy combines the outstanding scaling properties of the TA-Up approach, regarding τ_{aver}, and the TA estimation efficiency of the TAug-Up methodology for short averaging periods.

CHAPTER 3

Assimilation of Time-Averaged Observations into a Coupled 2-Scale Model

In this chapter the problem of estimating the Time-Averaged (TA) state of a model out of TA observations is revisited. The 2-component coupled model of Peña and Kalnay [2004] (PK2004) is used to perform a set of Data Assimilation (DA) experiments designed to shed light on the role of inter-scale coupling in the performance of for the different TA state estimation strategies described in chapter 2.

3.1 Experimental setting

3.1.1 Dynamical model

The PK2004 dynamical system features a coupling of two Lorenz [1963] (L63) models [Lorenz, 1963] with different time scales:

$$
\begin{aligned}
\dot{\mathbf{x}}_1 &= \sigma(\mathbf{x}_2 - \mathbf{x}_1) - c(s_a\mathbf{x}_4 + k) \\
\dot{\mathbf{x}}_2 &= r\mathbf{x}_1 - \mathbf{x}_2 - \mathbf{x}_1\mathbf{x}_3 + c(s_a\mathbf{x}_5 + k) \\
\dot{\mathbf{x}}_3 &= \mathbf{x}_1\mathbf{x}_2 - b\mathbf{x}_3 + c_z \mathbf{x}_6 \\
\dot{\mathbf{x}}_4 &= s_t(\sigma(\mathbf{x}_5 - \mathbf{x}_4)) - c(\mathbf{x}_1 + k) \\
\dot{\mathbf{x}}_5 &= s_t(r\mathbf{x}_4 - \mathbf{x}_5 - s_a\mathbf{x}_4\mathbf{x}_6) + c(\mathbf{x}_2 + k) \\
\dot{\mathbf{x}}_6 &= s_t(s_a\mathbf{x}_4\mathbf{x}_5 - b\mathbf{x}_6) - c_z \mathbf{x}_3,
\end{aligned}
\tag{3.1}
$$

where $(\mathbf{x}_1, \mathbf{x}_2, \mathbf{x}_3)^\dagger$ and $(\mathbf{x}_4, \mathbf{x}_5, \mathbf{x}_6)^\dagger$ are the fast and slow model components, respectively; $\sigma = 10$, $b = 8/3$, and $r = 28$ are the typical L63 parameter values, c (c_z) is the coupling strength for the $x - y$ (z) variables, s_a (s_t) is the amplitude (time) scale factor, and k is an "uncentering" parameter. Equations 3.1 constitute a minimalistic non linear dynamical system which allows as to focus on the role of coupling for the filtering of TA observations. All along our numerical exploration, we set $c = c_z$ (symmetric coupling) $k = -11$, $s_a = 1.0$ (equal amplitude scales) and $s_t = 0.1$ (fast component time scale ten times shorter than slow component one). It is important to mention that the actual time and scale ratios depend on the coupling details. We consider three configurations regarding the inter-component interaction: (i) no coupling: $c = 0.0$, (ii) weak coupling: $c = 0.1$ and (iii) strong coupling: $c = 0.5$. The numerical integration of the model equations is achieved via the standard Runge-Kutta method of fourth order with time step $\Delta t = 0.01$, where the model variables are represented by 64-bit FORTRAN real variables.

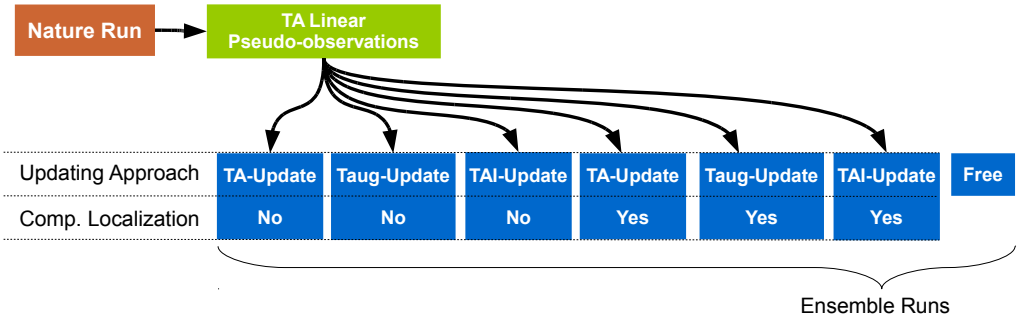

FIGURE 3.1: Schematic of the runs performed with the PK2004 model

3.1.2 Filter configuration and experiment characteristics

In our experiments we use ensembles with 20 members and a typical Ensemble Kalman Filter (EnKF) setting consisting of a stochastic analysis step [Burgers et al., 1998] (equation 2.9) and multiplicative inflation between 1% and 5% before the ensemble update. Additionally, in order to investigate the role of the inter-component interaction on the DA skill, we study the operation of the filter when the observations from the fast and slow components are allowed to impact only the state of fast and slow components, respectively. This filter configuration is achieved by setting to zero the covariance terms between state variables and observations corresponding to different model components. We refer to this procedure as component-wise covariance localization, or simply component localization.

We perform a set of standard "perfect model" Observation System Simulation Experiments (OSSEs)[1], meant to study the sensitivity of the DA scheme to the updating approaches introduced in section 2.2.1, as well as to the use of component-wise covariance localization. A diagram of the numerical exploration performed is provided in figure 3.1.

The model climatology is obtained by starting a model trajectory from a random initial condition and storing the model state every 5000 time steps. All ensemble runs are initialized identically from a random sampling of the model climatology that does not include the initial condition of the nature run. TA linear pseudo-observations are extracted from

[1] see section 2.1.3 for a description of OSSEs

the nature run following the equation 2.13, using the following instantaneous operator:

$$\widehat{\mathrm{H}} = \begin{pmatrix} 0 & 1 & 0 & 0 & 0 & 0 \\ 0 & 0 & 1 & 0 & 0 & 0 \\ 0 & 0 & 0 & 0 & 1 & 0 \\ 0 & 0 & 0 & 0 & 0 & 1 \end{pmatrix}, \tag{3.2}$$

which linearly measures the last two variables of each model component. Given that the variance of TA quantities decreases with time average length, for each τ_{aver} value we calculate the variance of the "clean" TA observation series and set the noise variance so as to keep a constant Signal-To-Noise ratio (SNR) equal to 10.0.

3.1.3 Diagnostic statistics

Given that the impact of time averaging on the error levels depends strongly on the time scale of the model internal variability, components with different time scales are expected to react differently to the same time averaging length. Accordingly, we analyze separately the error levels of slow and fast components. Analysis and forecast error levels are monitored by means of the root mean square error, **RMSE**, and the error decrease regarding the free run, $\mathcal{E}^{\text{Free}}_{\text{Reduction}}$, for the unobserved model variables ($\mathbf{x}_1$ and $\mathbf{x}_4$) after 10^5 analysis cycles[2]. The first 10^4 analysis cycles of the runs are regarded as spin-up period, and therefore they are not considered in the statistics.

[2]see section 2.1.3 for the definition of these diagnostic quantities

3.2 Results

3.2.1 Uncoupled configuration

3.2.1.1 Dynamics

For this configuration the dynamical system reduces to two independent L63 models, whose time scales present a ratio equal to 10 (see figure 3.3(a)). One consequence of this speed difference between the dynamics of the model components, is that their corresponding "butterfly" attractors are covered by a trajectory at different paces (see figure 3.3(b)). Given the absence of inter-component coupling, state variables corresponding to different components exhibit negligible correlations and their power spectra present no interaction (see figure 3.3(c) and 3.3(d)).

3.2.1.2 TA-Up performance using component localization

Given the independence of the model components, when component localization is employed our experimental setup setting effectively splits into two completely disconnected DA settings, each one comprising a L63 model and a EnKF assimilating TA observations.

Instantaneous quantities Due to the low-pass filtering action of the Time-Averaging operator, TA observations get gradually decorrelated from the instantaneous variables as τ increases. As a consequence, errors in the estimate of the instantaneous state, i.e., the instantaneous ensemble mean, tend to grow by increasing τ. This process can be readily seen in the red lines of figure 3.4(a), where the instantaneous forecast Root-Mean-Square (RMS) error for the fast (slow) component converge to the free run values at around $\tau = 1.0$ ($\tau = 3.3$). Analysis errors undergo an equivalent process but at a slightly slower pace.

Time-Averaged quantities As opposed to the instantaneous state, the TA state remains correlated to the TA observations regardless of the τ value. Consequently, TA

analysis error curves remain below their corresponding free run curves for much longer averaging periods than the instantaneous error curves (see figure 3.4(a)). Regarding TA forecasting skill, despite the considerable TA analysis skill for all τ values considered, the TA forecast errors saturate and reach the free run values at around $\tau = 1.0$ ($\tau = 4.0$) for the fast (slow) component (see figure 3.4(a)). This situation, where a DA method presents TA analysis skill for averaging periods where the TA forecasting skill is completely lost, has been previously observed in studies applying EnKF techniques on TA quantities [Huntley and Hakim, 2010; Bhend et al., 2012; Pendergrass et al., 2012; Steiger et al., 2014]. DA performed under these circumstances is currently labeled as "offline". This term is used to indicate that, under the randomizing action of chaotic model dynamics, at assimilation time the prior ensemble is completely decorrelated from the previous analysis state. As a consequence, the observational information cannot accumulate over time, as opposed to the typical application of DA for short-range prediction.

3.2.1.3 TA-Up performance without component localization

Considering the negligible correlation between variables belonging to different model components observed in figure 3.3(c), fast observations would not be expected to impact the slow component and *vice versa*. However, due to the finite ensemble size, in absence of component localization the filter still detects spurious inter-component covariances which allow inter-component observational influence. As a consequence, model components pollute each other during the EnKF analysis step, as it can be observed in figure 3.4(b), where the strong error increase of the fast component for τ_{aver} values around 0.6 gets imprinted in the error curves for the slow component. This inter-scale contamination phenomenon has been already observed in the first numerical test of the Time-Averaged Update (TA-Up) strategy on another uncoupled, 2-scale chaotic dynamical system [Dirren and Hakim, 2005].

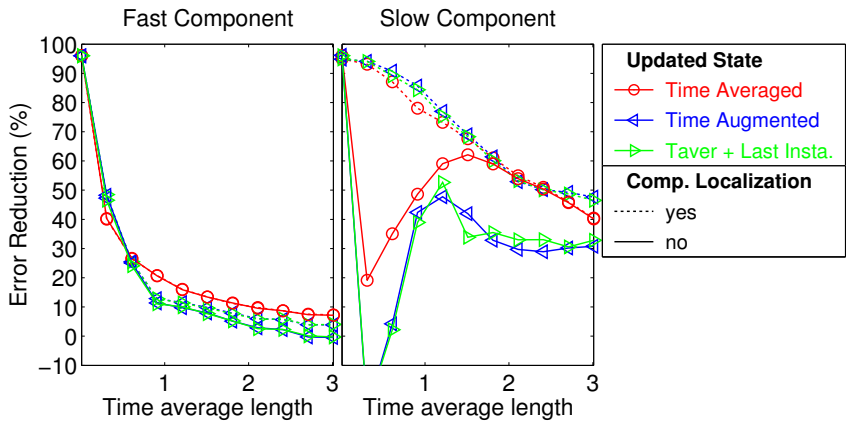

(a) Instantaneous Analysis quantities

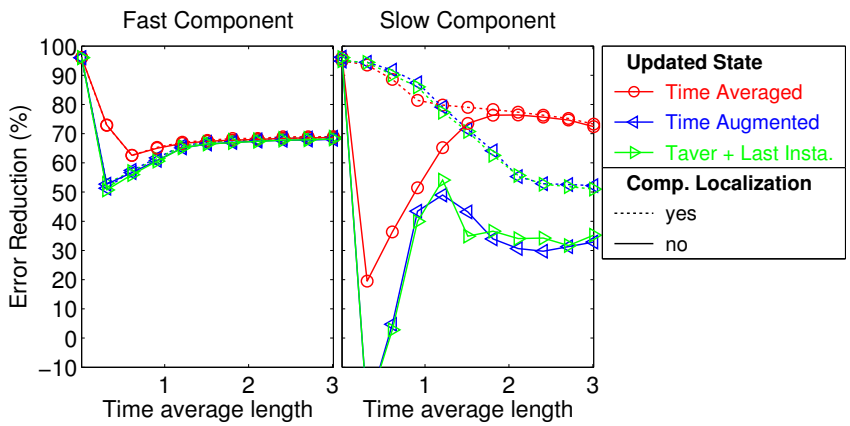

(b) Time-Averaged Analysis quantities

FIGURE 3.2: Analysis error reduction vs averaging period τ_{aver} for the uncoupled setting.

3.2.1.4 Comparison between update strategies

An interesting feature of figures 3.2(a) and 3.2(b) is the remarkable similarity of the error levels between Time-Augmented Update (TAug-Up) an Time-Averaged + Instantaneous Update (TAI-Up) approaches. Given this strong resemblance, only TAug-Up will be mentioned in the following comparison.

Instantaneous quantities In the presence of component localization, all update approaches exhibit similar performance, with a subtle supremacy of TAug-Up for short averaging periods and of TA-Up for long ones. Once component localization is turned off, the

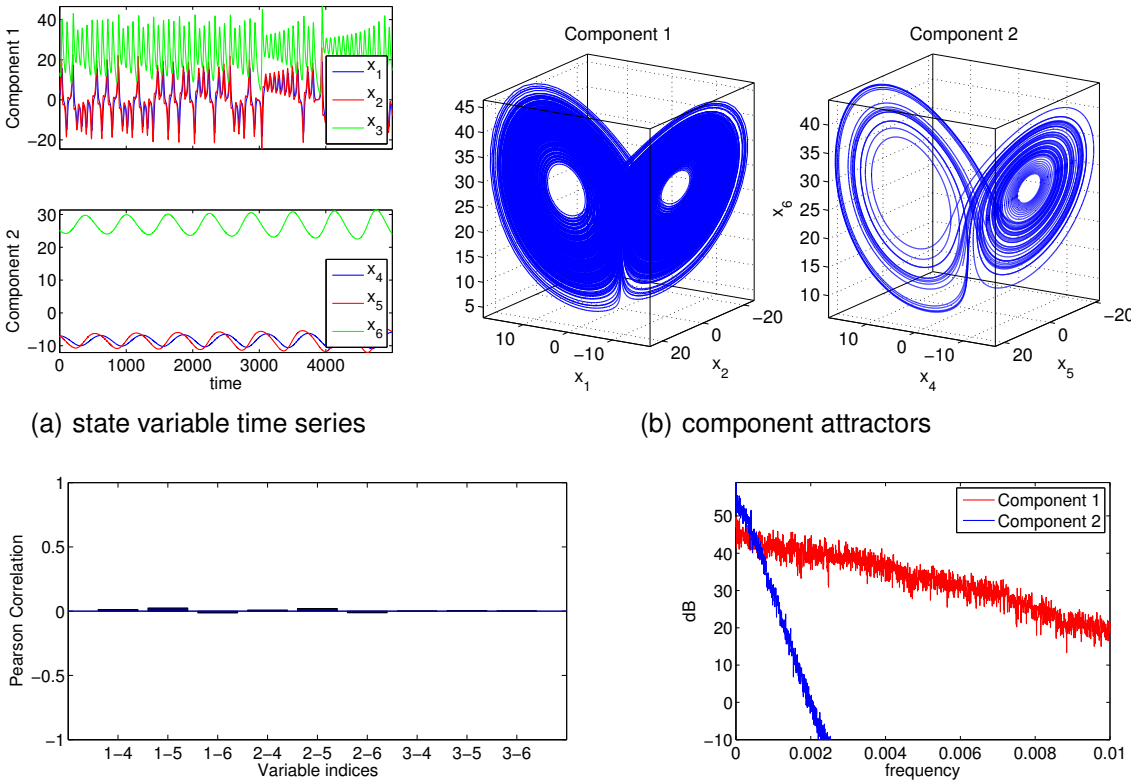

(a) state variable time series (b) component attractors

(c) inter-component variable correlations (d) power spectra

FIGURE 3.3: Some dynamical diagnostics for the uncoupled setting

error reduction levels for the fast component are only slightly modified, whereas for the slow component big changes take place: all the update strategies now become strongly affected by the above mentioned inter-scale contamination, with a clear edge of TA-Up over the other update techniques (see figure 3.2(a)).

Time-Averaged quantities Concerning TA assimilation skill, TA-Up is undoubtedly the dominant update approach. TAug-Up only shows a little advantage at τ_{aver} values around 1.0 for the slow component using component localization, while for larger τ_{aver} values the performance difference becomes striking, especially without component localization (see figure 3.2(b)).

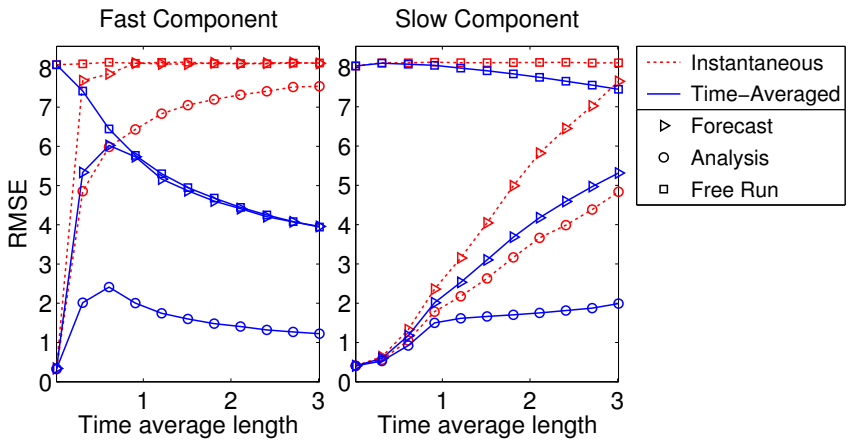

(a) with component localization.

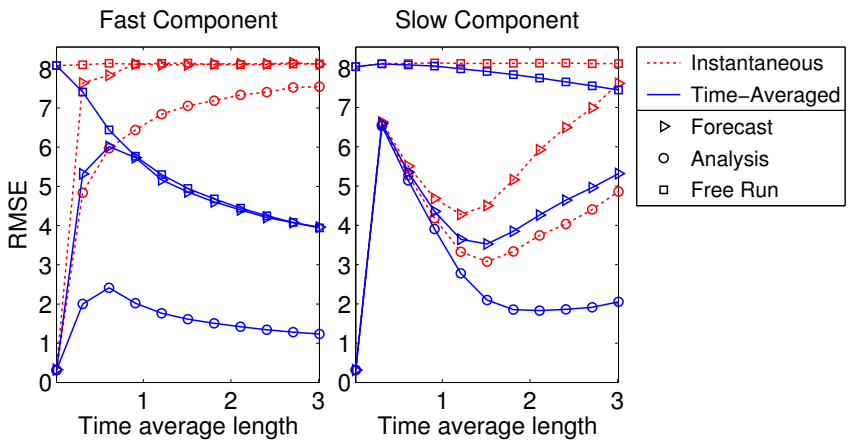

(b) without component localization.

FIGURE 3.4: Error levels vs averaging period τ_{aver} for the uncoupled setting using the Time-Averaged Update (TA-Up).

3.2.2 Weak coupling setting

3.2.2.1 Dynamics

An increasing the coupling constant from 0.0 to 0.1 barely affects the attractor structure as can be seen in figure 3.5(b). Nonetheless, the obtained weak interaction between components does lead to non-negligible inter-component correlations (see figure 3.5(c)) and enhancement of the low frequencies in the fast component spectrum (see figure 3.5(d).

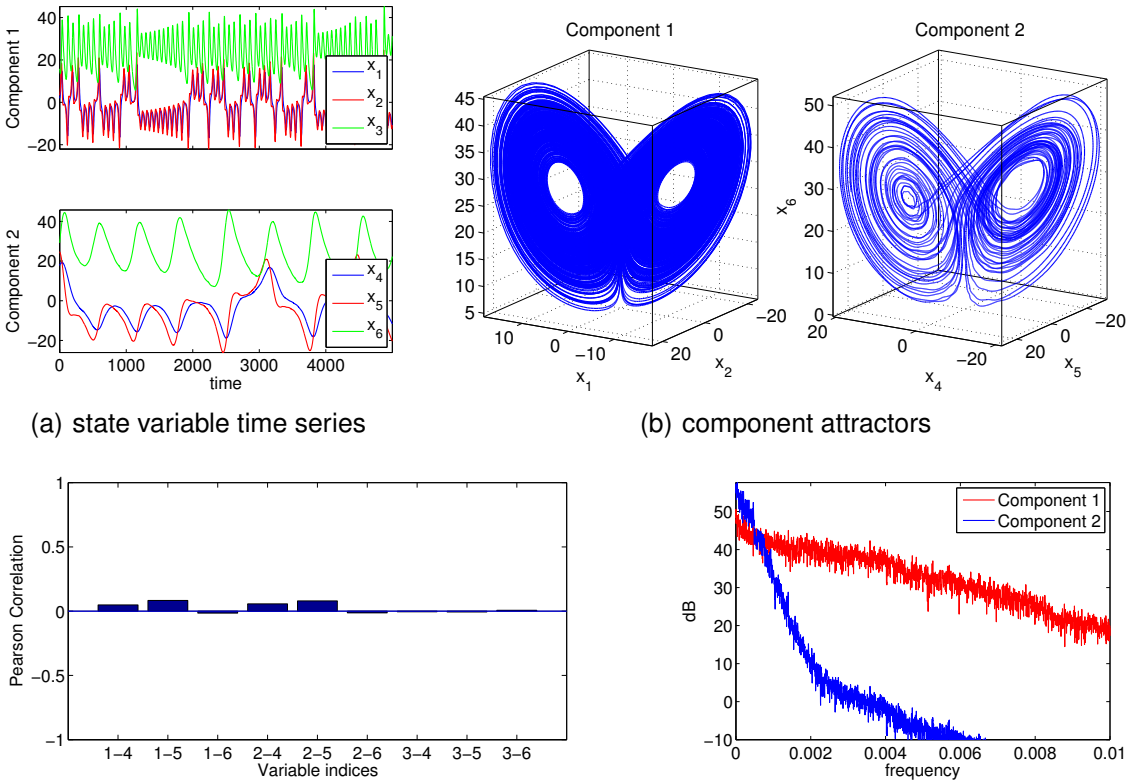

(a) state variable time series

(b) component attractors

(c) inter-component variable correlations

(d) power spectra

FIGURE 3.5: Some dynamical diagnostics for the weak coupling setting

3.2.2.2 DA skill dependence on averaging length

For our weakly coupled setting, the picture regarding analysis error levels remains considerably similar to the no coupling case (see figures 3.6(a) and 3.6(b)).

Short averaging regime The effect of the inter-scale contamination becomes smaller. This is consistent with the fact that for this configuration the components of the system do covary, although weakly, and therefore the inter-scale correlations detected by the filter are not completely spurious.

Long averaging regime The performance differences between the studied updating approaches are now considerably smaller. Regarding instantaneous quantities, TA-Up

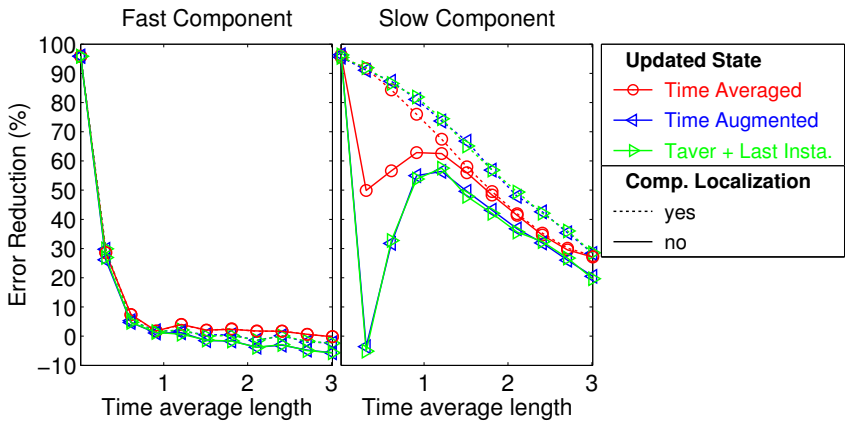

(a) Instantaneous analysis quantities

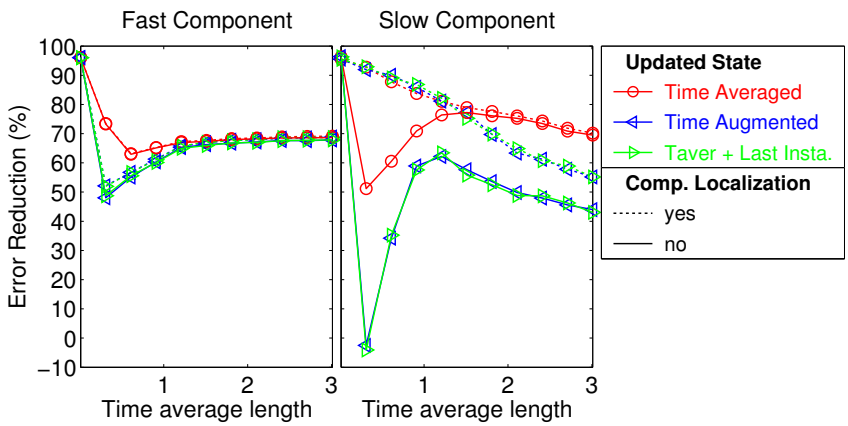

(b) Time-Averaged analysis quantities

FIGURE 3.6: Error reduction vs averaging period τ_{aver} for the weak coupling setting

is now outperformed by the other update strategies when component localization is employed.

3.2.3 Strong coupling setting

3.2.3.1 Dynamics

For coupling parameters in the range $0.22 \lesssim c \lesssim 0.55$, the components of the PK2004 model become strongly coupled. Accordingly the inter-component variable correlations come to be very significant and the spectra exhibit several dominant common frequencies

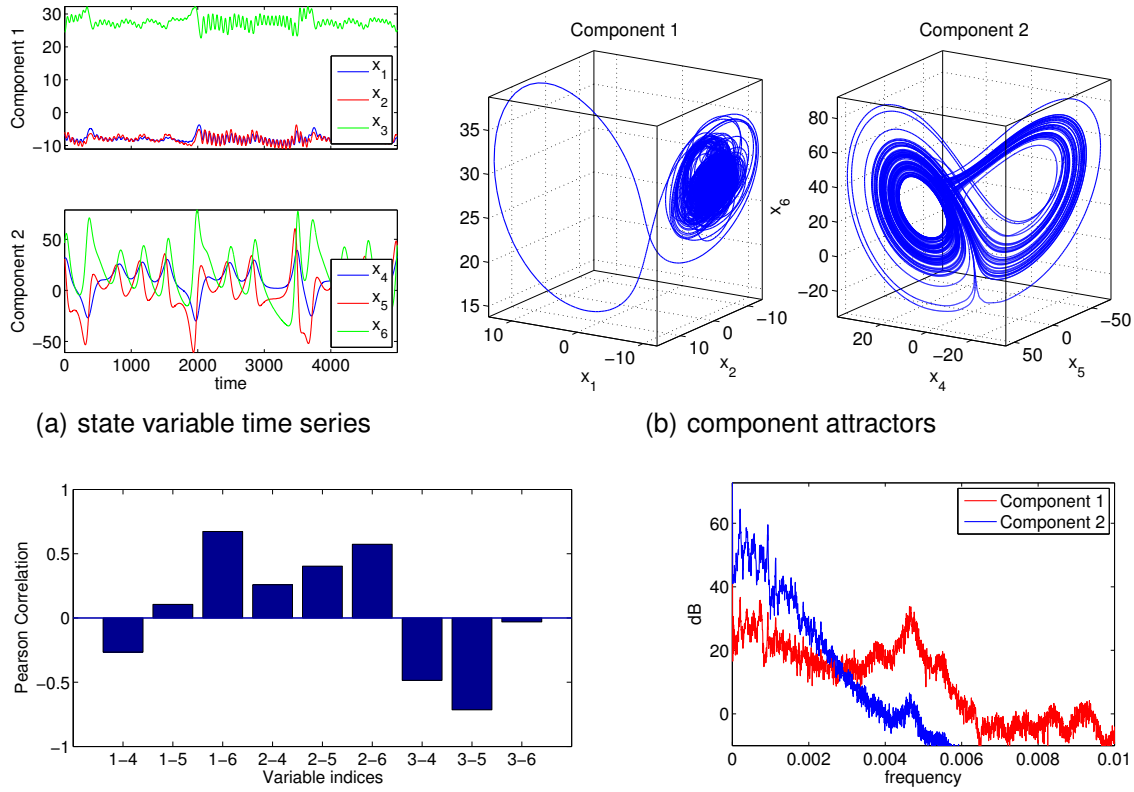

(a) state variable time series

(b) component attractors

(c) inter-component variable correlations

(d) power spectra

FIGURE 3.7: Some dynamical diagnostics for the strong coupling setting

(see figures 3.7(c) and 3.7(d)). In these conditions, the butterfly-like structure is still roughly preserved, however the dynamics in the fast attractor is now strongly asymmetric with one the lobes being much more visited than the other (see figure 3.7(a)).

3.2.3.2 DA skill dependence on averaging length

Short averaging regime Figures 3.8(a) and 3.8(b) show how by increasing the averaging length from $\tau_{\text{aver}} = 0$, TA-Up presents a sudden important drop in the error reduction, as opposed to TAug-Up whose error reduction decreases gradually. Analyzing in more detail the range of small τ_{aver} values (see figures 3.9(a) and 3.9(b)) it can be seen that TA-Up remains stable for very small τ_{aver} values ($0 \lesssim \tau_{\text{aver}} \lesssim 0.2$) and the onset of the above mentioned instability takes place at around $\tau_{\text{aver}} \approx 0.3$. Notice that component

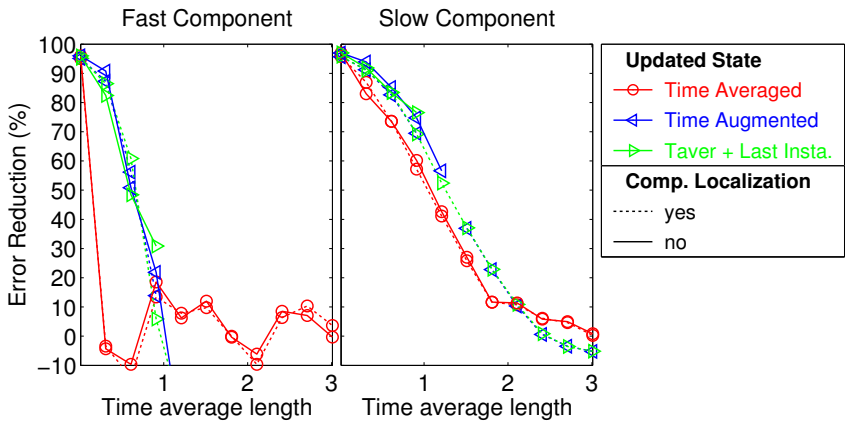

(a) Instantaneous analysis quantities

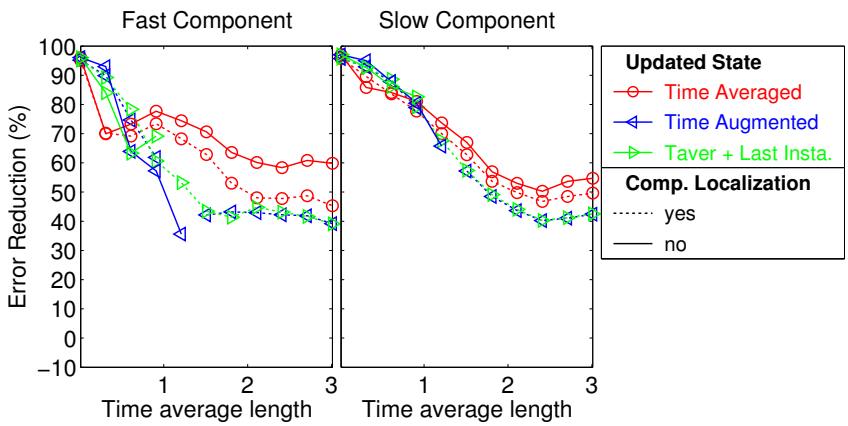

(b) Time-Averaged analysis quantities

FIGURE 3.8: Error reduction vs averaging period τ_{aver} for the strong coupling setting.

localization significantly alleviates TA-Up's skill loss for the slow component, while for the fast component the effect is hardly noticeable.

Long averaging regime The TA-Up strategy becomes again the dominant one, whith error reduction levels not significantly changed by the introduction of component localization. Au contraire, the TAug-Up and TAI-Up strategies becomes fairly unstable in the absence of component localization, exhibiting catastrophic filter divergence for $\tau_{\text{aver}} \gtrsim 1.0$. In presence of component localization, these two update approaches get stabilized, showing error reduction levels slightly smaller than the ones offered by TA-Up.

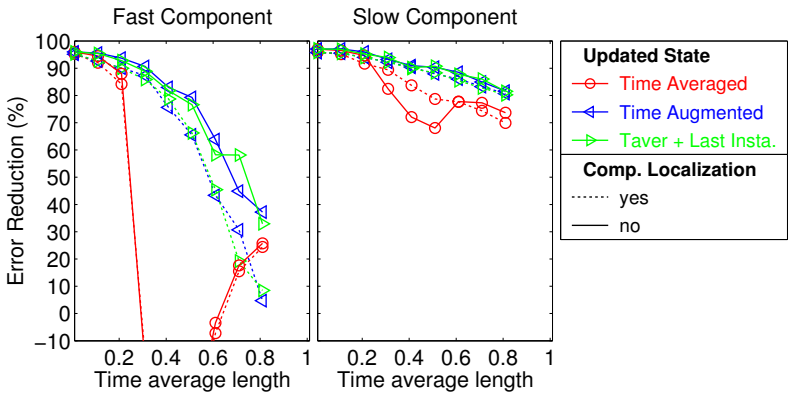

(a) Instantaneous analysis quantities

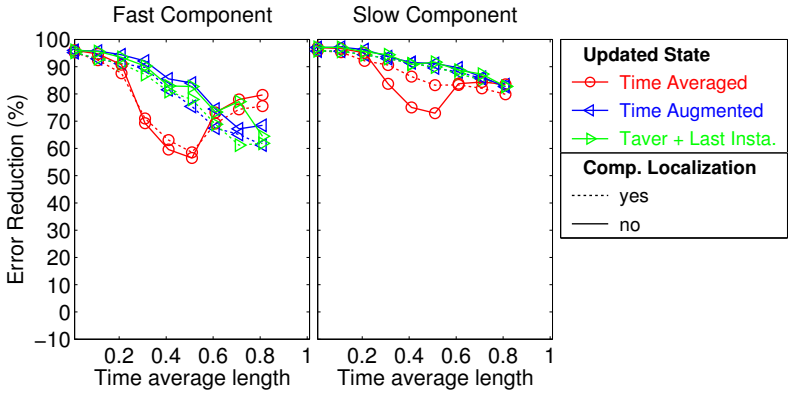

(b) Time-Averaged analysis quantities

FIGURE 3.9: Zoom of figure 3.8 for the short averaging regime.

3.3 Discussion and Outlook

3.3.1 TA updating strategies

Our EnKF experiments using the PK2004 model indicate that the currently used EnKF algorithms for Time-Averaged state estimation, i.e., TA [Dirren and Hakim, 2005] and Time-Augmented (TAUG) [Huntley and Hakim, 2010] algorithms, might exhibit significantly different performances when TA linear observations from a strongly coupled, multi-scale dynamical system are assimilated.

In our DA experiments employing the PK2004 model, the operation of the different updating approaches is heavily determined by the strength of the coupling between the

model components. For null or weak inter-component coupling, the TA-Up update approach showed the best overall performance, especially in absence of component-wise covariance localization, being less liable to inter-scale contamination than the other update approaches. On the other hand, when the components of the PK2004 model are allowed to interact strongly the situation regarding updating approaches becomes more complicated and the length of the averaging period starts playing a key role:

Short averaging periods: For τ_{aver} values where the fast scales of the system are still predictable, TAug-Up shows a very stable operation, as opposed to TA-Up which present significantly higher error error levels both for instantaneous and TA quantities.

Long averaging periods: TA-Up significantly recovers and shows again a reliable performance. On the other, TAug-Up presents either lower error reduction levels when component localization is employed, or catastrophic filter divergence otherwise.

It is worth mentioning that regarding the estimation of instantaneous quantities, the TAug-Up strategy is fully equivalent to the standard EnKF algorithm, whose skill assimilating TA observations decreases gradually by increasing the averaging length. This fact explains the stability of TAug-Up for short averaging periods, where the fast scale is still predictable.

Contrarily, the TA-Up strategy estimates instantaneous quantities by means of sequence of operations (TA decomposition, update of the TA state and TA recomposition) that according to our numerical results not necessarily preserves the instantaneous analysis skill for small τ_{aver} values. On the other hand, the stability of TA-Up for long averaging periods can be accounted for considering that it directly updates the TA state, which appear to be the best strategy for long averaging periods where the TA observations are significantly decorrelated from the instantaneous state of the system. To the contrary, TAug-Up keeps updating instantaneous states based on strongly decorrelated TA observations. Accordingly it generates instantaneous analysis states which can be far away from the attractor of the dynamical system and then the filter becomes prone to catastrophic divergence.

As mentioned in section 2.2.1, the only previous comparison of TA-Up and TAug-Up presented highly similar performance for a quasi-geostrophic atmospheric model [Huntley and Hakim, 2010] and since then TA-Up has been favored [Pendergrass et al., 2012; Steiger et al., 2014] due to its much lower computational cost. Accordingly, our results increase the knowledge on the EnKF-based estimation of TA states and call for caution at the moment of selecting the filtering approach to assimilate TA observations into a multi-component climate model.

Regarding more realistic paleo-DA experiments, we consider that given the the wealth of dynamical time scales present in the climate system and the broad range of time resolutions provided by proxy records, favorable conditions for both updating strategies will probably appear in the future. Consider for example El Niño Southern Oscillation (ENSO), which originates from the strong ocean-atmosphere coupling taking place in the tropics. In this geographical area one of the most important sources of paleoclimate information are coral records, which have a very stable yearly resolution. Given that the average period of ENSO is around 4 years MacMynowski and Tziperman [2008], the one year averaging period of coral records is well below ENSO's typical time scales and then TAug-Up might be the best choice. On the other hand, the typical decadal time resolution of ice cores is considerably longer than the time scales of most atmospheric-related processes and consequently the TA-Up strategy may prevail in this conditions.

3.3.2 Component-wise covariance localization

The localization of observations within their corresponding model components appeared to be a very effective measure against the inter-scale contamination. In the weak coupling regime, the inter-scale correlations observed by the EnKF are mostly spurious and accordingly the inter-scale contamination becomes strong. In these conditions the performance of filter can be greatly improved by component localization. On the other hand, under strong coupling conditions, inter-scale correlations are no longer dominantly artificial and then the effect of component localization is less evident. Still, it appears very

effective at preventing catastrophic filter divergence for the TAug-Up and TAI-Up updating approaches.

Regarding real-world applications, it is worthwhile to mention that proxy systems can be simultaneously driven by several components of the climate system. A clear example of this are trees, whose growth is strongly influence by atmospheric and soil conditions. In this circumstances, the assignment of the proxy record to one climate system component is not possible and then the component-wise localization is not adequate.

3.3.3 Hybrid updating strategy

All along our numerical exploration, the performance of the proposed hybrid updating algorithm (TAI-Up) was practically equivalent to the one of the TAug-Up algorithm. Consequently, as hypothesized in the previous chapter, our proposed hybrid updating algorithm successfully estimates the TA state without updating all the instantaneous forecast states contributing to the observation, and preserves the skill of the TAI-Up strategy for short averaging periods. The main advantage of TAI-Up over TAug-Up is its much lower computational cost given that only two EnKF updates need to be performed. Likewise TA-Up, for TAI-Up it is still necessary to aggregate the instantaneous ensemble states during the forecast step so that the TA state can be calculated at the end of the observation interval. Nonetheless, this aggregation is considerably cheaper than the several instantaneous EnKF updates required by TAug-Up, particularly for long averaging intervals. Accordingly, TAI-Up appears as an efficient alternative updating approach, convenient for the aforementioned conditions where the TA-Up strategy becomes inadequate.

CHAPTER 4

Fuzzy Logic Approach to Tree-Ring Growth Forward Modeling

Tree-ring growth forward models have reached a rather mature state of development. In particular within climate applications, there exists a sufficiently realistic yet affordable process-based forward model for Tree-Ring-Width (TRW) chronologies called Vaganov-Shashkin-Lite (VSL) Tolwinski-Ward et al. [2011, 2013]. This chapter is devoted to the analysis and extension of VSL's modelling approach by means of Fuzzy Logic (FL) theory. Firstly, it is shown that VSL's formulation can be completely reinterpreted in FL terms, which exposes multiple representations of the Principle of Limiting Factors (PLF). Secondly, the sensitivity of VSL's to three possible FL-based modifications is studied for a global network of TRW chronologies. The conceptual implications of the FL reinterpretation are discussed at the end of the chapter.

4.1 Vaganov-Shashkin-Lite (VSL) Model

The VSL model for TRW chronologies offers an intermediate complexity approach between ecophysiological and completely data-driven models [Tolwinski-Ward et al., 2011; Tolwinski-Ward, 2012], where the climate-driven component of tree-ring growth is parametrized by way of a simple representation of the PLF [Fritts, 1976]. This biological concept states that the pace at which a plant develops is controlled by the single basic growth resource, typically either energy or water, that is in shortest supply. Within VSL, the limiting factors relevant for tree-ring growth are near-surface air temperature T and soil moisture M. Their impacts on tree development are accounted for via the "growth response" functions g_T and g_M. Making use of the piece-wise linear "standard ramp" function [Tolwinski-Ward et al., 2014]

$$\Psi(u) = \begin{cases} 0 & \text{if} \quad 0 \geqslant u \\ u & \text{if} \quad 0 < u \leqslant 1 \\ 1 & \text{if} \quad u > 1, \end{cases}$$

VSL's growth responses at a particular time can be expressed as:

$$g_T = \Psi\left(\frac{T - T^L}{T^U - T^L}\right) \tag{4.1}$$

and

$$g_M = \Psi\left(\frac{M - M^L}{M^U - M^L}\right). \tag{4.2}$$

Here T^L and M^L denote lower thresholds below which there is no growth and trees are said to be dormant, while T^U and M^U designate upper thresholds above which tree growth is optimal. Given a pair of g_T and g_M values, the corresponding growth rate G_{MIN} is determined by the smallest growth response, i.e.,

$$G_{\text{MIN}} = \min\{g_T, g_M\}, \tag{4.3}$$

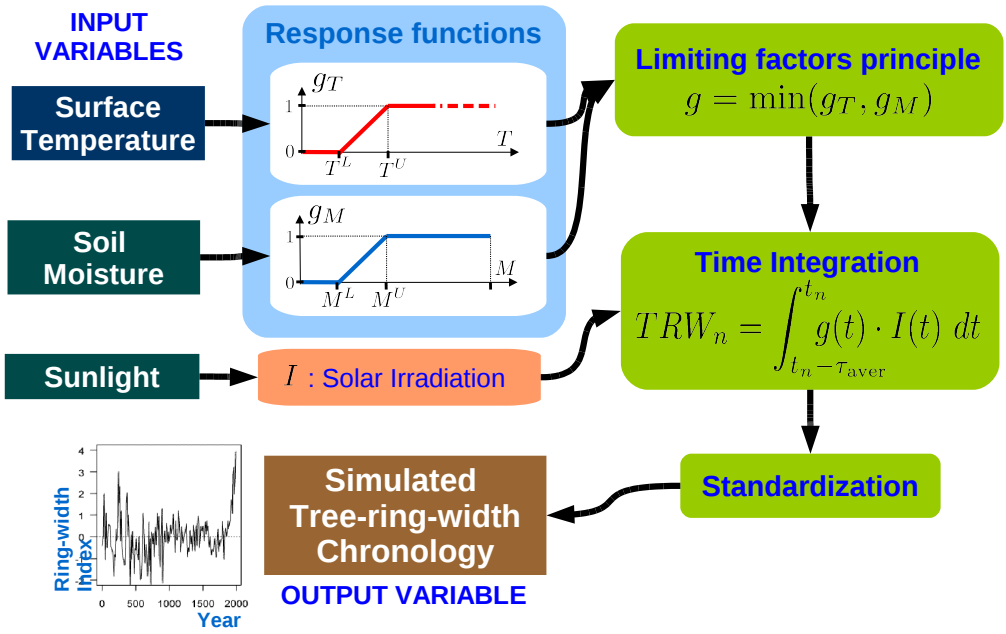

FIGURE 4.1: Schematic of VSL's formulation. Sharp (rounded) cornered boxes represent data (processes).

which defines a non-smooth surface in the $T - M$ plane, displaying 4 distinct growth regimes: (i) dormancy, (ii) optimal growth, (iii) temperature limited and (iv) moisture limited (see fig. 4.3(a)).

The TRW values W for each year are obtained via time integration of the growth rate function modulated by the relative local insolation I.

$$W_n = \int_{t_n-\tau}^{t_n} G_{\text{MIN}}(t) I(t)\, dt. \tag{4.4}$$

Finally, the obtained TRW series are standardized so as to allow for comparison against actual TRW chronologies, which are given as non-dimensional index series. The overall structure of VSL formulation can be visualized in figure 4.1.

It is important to notice that for climate forcing trajectories confined within either temperature- or moisture-limited zones (see figure 4.3(a)), VSL's formulation reduces to an univariate linear approach. In this case a single input variable is imprinted in the final TRW chronology, as opposed to the general case where tree growth is limited by T

and M in a fluctuating fashion resulting in a mixed chronology. This "response-switching" mechanism [Tolwinski-Ward et al., 2014] presents a challenge to inverse problem applications of VSL. As a matter of fact, in the context of simultaneous temperature-moisture reconstructions via Bayesian Hierarchical modeling, it has been linked to non-Gaussian, bimodal posterior probability densities [Tolwinski-Ward et al., 2014].

4.2 Basic Fuzzy Logic Concepts

FL mimics the kind of reasoning achieved by human language, and by doing so it provides a mathematical framework where definite conclusions can be drawn from imprecise data and vague knowledge of the underlying mechanisms. Accordingly, FL constitutes a powerful modeling approach in areas dealing with complex systems. As opposed to the classical Boolean logic, where a preposition can be either true or false, FL allows for partial truth values between 1 (completely true) and 0 (completely false), and then it provides a rigorous mathematical foundation for the implementation of approximate reasoning systems [Zadeh, 1975].

Since its introduction in the 1960s by Zadeh [1975], FL has greatly influenced many applied disciplines, most notably control theory Nguyen et al. [2002]. Within the environmental sciences, FL has also found numerous applications, including ecological and hydrological modeling Marchini [2011]; Salski [2006]; Se [2009]. Regarding climate proxy forward modeling, however, FL theory has not yet been explicitly employed. As we will show below, several of the tree growth modeling concepts have direct "fuzzy" analogues and in particular, VSL model can be completely reinterpreted in terms of FL.

Assuming U as the set of all elements or conditions considered in a particular application, e.g., all the climate conditions a tree can be subjected to, a classical set A in U can be defined by a membership function μ_A that assigns to each element of U a number from the set $\{0, 1\}$. Here 0 (1) represents non-membership (membership) to the set A. This definition can be rephrased in classical logic terms by interpreting the value $\mu_A(x)$ as the truth value of the preposition "x is in A", where x denotes a generic element of

U. Fuzzy set theory generalizes the classical one by extending the range of membership functions to the real interval $[0, 1]$. This modification allows the existence of elements with partial membership: $\{x : 0 < \mu_A(x) < 1\}$, for which the preposition "x is in A" is partially true [Zadeh, 1965].

Fuzzy membership functions can adopt very different shapes depending on the particular application. Piecewise-linear forms – such as ramps, triangles and trapezoids – are frequently used because of their simplicity in terms of implementation and interpretation. On the other hand, when smoothness is a concern, membership functions with continuous derivative are preferred, e.g., Gaussian and sigmoidal functions.

Given two fuzzy sets A and B, the intersection set $A \wedge B$ (or equivalently the truth value of the composed statement "x is in A" AND "x is in B") can be found by the following expression:

$$\mu_{A \wedge B} = T(\mu_A, \mu_A) \tag{4.5}$$

where T is a function, technically referred to as Triangular Norm (t-norm) [Nguyen et al., 2002], satisfying the following requirements:

$$\begin{aligned}
&\text{Commutativity: } T(a, b) = T(b, a), \\
&\text{Associativity: } T(a, T(b, c)) = T(T(a, b), c), \\
&\text{Monotonicity: } T(a, b) \leq T(c, d) \text{ if } a \leq c \text{ and } b \leq d, \\
&\text{Number } 1 \text{ is an identity element} : T(a, 1) = a,
\end{aligned} \tag{4.6}$$

which determine the admissible representations of the fuzzy intersection or equivalently the fuzzy AND operation.

T-norms constitute a rather ample class of functions, from which the first and most popular example is the minimum function, also called Gödel t-norm [Zadeh, 1965]. Abundant types of t-norms have been studied [Nguyen et al., 2002] and, similar to membership functions, the selection of the particular t-norm depends heavily on the problem considered.

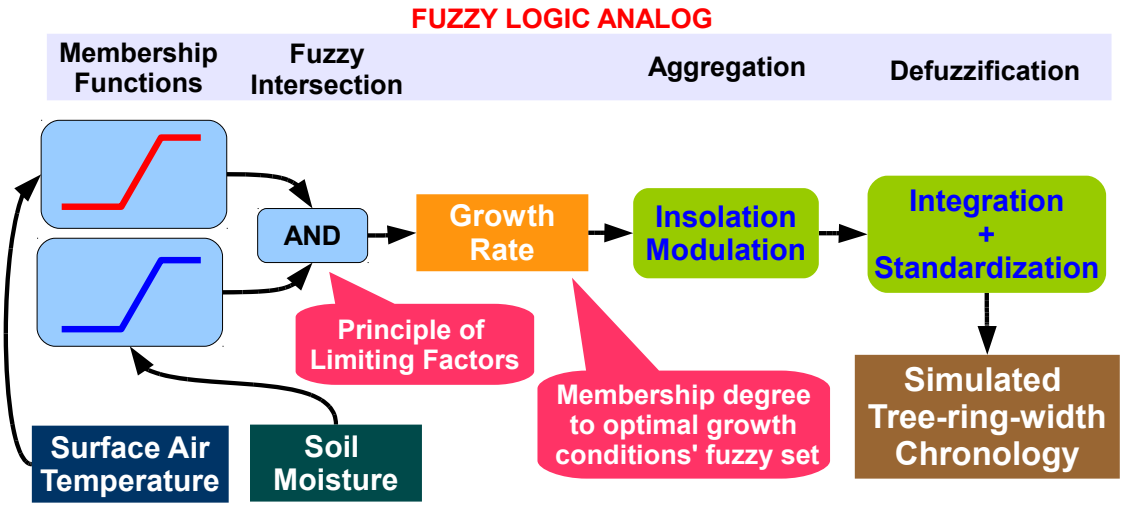

FIGURE 4.2: Schematic of VSL's fuzzy logic reinterpretation. Sharp (rounded) cornered boxes represent data (processes).

4.3 VSL Model from the Fuzzy Logic Perspective

Bearing in mind the concepts introduced in section 4.2, VSL's growth response g_T (g_M) can be understood as a membership function defining the fuzzy set S_T (S_M) of climate states whose temperature (moisture) values are optimal for tree growth. Furthermore, the minimum function used to obtain the growth rate can be regarded as a t-norm that determines the fuzzy intersection set $S_{T \wedge M}$ in the $T - M$ plane. Analogously, the growth rate can be interpreted as the degree of truth of the statement "temperature AND moisture values are optimal for tree growth".

Therefore, we claim that VSL 's formulation of the PLF – which is inherited from the full Vaganov-Shashkin (VS) model [Vaganov et al., 2006] – essentially determines the fuzzy set of temperature-moisture conditions that are optimal for tree growth. The final two steps of VSL's TRW calculation, insolation modulation and time integration, can also be translated to fuzzy terms as examples of aggregation and defuzzification methods (see figure 4.2). Furthermore, the whole mathematical formulation of VSL can be viewed as a zero-order Sugeno-type fuzzy inference system [Sugeno, 1985] with $2m$ arguments , i.e.,

monthly temperature and moisture values for m months, and one output, i.e., TRW (see Nguyen et al. [2002] for details).

An important consequence of representing the fuzzy intersection via the minimum t-norm is that the growth rate at an specific time is only determined by the most limiting factor. This fact implies that the growth limitation is exclusive and that the transitions between growth-limited regimes necessarily take place in a sharp manner. Notice that this abrupt response-switching mechanism might be problematic for the application of VSL model as observation operator within a Data Assimilation (DA) setting, given that completely smooth growth responses would typically lead to non-smooth growth rate functions. Consequently, we make use of the freedom we have to select the fuzzy intersection representation and study three alternative t-norms (see figure 4.3): (i) the algebraic product:

$$G_{\text{PROD}} = g_T \cdot g_M, \tag{4.7}$$

(ii) Yager t-norm of second order:

$$G_{\text{YAG}} = \max\{0, ((1 - g_T)^2 + (1 - g_M)^2)^{1/2}\}, \tag{4.8}$$

and (iii) Lukasiewicz t-norm:

$$G_{\text{LUK}} = \max\{0, g_T + g_M - 1\}. \tag{4.9}$$

All of these new representations of the PLF exhibit an additional regime where T and M concurrently limit tree-ring growth (see zones (v) in figure 4.3), which allows a gradual transition between temperature- and moisture-limited modes and thus a progressive alternation of the recorded variable. In the case of G_{YAG} this transition is perfectly smooth while for G_{PROD} there are still two subtle edges in the growth rate surface (see figure 4.3(b)). Nonetheless, the product t-norm offers high stability to input variable errors and membership function selection, given that it exhibits the smallest average sensitivity among all t-norms [Nguyen et al., 2002]. Finally, for the Lukasiewicz t-norm, the temperature-moisture limited growth area presents a perfectly linear dependence, unfortunately at the expense of increasing the sharpness of the above mentioned edges.

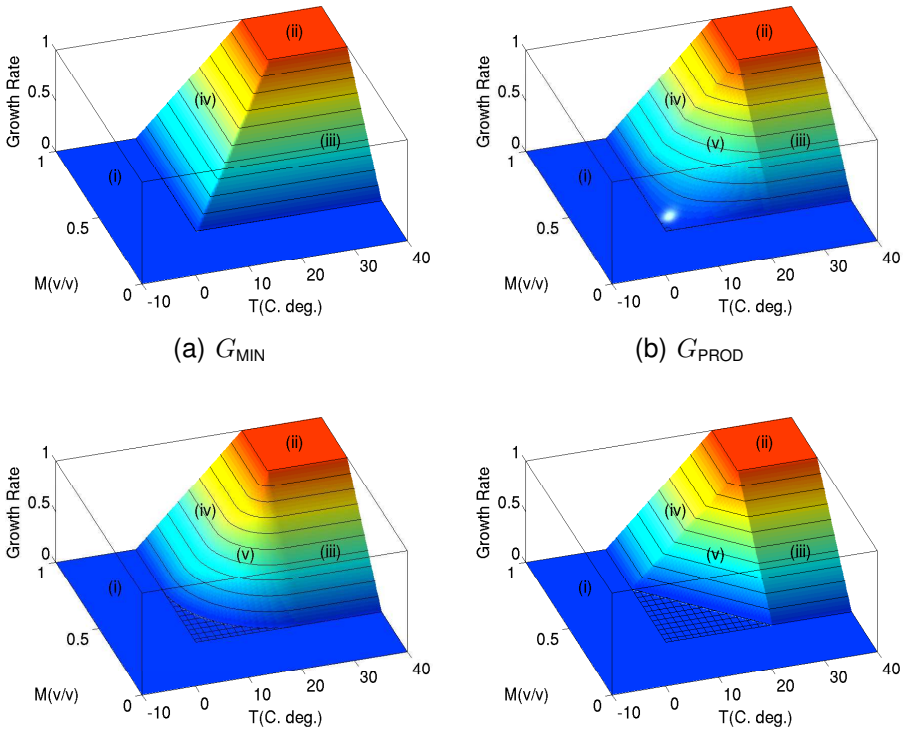

(a) G_{MIN} (b) G_{PROD}

(c) G_{YAG} (d) G_{LUK}

FIGURE 4.3: Growth rate surfaces for different representations of the fuzzy intersection operation. (a) minimum, (b) product, (c) Yager and (d) Lukasiewicz t-norms. Growth regimes: (i) dormancy, (ii) optimal, (iii) moisture limited, (iv) temperature limited and (v) temperature-moisture limited. Crossed hatched areas correspond to additional dormancy conditions introduced by the t-norm used. (Threshold values: $T_1 = 5$ C.deg, $T_2 = 25$ C.deg, $M_1 = 0.3$ v/v and $M_2 = 0.70$ v/v).

One important feature of the growth rate surfaces obtained using Yager and Lukasiewicz t-norms is the appearance of new points in the $T - M$ plane leading to null growth rates, regardless none of their corresponding growth responses is null (see figures 4.3(c) and 4.3(d)). This new dormancy area is due to the presence of the maximum function in equations 4.8 and 4.9.

4.4 VSL's Sensitivity to the Representation of the Principle of Limiting Factors

4.4.1 Climate and Tree-Ring-Width (TRW) data

In order to test the robustness of VSL's performance to the use of a particular PLF representation, we perform a validation study using the global TRW network recently compiled by Breitenmoser et al. [2014]. This dataset comprises 2918 chronologies from 163 different tree species, which are freely available at the International Tree Ring Data Bank (ITRDB, http://www.ncdc.noaa.gov/paleo/treering.html). These chronologies were gathered in raw format (individual ring width series from each tree of the chronology), corrected for data and metadata errors, and systematically processed with standard dendroclimatological methods using the the program ARSTAN [Cook, 1985] (see [Breitenmoser et al., 2014] for more details of the chronology development methodology). Finally, for our sensitivity study we selected from the whole network the series that completely covered the period $1901 - 1970$, which yielded a subset with 2415 chronologies.

As for the climate data, monthly time series of surface temperature and precipitation were extracted from the Climatic Research Unit Time Series (CRU-TS) product version 3.21, generated by University of East Anglia [Harris et al., 2014]. This dataset provides high-resolution gridded fields ($0.5° \times 0.5°$) of many climatic variables for the period Jan. 1901 - Dec. 2012, based on more than 4000 weather stations distributed around the world. In order not to interfere with the gridding algorithm of the dataset, we refrain from interpolating and utilize the times series corresponding to the nearest grid point to the chronology site as forcing data for VSL.

4.4.2 Modeling setting

We utilize the version 2.3 of VSL model, which is freely available at the USA's National Oceanic and Atmospheric Administration (NOAA) Paleoclimatology software library. This matlab software provides implementations of the forward model itself, a hydrological

model and a Bayesian tuning framework. For the present study we extend both the forward model and its tuning scheme so that the growth rate function can be calculated using any of the previously introduced t-norms, i.e., minimum, product, Yager and Lukasiewicz t-norms. The TRW forward models obtained in this fashion will be refer to as VSL-Min, VSL-Prod, VSL-Yager and VSL-Luka, respectively

4.4.2.1 Forward model

VSL v2.3 requires as input data the latitude of the studied site as well as monthly time series of local temperature and soil moisture. After calculating the response and growth rate functions, the obtained monthly growth rate time series is integrated over a moving window. Notice that this integration time window has previously set to a length of 16 months (starting in September of the previous year) in order to account for the autocorrelation observed in real TRW chronologies [Tolwinski-Ward et al., 2011; Breitenmoser et al., 2014; Acevedo et al., 2013]. Accordingly, for the sake of comparability, we use the same integration period in the present study.

4.4.2.2 Hydrological model

Given the very limited availability of soil moisture data in historical observational records, VSL's code provides also an implementation of the USA's Climate Prediction Center Leaky Bucket Model (CPC-LBM) [Huang et al., 1996]. This hydrological model simulates the water balance cycle considering most of the relevant water exchange processes (precipitation, evapo-transpiration, surface and subsurface runoff, and groundwater loss) and provides soil moisture monthly time series out of latitude data, and monthly time series of temperature and precipitation.

4.4.2.3 Model calibration

VSL v2.3 code allows to estimate probabilistically the model parameters, i.e., temperature and moisture response thresholds, by means of a Markov Chain Monte Carlo (MCMC)

strategy [Tolwinski-Ward et al., 2013]. Within this Bayesian tuning framework –given climate and TRW data, as well as a literature-informed prior Probability Density Function (PDF) of the parameters– the posterior PDF of the parameters is inferred by way of a set of random walkers, known as chains, which sample the parameter space and whose distribution converges to the sought posterior PDF.

For the present sensitivity study, the modeling time period is splited randomly into two disjunct equally-sized sequences of years to be used to calibrate and validation, respectively. For the calibration period, VSL's parameters are tuned using the setting described by Tolwinski-Ward et al. [2013], which consist of three chains ran during 30000 iterations after a spin-up period of 300 iterations. Subsequently, the obtained sample sequences are sub-sampled every 50th value so as to remove the autocorrelation of the chains, yielding a collection of 1800 approximately independent samples. Finally, the optimal parameter values and their uncertaities are estimated from the medians and the interquartile ranges of the smaple collections

The performance of the model is assessed by means of the Pearson correlation between actual and simulated chronologies, denoted by the letter ρ, and the corresponding statistical significance $s = 100\%(1 - P_{\text{VALUE}})$. Notice that due to the significant autocorrelation of TRW chronologies, every P_{VALUE} is corrected for the effective number of degrees of freedom.

4.4.3 Results

Figures 4.4 and 4.5 illustrate the quantities involved in VSL's modeling process for two different chronologies. For the first TRW record, VSL presents the best performance over the whole network, characterized by ρ values around 0.9 both for the calibration and validation periods. Growth limitation appears to be dominated by moisture from April to November, and by temperature during the rest of the year. Notice that the lower threshold both for temperature and moisture were hardly altered by the tuning procedure whereas the upper threshold did experience strong changes (see figure 4.4). On the other hand, for the second chronology VSL's performance is much more modest, with rather low ρ

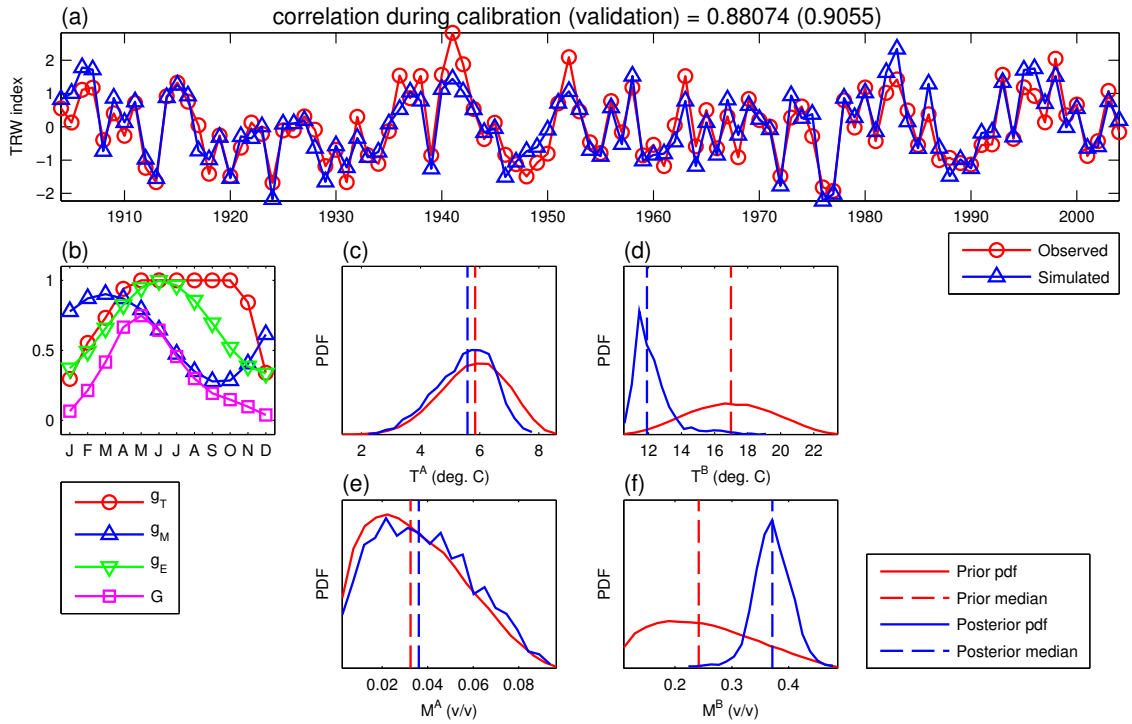

FIGURE 4.4: VSL-Min modeling output for a blue oak TRW chronology. (Location= Mt. Diablo state Park, lon.= $-121.9500°$, lat.= $37.8667°$, alt.= 245 m.). Actual and simulated chronologies (a), multi-year monthly means of growth response and growth rate (b), and parameter PDFs (c-f).

values around 0.2. tree growth is limited in this case only by temperature during the whole year and only parameter modified by the tuning scheme was the upper moisture threshold (see figure 4.5).

Regarding global performance, VSL is considerably skillful in most of the globe (as previously observed by Breitenmoser et al. [2014]), presenting areas of high model-data agreement in USA, central Europe, Scandinavia and eastern/central Siberia (see figure 4.6(a)). There are, nonetheless, problematic areas where the correlations between real and modeled chronologies can be near to zero or even negative, as is the case of New Zealand, Tasmania, Alaska, North West/South East band going from central Canada to North East USA, and southern Europe.

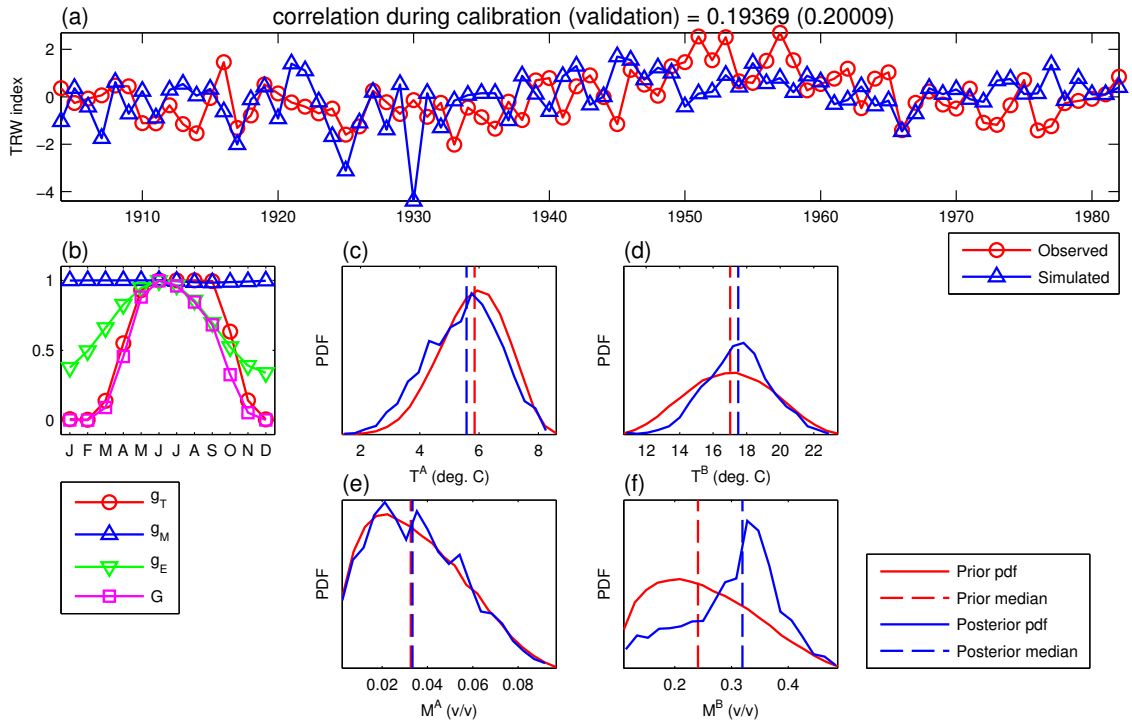

FIGURE 4.5: VSL-Min modelling output for a chestnut oak TRW chronology. (Location= Blue Ridge Parkway, lon.= $-79.4500°$, lat.=$37.5500°$, alt.= 1000 m.). Actual and simulated chronologies (a), multi-year monthly means of growth response and growth rate (b), and parameter PDFs (c-f).

Figure 4.6(b) shows that for all the t-norm studied, ρ values were very similarly distributed. VSL-Min and VSL-Prod presented almost equivalent network histogram median values around 0.23. This constitutes a subtle improvement over VSL-Yager and VSL-Luka, which behaved very similarly with median values around 0.21. Regarding the statistical significance of real-modeled chronology inter-correlations, the performance difference between t-norms is more noticeable with VSL-Prod exhibiting the highest significance median, being followed first by VSL-Min and then by the other two models

Finally, concerning the behavior of the tuning framework at global scale, figure 4.7(a) shows that the use of the four studied t-norms to represent the PLF does not change greatly the network histogram of optimal parameter values. Notice that the only big differences in the network histogram medians took place with VSL model with PLF represented by the Yager t-norm (VSL-Yager) and VSL model with PLF represented by the Lukasiewcz

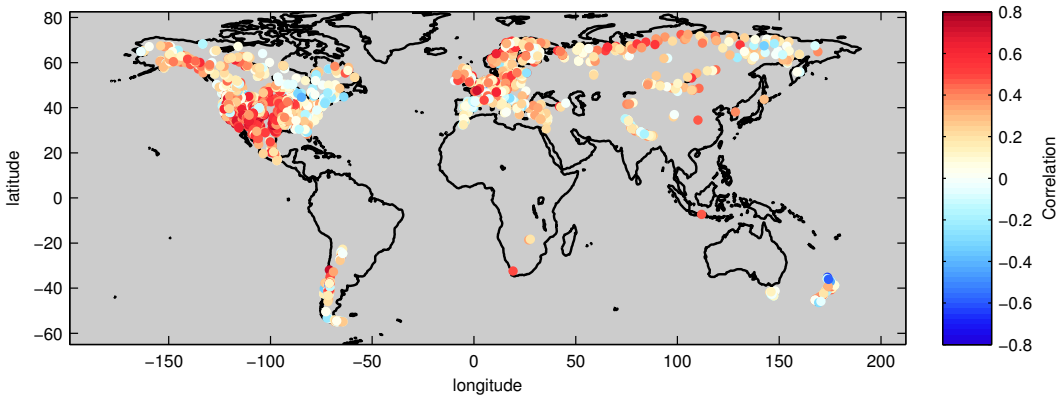

(a) World map of correlations between actual and simulated chronologies for VSL-Min

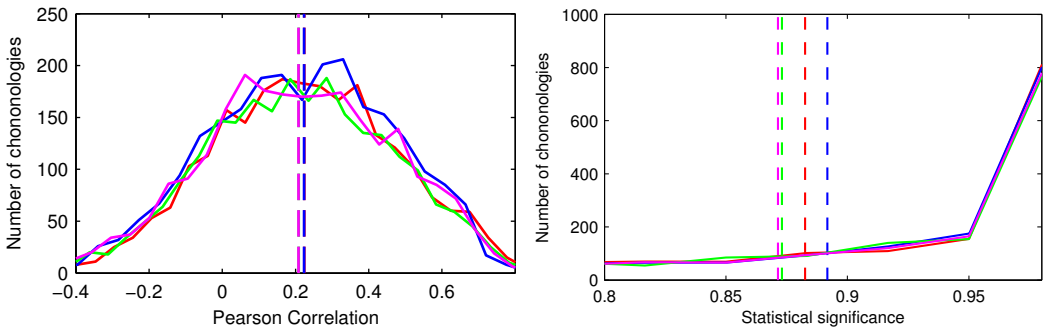

(b) Histograms of correlations and their significances , between actual and simulated chronologies. T-norms studied: Minimum (red), product (blue), Yager (green) and Lukasiewicz (purple). Solid (dashed) lines represent histograms (median values).

FIGURE 4.6: VSL's performance statistics over the chronology network during the validation period.

t-norm (VSL-Luka) for the lower and upper moisture thresholds, respectively. As for the parameter uncertainties, figure 4.7(b) reveals that the lower moisture threshold is the only parameter significantly sensitive to the the PLF representation.

4.5 Discussion and Outlook

The validation studies described in this chapter reveal that at global scale VSL model is remarkably insensitive, both in terms of model-data agreement and parameter optimization, to the particular representation of the PLF by means of different t-norms. This fact supports our hypothesis that VSL's formulation can be embedded into the FL framework

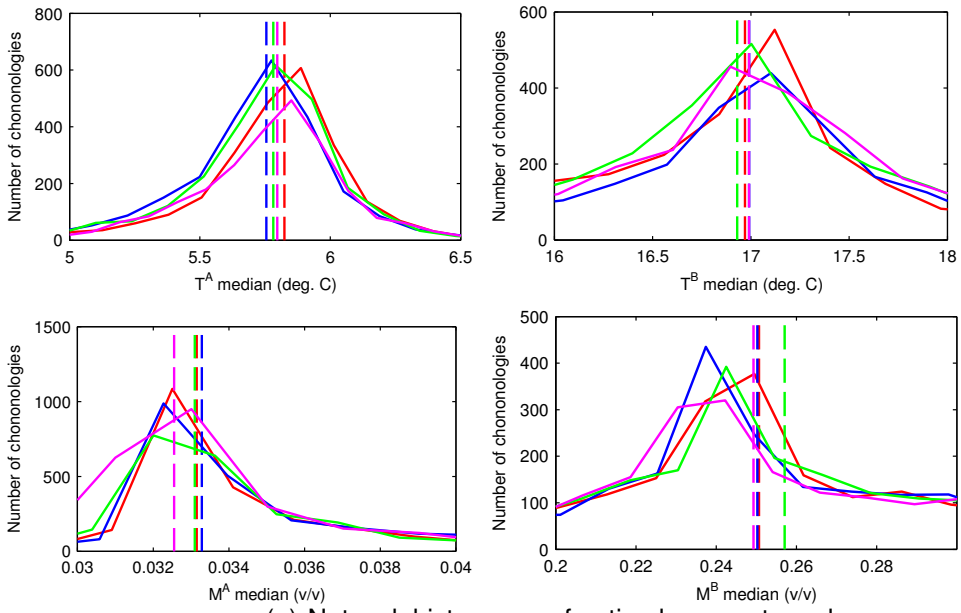

(a) Network histograms of optimal parameter values

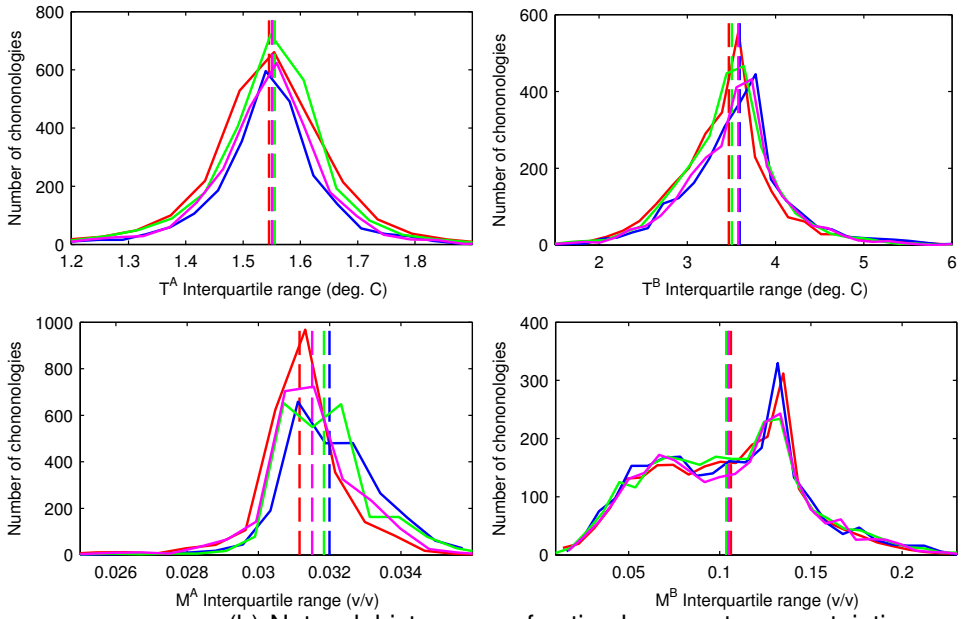

(b) Network histograms of optimal parameter uncertainties

FIGURE 4.7: Network statistics of posterior parameter PDFs. t-norms studied: Minimum (red), product (blue), Yager (green) and Lukasiewicz (purple). Solid (dashed) lines represent histograms (median values).

and that the traditional mathematical formulation of the PLF corresponds to a particular representation of a fuzzy AND operation.

An important conceptual implication of this viewpoint shift is that the exclusory character of growth limitation, implied by the minimum function, becomes an unnecessary feature of a tree growth model. From the FL perspective, the real essence of the PLF is then that tree growth takes place only when all limiting factors are simultaneously favorable, which naturally defines a fuzzy AND operation. Accordingly, we claim that the abrupt shifting of growth limitation regime is not a necessary component of the PLF but rather a consequence of the specific formulation of VSL. Notice that this new interpretation of tree growth limitation provides freedom to select the representation depending on the application at hand and accommodates the possibility of several factors concurrently regulating tree development, which is currently refer to as co-limitation. This growth limitation regime was initially recognized by Singh and Lal [1935], who called attention to the limitations of the original formulation of the PLF due to Blackman [1905]. Within the ecological research community, co-limitation has been widely acknowledged as an crucial resource limitation phenomenon [Harpole et al., 2011], with abundant observational support both in terrestrial [Niinemets and Kull, 2005] and aquatic [Saito et al., 2008] environments. Interestingly, within the vegetation modeling community the original PLF formulation is still the predominant approach to model photosynthesis [Yin and Struik, 2009].

The translation of VSL into the FL language suggest other possible extensions for VSL. (i) growth response functions can be generalized using the extensive knowledge on membership functions gathered in the FL research community [Nguyen et al., 2002]. In particular, it might be possible to tailor the shape of the growth response functions so as to optimize the performance of VSL regarding the particular application at hand, (ii) additional limiting factors, e.g., CO^2 concentration, can in principle be incorporated by adding to the fuzzy inference system new rules designed to mathematically express the expert knowledge about the influence of these factors on tree growth. (iii) the intrinsic uncertainty on the VSL parameters might be taken into account for the first time making use of the emerging theory of stochastic FL [Luhandjula and Gupta, 1996]. Furthermore, this ability of the FL approach to efficiently simulate complex processes involving vaguely

understood mechanisms can be used in the development of new proxies forward models, as well as the extension of the existing ones, following the rationale of our proposed modifications to VSL (see Reviewer 1 comments in appendix B).

Finally, regarding the application of VSL as a observation operator within a DA setting, we will show in the next two chapters how co-limitation-permitting representations of the PLF, particularly the product t-norm, can be more compatible with an Ensemble Kalman Filter (EnKF) approach that the minimum t-norm. Given the essentially equivalent forward modeling skill observed in our sensitivity study, these alternative t-norms appear as promising options within a EnKF-based paleo-reanalysis scheme.

CHAPTER 5

Assimilation of Pseudo-Tree-Ring-Width Observations into a 2-Scale Nonlinear Model

This chapter investigates the applicability of the Vaganov-Shashkin-Lite (VSL) forward model for Tree-Ring-Width (TRW) chronologies as observation operator within a proxy Data Assimilation (DA) setting. Based on the Principle of Limiting Factors (PLF), VSL combines temperature and moisture time series in a nonlinear fashion to obtain simulated TRW chronologies. When used as observation operator, this forward modeling approach implies two nonlinear characteristics: (i) "switching recording" of 2 variables and (ii) bounded response windows leading to "thresholded response". The impact of these compounding, challenging features on the Ensemble Kalman Filter (EnKF) estimation of the Time-Averaged (TA) state is studied using a 2-scale chaotic model meant to be serve as a cartoon of the atmosphere-land system.

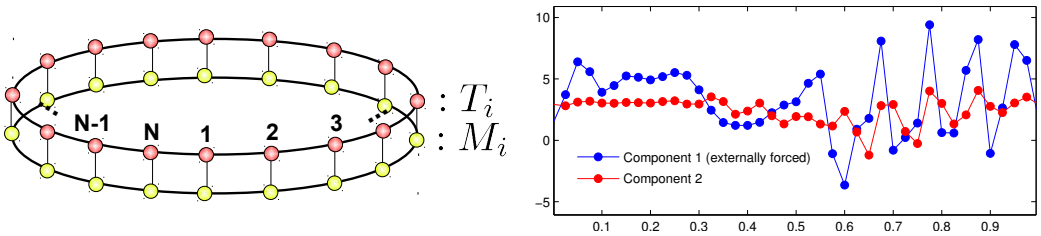

(a) (b)

FIGURE 5.1: (a) Model grid schematics and (b) State Variables Snapshot for the two-scale Lorenz [1996] model model.

5.1 Experimental Setting

5.1.1 Dynamical system

Soil processes are known to have a significantly longer memory than atmospheric ones [Wanru and Dickinson, 2004] and, consequently their corresponding variables present significantly different time scales. In order to mimic this multi-scale environmental driving on tree growth, we utilize the chaotic two-component dynamical system introduced by Lorenz [1996], given by the following nonlinear equations:

$$\begin{aligned} \dot{T}_i &= T_{i-1}(T_{i+1} - T_{i-2}) - T_i - \frac{hc}{b}\sum_{j=1}^{n} M_{j,i} + F, \\ \dot{M}_{j,i} &= cbM_{j+1,i}(M_{j-1,i} - M_{j+2,i}) - cM_{j,i} + \frac{hc}{b}T_i, \end{aligned} \tag{5.1}$$

where $i = 1 \ldots m$, $j = 1 \ldots n$, F is a constant forcing term, c and b are factors controlling the time scale and amplitude of the component M, and h is the coupling constant. Additionally, T and M variables are assumed to be periodic, i.e., $T_1 = T_{n+1}$; $M_1 = M_{n+1}$ (see figure 5.2(a)). Model state trajectories are obtained numerically via the standard Runge-Kutta method of fourth order with time step $\Delta t = 0.01$, where the model variables are represented by 64-bit FORTRAN real variables. The results shown in this paper correspond to the parameter setting $m = 40$, $n = 1$, $F = 8.0$, $c = 0.5$, $b = 1.0$ and $h = 1.0$, which is representative of our whole numerical exploration. For these parameter values,

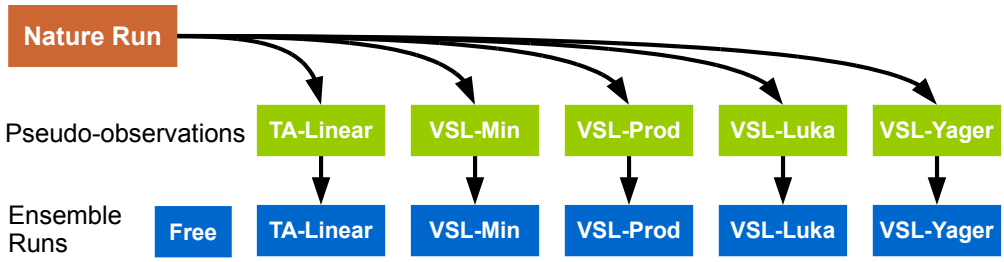

FIGURE 5.2: Schematic of the runs performed with the L96 model

the faster component T oscillates with roughly 2.5 times the amplitude of the slow component M. Moreover, the predictability horizon for instantaneous quantities is roughly four times longer in the slow component than in the fast one (see figure 5.5(a)). This configuration is meant to resemble the typical ratios of predictability time scale and amplitude between near-surface air temperature and soil moisture variables. Notice that the use of the letters T and M to denote fast and slow variables is made only for the sake of notation simplicity and there is no actual relation to the details of atmosphere-land interaction.

5.1.2 Experiment characteristics and filter configuration

In this chapter we present the results of a set of standard "perfect model" Observation System Simulation Experiments (OSSEs)[1] designed to study the influence of the representation of the PLF on the filter performance when VSL-based pseudo-TRW observations are assimilated. Four different sets of pseudo-observations and their corresponding observationally constrained runs are generated using the four Triangular Norms (t-norms) introduced in section 4.3. Furthermore, in order to have a reference that allows us to assess the loss of optimality due to the nonlinearities of VSL, we perform an additional ensemble run, $\mathbf{X}^{\text{DA}}_{\text{TA-Linear}}$, constrained by TA linear observations. The details of the creation of these pseudo-observations are provided in section 5.1.3. An schematic representation of the OSSEs performed can be found in figure 5.2.

Concerning the ensemble filter, we utilize an EnKF comprising 20 members, a stochastic analysis step with multiplicative inflation between 1% and 5%, and B-localization,

[1] see section 2.1.3 for a description of OSSEs

given the spatially extended nature of the L96 model. This was obtained using the Gaspari-Cohn function [Gaspari and Cohn, 1999] with localization radius $r = 2$, assuming a grid spacing $\Delta x = 1$.

5.1.3 Pseudo-observation generation

We create VSL-based pseudo-TRW observations from the nature run, by using the time series of fast and slow variables of the L96 model, T and M, as input data for the VSL model. We follow the steps outlined in section 4.1 employing the four t-norms introduced in section 4.3 to compute the growth rate[2] and add a final contamination step with unbiased Gaussian noise. We set the period between observations equal to the length of the integration period τ. Since the variance of the clean pseudo-TRW observations changes with τ, we set the variance of the noise so as to keep a constant Signal-To-Noise ratio (SNR). Our focus in this paper are the additional challenging features of VSL as an observation operator, therefore for our experiments we use optimistic observability conditions, i.e., observations at every grid point and SNR $= 10$, unless otherwise stated.

Given that our interest lies in the non-linear combination of 2 variables performed by VSL, we present results corresponding to mixed pseudo-TRW observations, obtained by setting the growth response windows to the values:

$$\begin{aligned} [T^L, T^U] &= [\overline{T} - R^A\sigma(T),\ \overline{T} + R^B\sigma(T)], \\ [M^L, M^U] &= [\overline{M} - R^A\sigma(M),\ \overline{M} + R^B\sigma(M)]. \end{aligned} \tag{5.2}$$

Here $\overline{*}$ and $\sigma(*)$ denote the mean and standard deviation values of the quantity $*$, estimated during the nature run; while R^A and R^B are constants that control the position of upper and lower response thresholds, respectively. We will focus on two particular configurations for the response functions: (i) wide windows ($R^A = R^B = 3.0$) and (ii) narrow windows ($R^A = R^B = 1.5$). In the first case, most of the climatological values of T and M are contained within the response windows and hence the response functions basically

[2]Given that the forcing term of the dynamical system used is constant, we replace the insolation term I by the unity

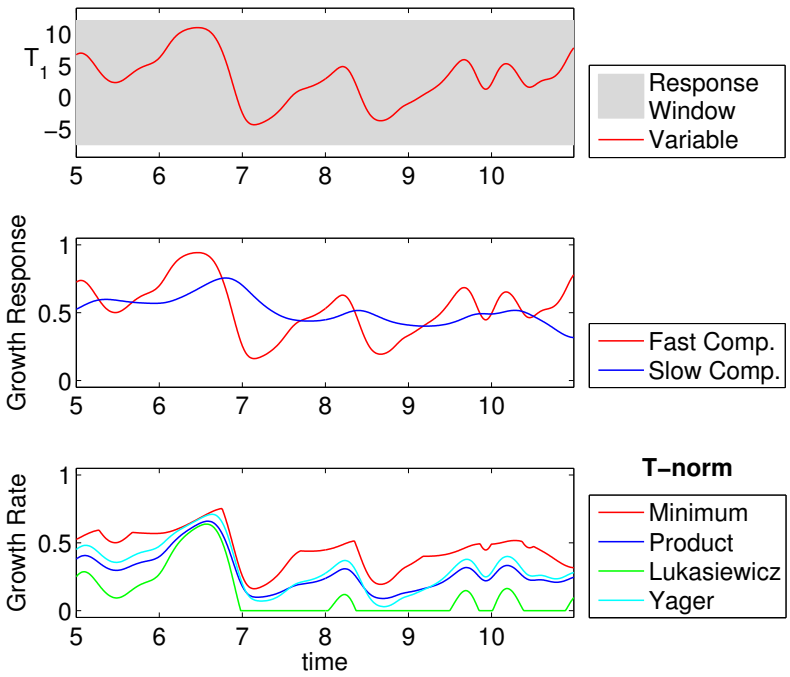

(a) Wide response windows

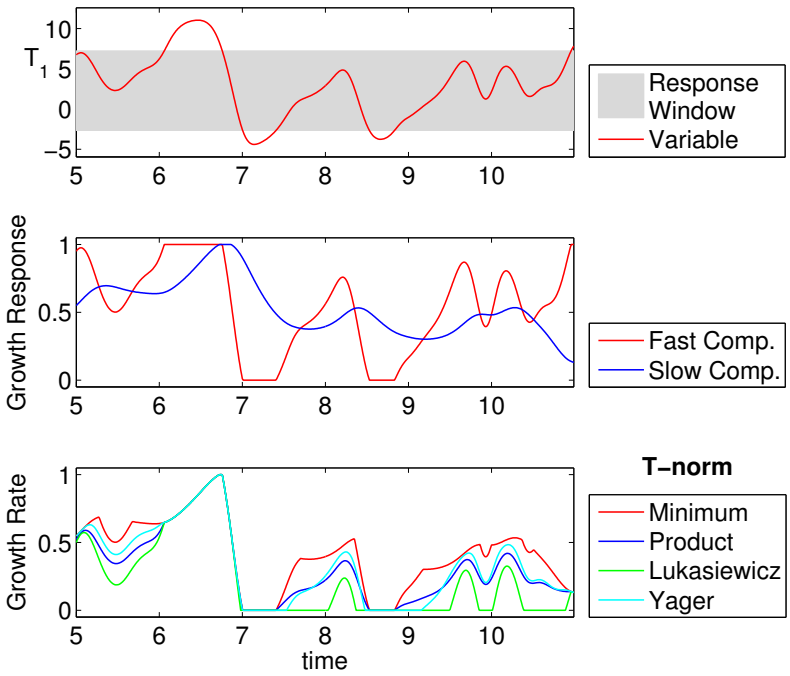

(b) Narrow response windows

FIGURE 5.3: Example time series of the quantities involved in the generation of pseudo-TRW observations. (For simplicity the quantities corresponding to the slow component are not shown in the upper panels).

act as linear rescaling operators (see figure 5.4(a)). Contrarily, in the second case, T and M time series are constantly cropped by the response functions and thus the recording thresholding becomes significant (see figure 5.4(b)).

As previously mentioned, we perform an additional ensemble run constrained by TA linear observations, obtained with the following instantaneous observation operator:

$$H_L = g_T + g_M, \; R^A = R^B = 3.0. \tag{5.3}$$

This setting corresponds to the wide response window configuration where the response thresholding is negligible. In these conditions, as mentioned in the previous paragraph, the response functions become lineal.

5.1.4 Diagnostic statistics

Similarly to the experiments presented in chapter 3, for a particular run $\mathbf{X}^{\text{DA}}_{\text{VSL}}$ constrained with VSL-based pseudo-TRW observations, the filter operation is evaluated by way of the root mean square error, $\textbf{RMSE}(\mathbf{X}^{\text{DA}}_{\text{VSL}})$, and the error decrease regarding the free run, $\mathcal{E}^{\text{Free}}_{\text{Reduction}}(\mathbf{X}^{\text{DA}}_{\text{VSL}})$. Additionally, in order to quantify the DA skill loss due to the nonlinearity of VSL we calculate the error increase regarding $\mathbf{X}^{\text{DA}}_{\text{TA-Linear}}$, $\mathcal{E}^{\text{NonLinObs}}_{\text{Increase}}(\mathbf{X}^{\text{DA}}_{\text{VSL}})$, given by the following expression:

$$\mathcal{E}^{\text{NonLinObs}}_{\text{Increase}}(\mathbf{X}^{\text{DA}}_{\text{VSL}}) = 100\% \cdot \left(\frac{\textbf{RMSE}(\mathbf{X}^{\text{DA}}_{\text{VSL}})}{\textbf{RMSE}(\mathbf{X}^{\text{DA}}_{\text{TA-Linear}})} - 1 \right). \tag{5.4}$$

We will refer to $\mathcal{E}^{\text{NonLinObs}}_{\text{Increase}}(\mathbf{X}^{\text{DA}}_{\text{VSL}})$ as the error increase due to observation nonlinearities.

The above mentioned diagnostic quantities are calculated for each model variable during 5×10^4 analysis cycles, and afterwards averaging within each component. The first 5×10^3 analysis cycles of the runs are regarded as spin-up period, and therefore they are not considered in the statistics.

5.2 Results

5.2.1 Assimilation of Time-Averaged linear observations

5.2.1.1 Instantaneous quantities

Due to the low-pass filtering action of the Time-Averaging operator, TA observations get gradually decorrelated from the instantaneous variables as τ increases. As a consequence, errors in the estimate of the instantaneous state, i.e., the instantaneous ensemble mean, tend to grow by increasing τ. This process can be readily seen in the red lines of figure 5.5(a), where the instantaneous forecast Root-Mean-Square (RMS) error for the fast (slow) component converge to the free run values at around $\tau = 0.8$ ($\tau = 2.8$). Analysis errors undergo an equivalent process but at a slightly slower pace. Notice that for the fast component the analysis error curve presents a clear overshoot around $\tau = 1.0$, where the analysis skill is negative and then the DA run performs worse than the free ensemble run.

5.2.1.2 Time-Averaged quantities

As opposed to the instantaneous state, the TA state remains correlated to the TA observations regardless of the τ value. Consequently, TA analysis error curves remain below their corresponding free run curves for much longer averaging periods than the instantaneous error curves (see figure 5.5(a)). Notice that the TA analysis skill is moderately sensitive to to the noise level and can be considerably diminished for low SNR values (see figure 5.5(b)).

Regarding TA forecasting skill, despite the considerable TA analysis skill for all τ values considered, the TA forecast errors saturate and reach the free run values at around $\tau = 1.0$ ($\tau = 4.0$) for the fast (slow) component (see figure 5.5(a)). This situation, where a DA method presents TA analysis skill for averaging periods where the TA forecasting skill is completely lost, has been previously observed in studies applying EnKF techniques on

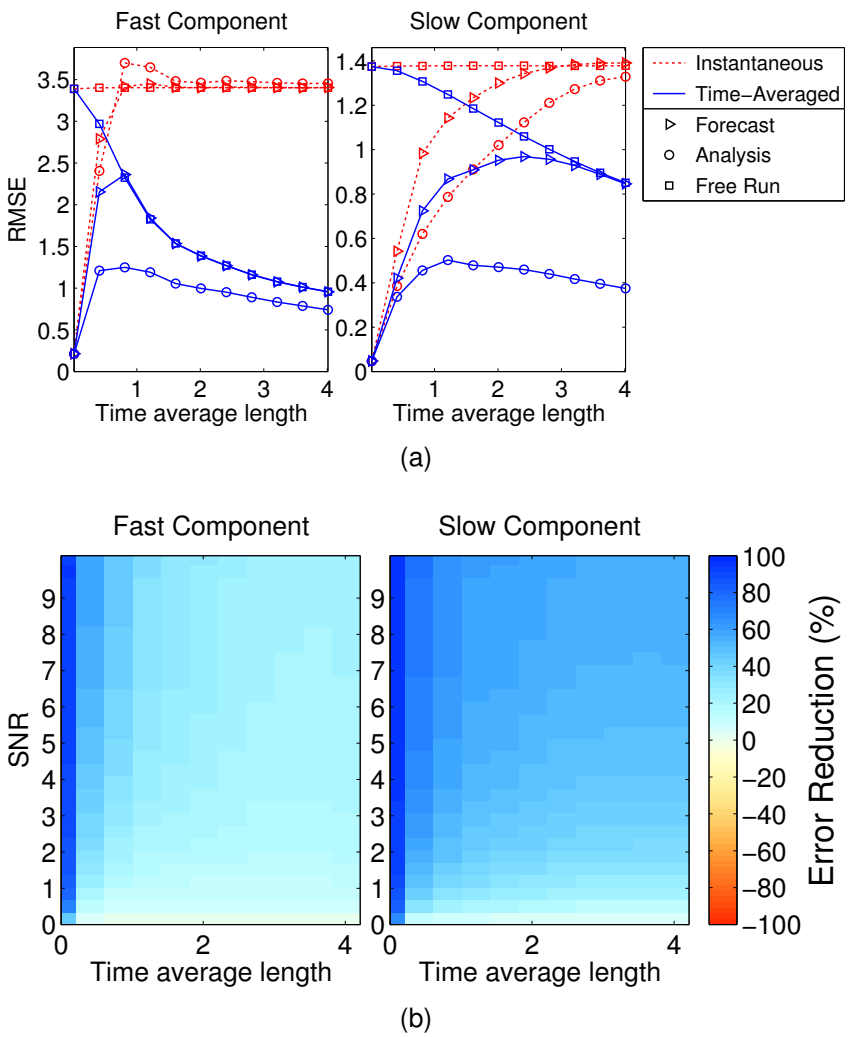

FIGURE 5.4: Error statistics for DA experiments assimilating TA linear observations. (a) RMS error vs averaging period τ for SNR $= 10$. Free Run curves correspond to an ensemble run without DA. (b) Time-Averaged Analysis Error Reduction (regarding a free run) vs τ and Signal-To-Noise ratio.

TA quantities Huntley and Hakim [2010]; Bhend et al. [2012]; Pendergrass et al. [2012]; Steiger et al. [2014]. DA performed under these circumstances is currently labeled as "off-line". This term is used to indicate that, under the randomizing action of chaotic model dynamics, at assimilation time the prior ensemble is completely decorrelated from the previous analysis state. As a consequence, the observational information cannot accumulate over time, as opposed to the typical application of DA for short-range prediction.

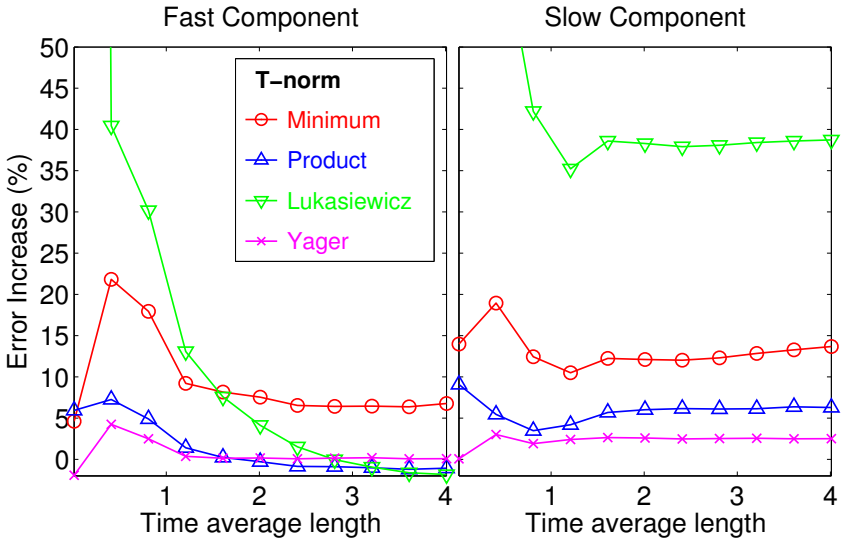

(a) Wide response windows

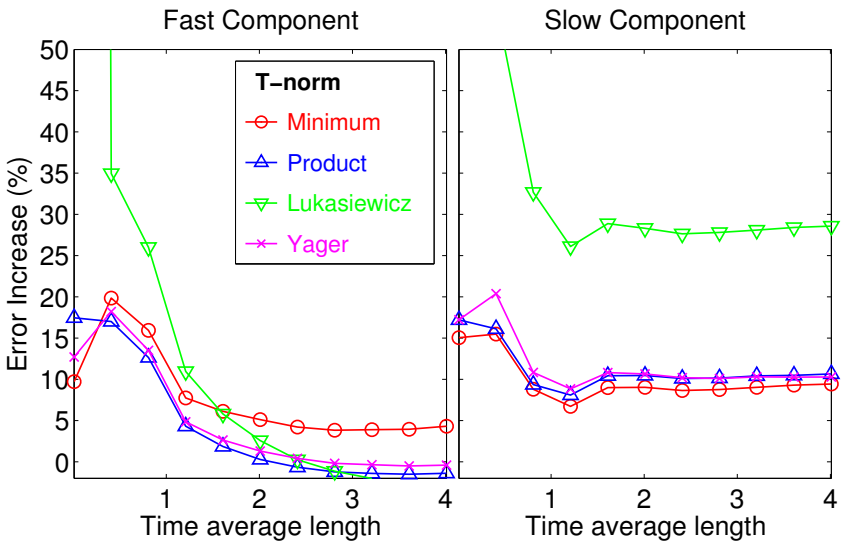

(b) Narrow response windows

FIGURE 5.5: Averaging period length dependency of the TA analysis error increase due to observation nonlinearities.

5.2.2 Assimilation of pseudo-TRW observations

As expected, assimilation experiments involving pseudo-TRW observations presented higher error levels than the ones already analyzed for linear observations. The recording efficiency of the different growth rate functions considered strongly depends on the

characteristics of the response windows.

Wide response windows

For this configuration of the response thresholds, as discussed in section 5.1.3, g_T and g_M reduce to linear rescaling operators and therefore the only nonlinearities present in the pseudo-TRW observations are those introduced by the particular t-norm used to represent the fuzzy intersection. Figure 5.4(a) shows how, in absence of recording thresholding coming from the response functions, G_{PROD} generates a completely smooth growth rate curve, as opposed to G_{MIN} whose corresponding line exhibits a cusp at every intersection of the growth response functions. G_{YAG} also leads to very smooth g curves, however, in this case there is already a subtle lower thresholding arising from the additional dormancy area generated by this t-norm, as discussed in section 4.3. Finally, for G_{LUK} this lower response thresholding effect is remarkably stronger.

Concerning the filter performance detriment caused by the nonlinerities of pseudo-TRW observations, figure 5.6(a) reveals that the t-norms yielding the smoothest growth rate curves (G_{YAG} and G_{PROD}) are the ones displaying the smallest optimality losses, as measured by the error increases with regard to the ensemble run assimilating linear observations. G_{MIN} showed considerably larger error increase values, particularly for short time averaging periods, while G_{LUK} clearly presented the poorest performance, with an error increase value for the slow component of around 40 % in the offline zone.

Narrow response windows

For this configuration of the response thresholds, the recording thresholding becomes evident in all growth rate curves (see figure 5.4(b)) and accordingly the optimality losses become more pronounced (see figure 5.6(b)). Interestingly, G_{MIN} and G_{LUK} curves are barely affected by the addition of recording thresholding. Accordingly, the performance level of all growth rate functions considered becomes comparable, with the only exception being G_{LUK} whose operation for the slow component remains especially poor.

Asymmetric impact of lower and upper thresholding

The impact of the response threshold positions on the analysis skill varies strongly between different growth rate function, as shown in figure 5.6. A common feature is the existence of high error areas for strong lower thresholding conditions, corresponding to small values of R^A. On the other hand, strong upper thresholding, corresponding to small values of R^B, has a much milder impact on the filter performance with the only exception of G_{MIN} which behaves in very special way for the fast component, presenting its minimum error levels for T^L values around 1.4. This markedly asymmetric effect of lower and upper response thresholds on the assimilation skill, can be explained by the fact that the upper parts of g_T and g_M time series are considerably suppressed by the action of the fuzzy intersection operators and become scarcely imprinted in the growth rate time series.

An interesting aspect of the RMS error surfaces for G_{YAG} and G_{LUK} is the presence of a zone of large errors in the left upper corners of the plots. This behavior can be attributed to the additional dormancy area characteristic of these two t-norms, which becomes particularly sizable for large values of R^B (see section 4.3) .

In summary, among the four growth rate functions studied, the TA ensemble Kalman filter presented the most consistent performance for G_{PROD}. Representing the fuzzy intersection by means of the product t-norm increases the smoothness of the growth rate time series with regard to the minimum t-norm, without exhibiting the added lower response thresholding present for Yager and Lukasiewicz t-norms. Additionally, its low sensitivity to input data uncertainty (see section 4.3) appears to make the t-norm particularly robust to the response thresholding phenomenon.

5.3 Discussion

Our numerical experiments with the L96 model suggest that VSL's nonlinear, time integral formulation of TRW chronologies is compatible in general terms with the TA EnKF technique.

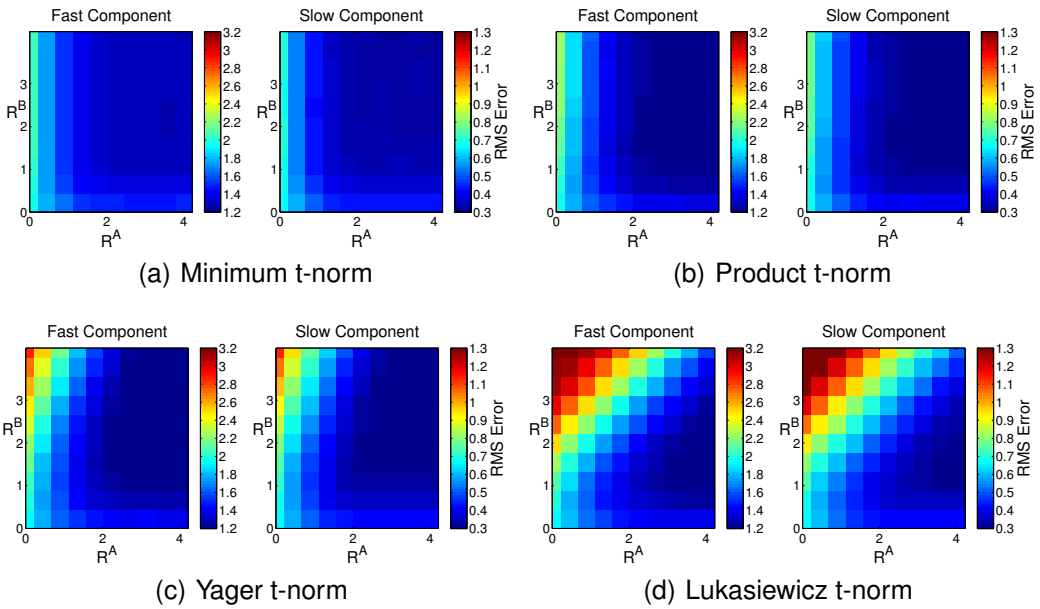

(a) Minimum t-norm (b) Product t-norm

(c) Yager t-norm (d) Lukasiewicz t-norm

FIGURE 5.6: Dependency of the TA analysis **RMSE** on the growth response thresholds (see equation 5.2) for the different growth rate functions considered ($\tau = 2.0$).

5.3.1 Switching recording

We found that the switching recording of two variables, implied by the PLF, does not necessarily deteriorate the filter performance in a dramatic way. However, when the transition between growth-limited modes occurs abruptly, as in the case of the original growth rate function, the lack of smoothness of the growth rate time series may significantly increase the optimality loss in the estimation of TA model state. Adopting the interpretation of growth response as membership functions and the minimum function as a t-norm representing the fuzzy intersection operation, it is pertinent to consider other examples of t-norms leading to alternative growth rate functions. Following this train of thought, we found that the smoothness of the particular t-norm employed plays an important role for the operation of the TA EnKF approach. This outcome is consistent with the smooth character of the trajectories of the deterministic model considered. Smooth t-norms allow a progressive switching of the recorded variables that decreases the roughness of the growth rate time series and, ultimately, benefits the filter operation. Among the alternative growth rate functions studied, the one based on the product t-norm provided the

best overall performance. We attribute this primacy of the product t-norm to its smoothness and its improved stability to input variable errors and membership function selection, which makes the product t-norm particularly appealing for the observation operator application investigated here.

5.3.2 Response thresholding

We found that the response thresholding phenomenon, arising from the bounded growth response windows, influences the assimilation skill in a strongly asymmetric fashion, being the lower thresholding significantly more detrimental than the upper one. This finding is rather fortunate in the view of more realistic DA experiments involving actual TRW chronologies, given the strong insensitivity of VSL to the lower moisture response threshold M^L, observed in Tolwinski-Ward et al. [2013]. With that, there exist a relative freedom to set the value of M^L, which could in principle be used to reduce the adverse effects of the lower moisture response thresholding, without compromising the TRW simulation competence of VSL.

CHAPTER 6

Assimilation of Pseudo-Tree-Ring-Width Observations into an Atmospheric General Circulation Model

In this chapter the problem of assimilating Tree-Ring-Width (TRW) chronologies is revisited, this time within the more realistic setting of an Atmospheric General Circulation Model (A-GCM). Following the rationale used in the experiments of chapter 5, pseudo-TRW observations are generated using Vaganov-Shashkin-Lite (VSL) as observation operator. Afterwards, the Time-Averaged (TA) state of the atmosphere is estimated via Ensemble Kalman Filter (EnKF) and the Time-Averaged Update (TA-Up) approach. The impact of the representation of the Principle of Limiting Factors (PLF) on the filter performance is studied using as reference the assimilation of TA linear observations.

6.1 Experimental setting

6.1.1 SPEEDY model

SPEEDY's logo

The Simplified Parametrizations, primitivE-Equation Dynamics (SPEEDY) model [Molteni, 2003] is an intermediate complexity Atmospheric General Circulation Model (A-GCM) comprising a spectral dynamical core and a set of simplified physical parametrizations, based on the same principles as state-of-the-art A-GCM but tailored to work with just a few vertical levels.

SPEEDY's dynamical core solves the hydrostatic primitive equations by means of the spectral transform developed by Bourke [1974], which uses absolute temperature, logarithm of the surface pressure, specific humidity, divergence and vorticity as basic prognostic variables. The time stepping is performed via a leapfrog scheme with an standard Robert–Asselin filter [Robert, 1966]. The sub-grid scale processes parametrized in SPEEDY are convection, large-scale condensation, clouds, short- and long-wave radiation, surface fluxes, and vertical diffusion.

In this dissertation we employ the version 32 of SPEEDY, featuring seven levels in the vertical (L7) and standard Gaussian grid of 96 by 48 points in the horizontal, which correspond to a triangular spectral truncation at total wave number 30 (T30). The top and bottom layers are meant to represent the stratosphere and the planetary boundary layer, respectively. Despite of its low resolution and the relative low complexity of its parametrizations, SPEEDY still captures many observed global climate features in a realistic way, while its computational cost is at least one order of magnitude lower than the one of sophisticated state-of-the-art A-GCMs at the same horizontal resolution [Molteni, 2003]. This latter virtue, makes SPEEDY specially suitable for studies involving long ensemble runs, like the ones presented in this chapter.

6.1.2 Filter implementation

Miyoshi [2005] adapted SPEEDY's code for Data Assimilation (DA) purposes and embedded it into the ensemble DA framework called SPEEDY-LETKF, which provides a parallel FORTRAN 90 implementation of the Local Ensemble Transform Kalman Filter (LETKF) [Hunt et al., 2007]. This particular flavor of EnKF is specially promising for high resolution model given that the calculation of the analysis for a particular grid point requires only the information of the neighboring grid points. With that, LETKF offers outstanding scalability properties.

SPEEDY-LETKF is an open-source software which have already been used for several DA studies: [Li et al., 2009; Miyoshi, 2010; Lien et al., 2013; Ruiz et al., 2013; Amezcua et al., 2014]. For the present study, it was extended for the assimilation of TA linear observations and pseudo-TRW observations. This task involved (i) the modification of the model time cycling, (ii) the addition of the TA-Up updating approach and (iii) the development of the VSL-like observation operator.

For the experiments presented in this section, we employed ensembles of 24 members and constant multiplicative inflation of 1% after the ensemble update. R-localization is achieved using the following formula:

$$R_{loc} = R * \exp\left((r_h/2\lambda_h)^2 + (r_v/2\lambda_v)^2\right) \tag{6.1}$$

where r_h and r_v stand for the horizontal and vertical distances, respectively. Their corresponding scaling parameters where set to the values $\lambda_h = 500$ Km and $\lambda_v = 0.4 \ln p$. Additionally, in order to avoid catastrophic filter divergence, observations differing too much from their corresponding predicted values are not taken into account. This sort of observation quality control is achieved within SPEEDY-LETKF via the following strategy: observations whose corresponding innovation vector norm (absolute mismatch regarding the forecast observation) is bigger that 10 times its error standard deviation, are discarded.

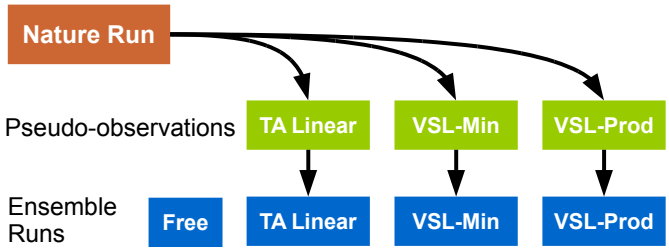

FIGURE 6.1: Schematic of the runs performed with SPEEDY model

6.1.3 Runs' characteristics

In this chapter, our modified version of SPEEDY-LETKF is utilized to carry out a set of standard "perfect model" Observation System Simulation Experiments (OSSEs)[1] completely analogous to the one performed with the two-scale Lorenz [1996] model (L96) in chapter 5. Nonetheless, in this chapter for the sake of simplicity and computational affordability, only two representations of the PLF are considered: the minimum and the product Triangular Norms (t-norms). This selection is based on the results of our experiments with the L96 model. An schematic representation of the OSSE set performed can be found in figure 6.1.

SPEEDY model is forced with the boundary conditions included in the version 32 of the code, which comprises the EOF-reconstructed Sea Surface Temperature (SST) dataset produced by Smith et al. [1996], as well as climatological maps derived from input data of the ECMWF's reanalysis [Gibson et al., 1997]. The latter consist of soil wetness, land temperature, snow depth, ice cover, vegetation cover and albedo monthly maps. Initially, a one-year long spin-up run is performed, starting from January 1st, 1950. The final state of this model trajectory is subsequently used as initial condition for a 30 years long nature run. Ensemble runs with and without DA are identically initialized from a set of states gathered daily from the last month of the spin-up run. Notice that the nature run and the different ensemble runs are generated driving SPEEDY with the same time varying forcing fields.

[1] see section 2.1.3 for a description of OSSEs

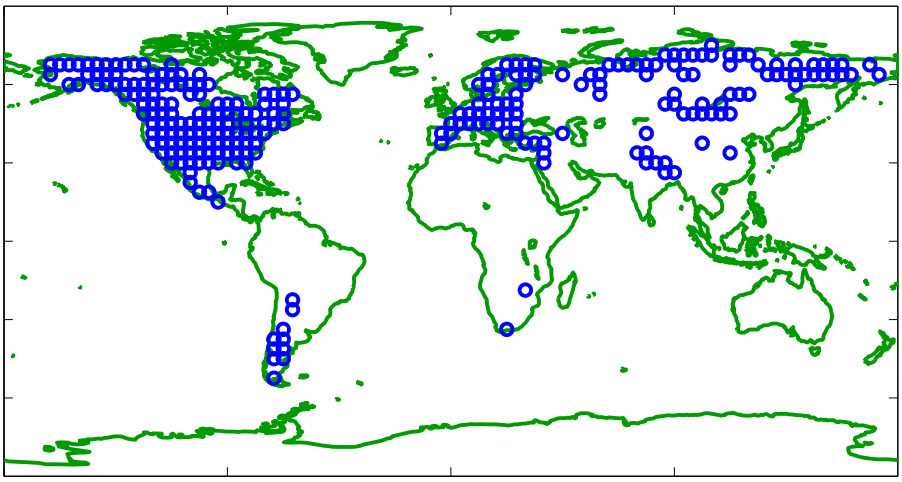

FIGURE 6.2: Station set resembling real TRW network from Breitenmoser et al. [2014]

6.1.4 Observation generation

Similarly to the OSSEs of the previous chapter, pseudo-TRW observations are produced following VSL's formulation (see section 4.1), plus a final white noise addition step, where random draws from a Gaussian distribution are added to the clean TA observations, so as to obtain a Signal-To-Noise ratio (SNR) equal to 10.0. Surface temperature data was extracted from the lowest level of the state vector, while soil moisture was taken from the surface boundary conditions. Notice that temperature is a prognostic variable of the model, whereas soil moisture is a prescribed variable with yearly periodicity. It is worthwhile to mention that although soil moisture is not a prognostic variable of SPEEDY, it does affect prognostic variables, such us humidity, through the parametrizations.

Regarding the geographical distribution of observations, we place a station at every grid box where at least one actual TRW chronology from the database of Breitenmoser et al. [2014] is present. This strategy yields an observational network comprising 257 stations (see figure 6.2). Concerning the configuration of the observation operator, for our OSSEs involving SPEEDY we focus on the effect of the first VSL's nonlinearity, i.e., the shifting of recorded variable. Consequently, we configure VSL so that no thresholding takes place. This we achieve by setting the upper and lower response thresholds to the

maximum and minimum values during the nature run, respectively, so that the response functions reduce to linear rescaling operators.

6.1.5 Diagnostic statistics

Given the annual resolution of TRW chronologies, we study the filter performance for a fixed averaging period length of one year. Similarly to the OSSEs conducted with the L96 model, we monitor the behavior of our ensemble runs by way of the ensemble mean, ensemble spread, Root Mean Square Error (**RMSE**), error decrease regarding the free run, $\mathcal{E}^{\text{Free}}_{\text{Reduction}}$, and error increase regarding the ensemble run constrained with TA linear observations, $\mathcal{E}^{\text{NonLinObs}}_{\text{Increase}}$. Nonetheless, in this chapter we redefine the latter two diagnostics so as to consider their absolute values:

$$\mathcal{E}^{\text{Free}}_{\text{Reduction}}(\mathbf{X}^{\text{DA}}) = \textbf{RMSE}(\mathbf{X}^{\text{Free}}) - \textbf{RMSE}(\mathbf{X}^{\text{DA}}), \tag{6.2}$$

$$\mathcal{E}^{\text{NonLinObs}}_{\text{Increase}}(\mathbf{X}^{\text{DA}}_{\text{VSL}}) = \textbf{RMSE}(\mathbf{X}^{\text{DA}}_{\text{VSL}}) - \textbf{RMSE}(\mathbf{X}^{\text{DA}}_{\text{TA-Linear}}). \tag{6.3}$$

This reformulation of $\mathcal{E}^{\text{Free}}_{\text{Reduction}}$ and $\mathcal{E}^{\text{NonLinObs}}_{\text{Increase}}$ is motivated by fact that –opposed to the models previously used in this manuscript, i.e., PK2004 and L96 models– SPEEDY presents spatially heterogeneous internal variability. Due to this feature, for a particular time averaging length, there will typically be regions with very low internal variability for which **RMSE**$(\mathbf{X}^{\text{Free}})$, **RMSE**$(\mathbf{X}^{\text{DA}}_{\text{TA-Linear}})$ and **RMSE**$(\mathbf{X}^{\text{DA}}_{\text{VSL}})$ concurrently present very low values. In these conditions, the letter three quantities are strongly dominated by statistical errors and consequently the relative error increase/decrease become overly noisy over low internal variability areas.

Diagnostic statistics are calculated for three SPEEDY variables: temperature, humidity and Zonal Wind (u-wind). In order to reduce the dimensionality of these 4-dimensional fields, we study their zonal means as well as a selected sigma level for each variable: 0.925 (≈ 925 hPa) for temperature, 0.850 (≈ 850 hPa) for humidity and 0.300 (≈ 300 hPa) for u-wind.

6.2 Results

6.2.1 Free ensemble run

An A-GCM is an example of non-autonomous systems and accordingly the evolution of its state is determined by both the atmospheric dynamics and the external forcings. The influences of these two distinct factors can be disentangle to a good extend by considering the atmospheric variability as a linear superposition of an internal component, caused by the intrinsic dynamics, and an external one, resulting from the variations of the boundary conditions [Deza et al., 2014]. Under this assumption, internal and external variability can be separated by way of a free ensemble run, using the ensemble mean as an estimate of the forced component. The magnitude of the internal variability can then be estimated from the ensemble spread. Notice that using an ensemble DA method is only profitable in the presence of internal variability, given that the forced variability can be well described by an unconstrained ensemble run.

Ensemble mean Figure 6.3 shows how the forced component of SPEEDY's variability at yearly time scales clearly exhibits important large scale patterns. Surface temperature shows a roughly latitudinal global distribution, disrupted by the irregular land distribution and zones of particularly high altitude, e.g. the Himalaya, or high albedo, e.g. Greenland and Antarctica. Humidity appears strongly localized near the surface around the equator, in the so-called Inter-Tropical Convergence Zone (ITCZ). Finally, u-wind is maximal near the tropopause at latitudes around $\pm 40°$. These two bands correspond to the subtropical jet streams [Holton, 1992].

Ensemble spread The time averaging operator acts as a low pass filter that reduces the amplitude of fluctuations with time scales shorter than the averaging period. Subsequently, geographical areas dominated by fast processes, compared to τ_{aver}, tend to present constant average values, or equivalently no internal time averaged variability. In

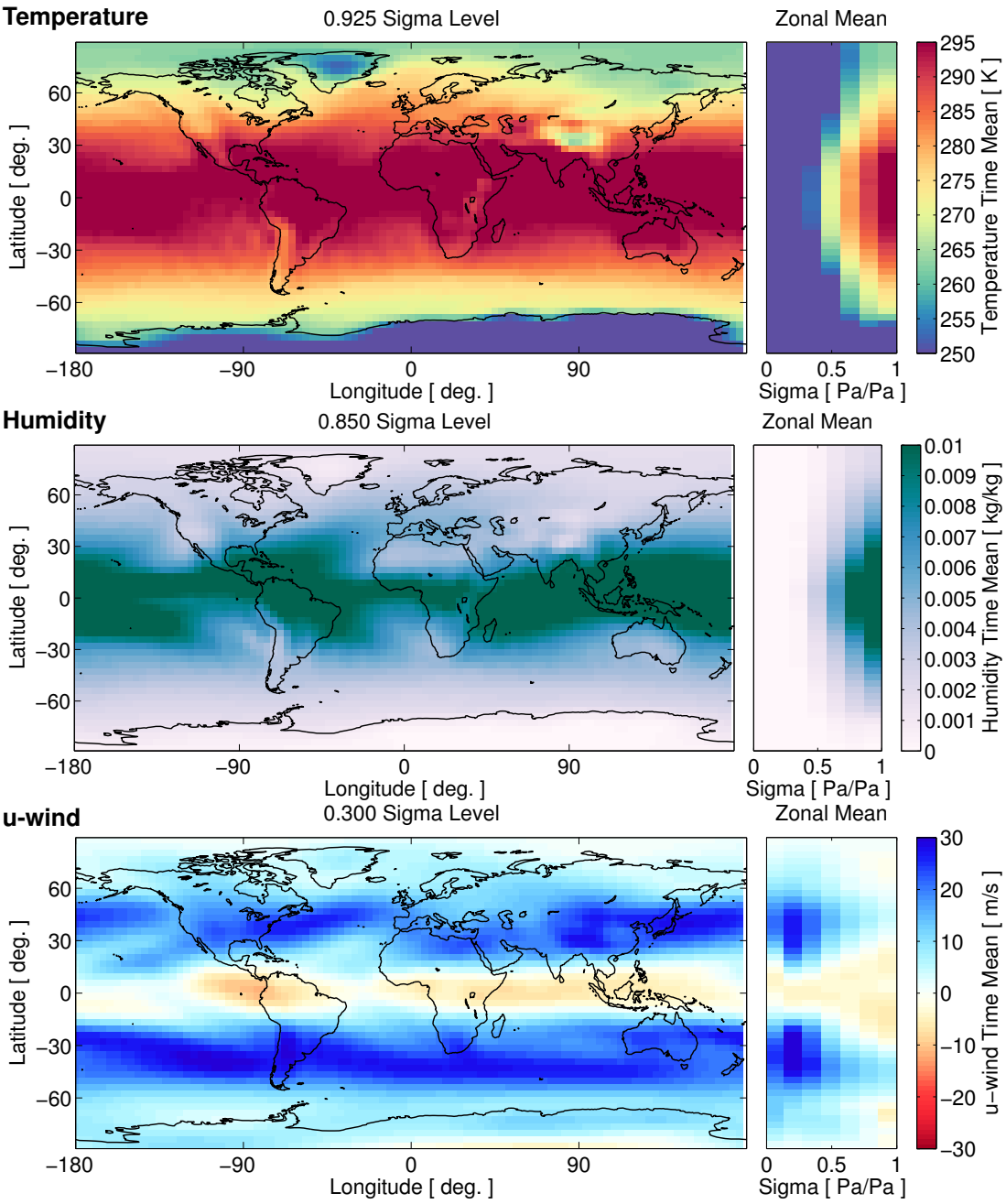

FIGURE 6.3: Ensemble mean for the yearly quantities of the free ensemble run.

the case of TRW chronologies, the characteristic one-year averaging period is considerably long for atmospheric phenomena, and as consequence several areas present very low yearly internal variability for particular variables. A clear example of this is temperature around the equator (see figure 6.4). In this zone temperature variability is dominated

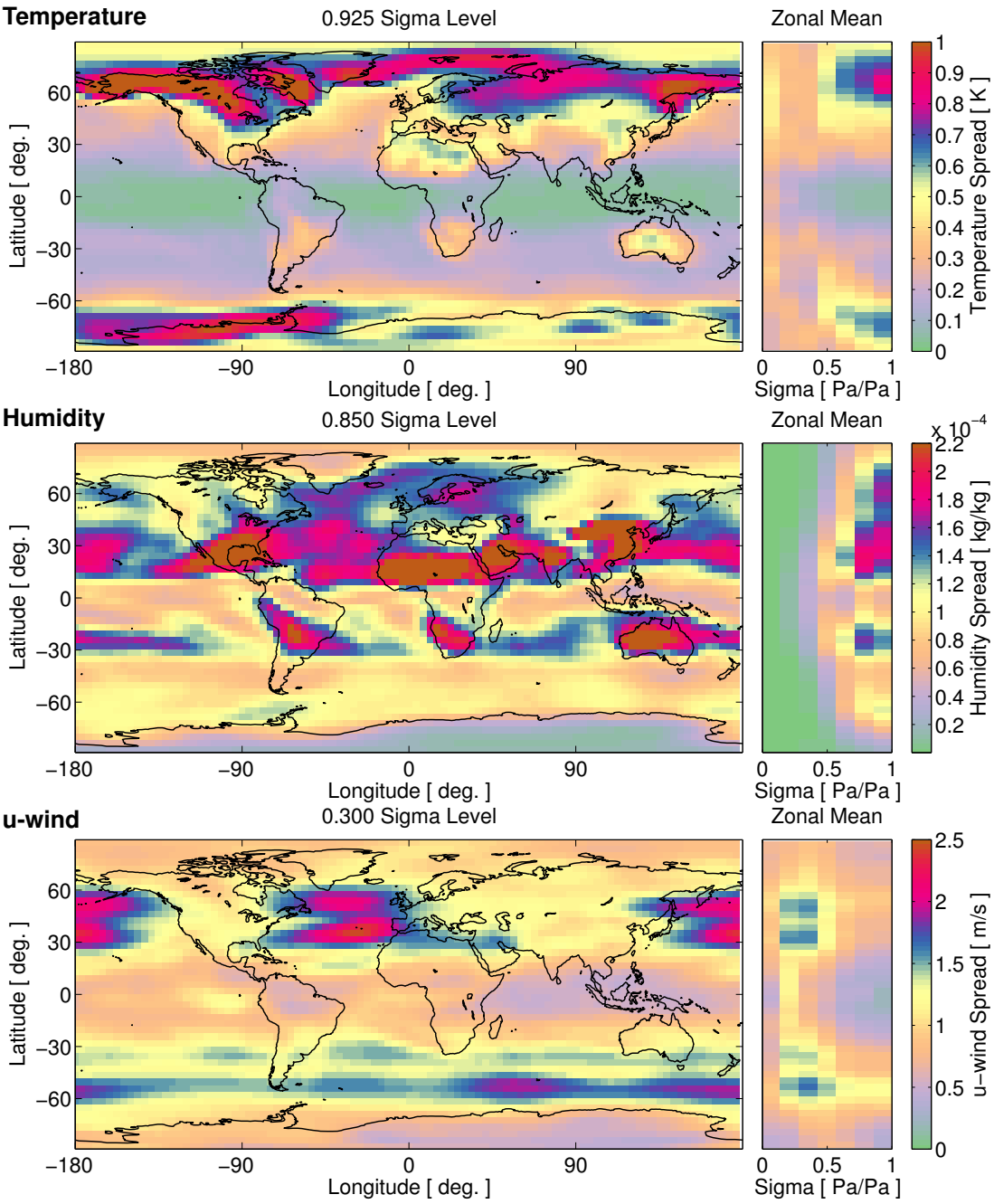

FIGURE 6.4: Ensemble spread for the yearly quantities of the free ensemble run.

by the daily cycle and accordingly it gets strongly attenuated by the a yearly averaging. On the other hand, planetary scale patterns are not completely stationary but present fluctuations over long time scales. These slow processes introduce internal variability in the yearly means, as can be seen in figure 6.4. Maximum temperature spread takes

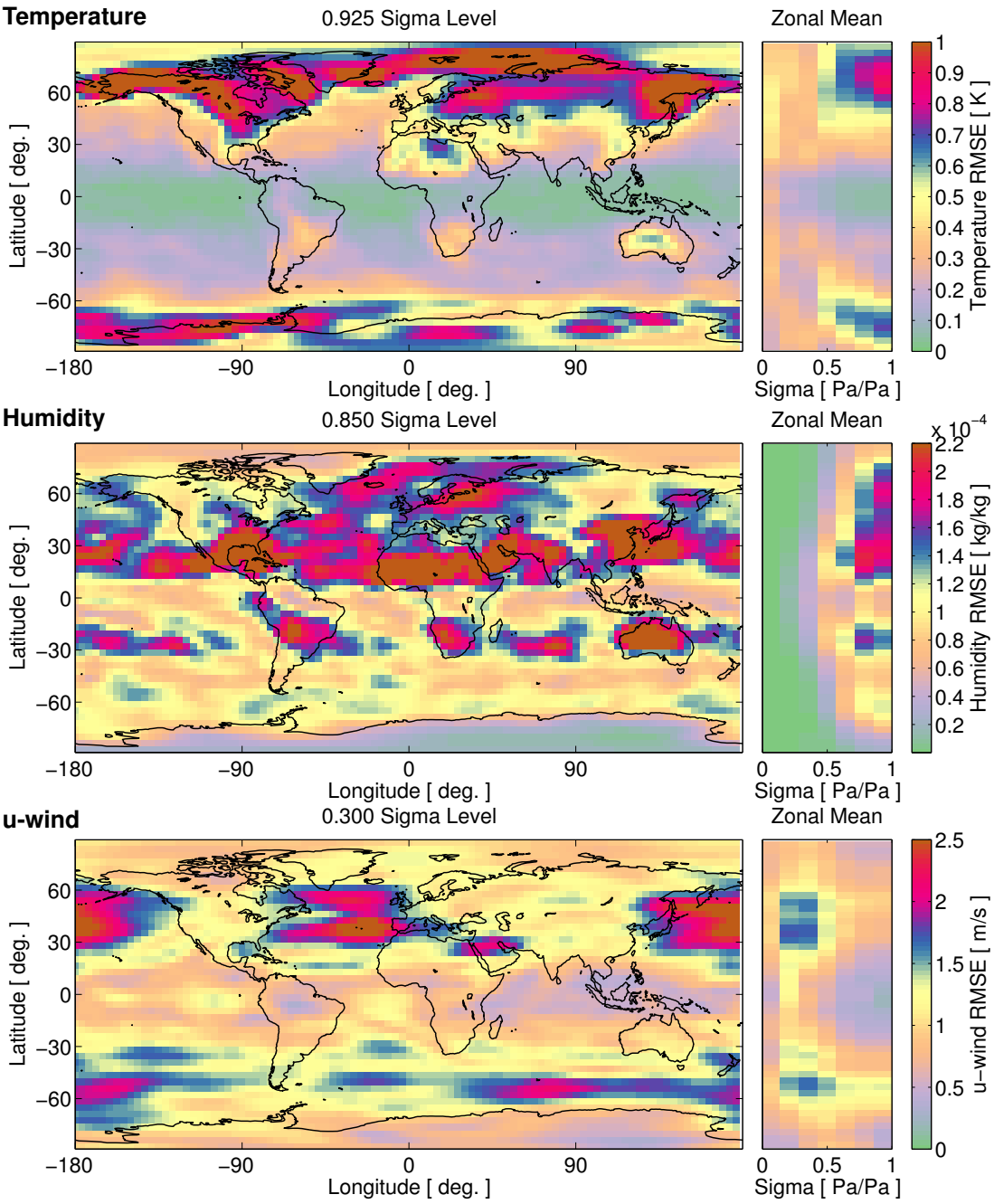

FIGURE 6.5: Forecast **RMSE** for the yearly quantities of the free ensemble run.

place near the surface at high latitudes around $\pm 70°$. Humidity and u-wind spreads are maximal in the edges of the ITCZ and the subtropical jet stream, respectively. These yearly internal variability maxima can be related to leading variability modes of the global circulation, such as the "annular modes" [Thompson and Wallace, 2000], migrations of

the ITCZ [Schneider et al., 2014], as well as jet stream displacements [Woollings et al., 2011].

An important consequence of the spatially heterogeneous yearly internal variability of SPEEDY, is that the nature run variables at geographical areas with low internal variability can be well predicted by the ensemble mean of the free ensemble run, as it can be readily seen in figure 6.5 for the tropical surface temperature. On the other hand, **RMSE** extremes take place in areas of maximal internal variability (compare figures 6.5 and 6.4). Generally speaking, the error of the free ensemble run, used as a predictor of the nature run, is essentially the projection of the nature run trajectory on the internal variability component.

6.2.2 Observationally constrained ensemble runs

6.2.2.1 Assimilating TA linear observations

The assimilation of TA linear observations leads to low temperature **RMSE** levels in all geographical areas adjacent to the observation network (see figure 6.6). The situation for moisture is very similar, however in this case there exist few areas with considerable error despite the presence of a nearby observational station, e.g., south-west China and Texas. On the other hand, u-wind and v-wind (not shown) analysis fields present no noticeable bettering in any part of the globe.

For our DA runs a low **RMSE** value for the yearly mean of a particular variable might be due to observational constraint or/and to lack of internal variability a that time scale. In these conditions, the error reduction with reference to the free run, $\mathcal{E}^{\text{FREE}}_{\text{REDUCTION}}$, appears as a very convenient quantity to assess the real benefit of performing DA. Figure 6.7 shows the existence of considerable error reduction for temperature and moisture in some geographical areas, whereas for u-wind $\mathcal{E}^{\text{FREE}}_{\text{REDUCTION}}$ exhibits negligible values as it is expected from the analysis of figure 6.6. This absence of observational constraint on the wind variables was common to all our simulations and accordingly wind-related quantities will not be analyzed hereafter.

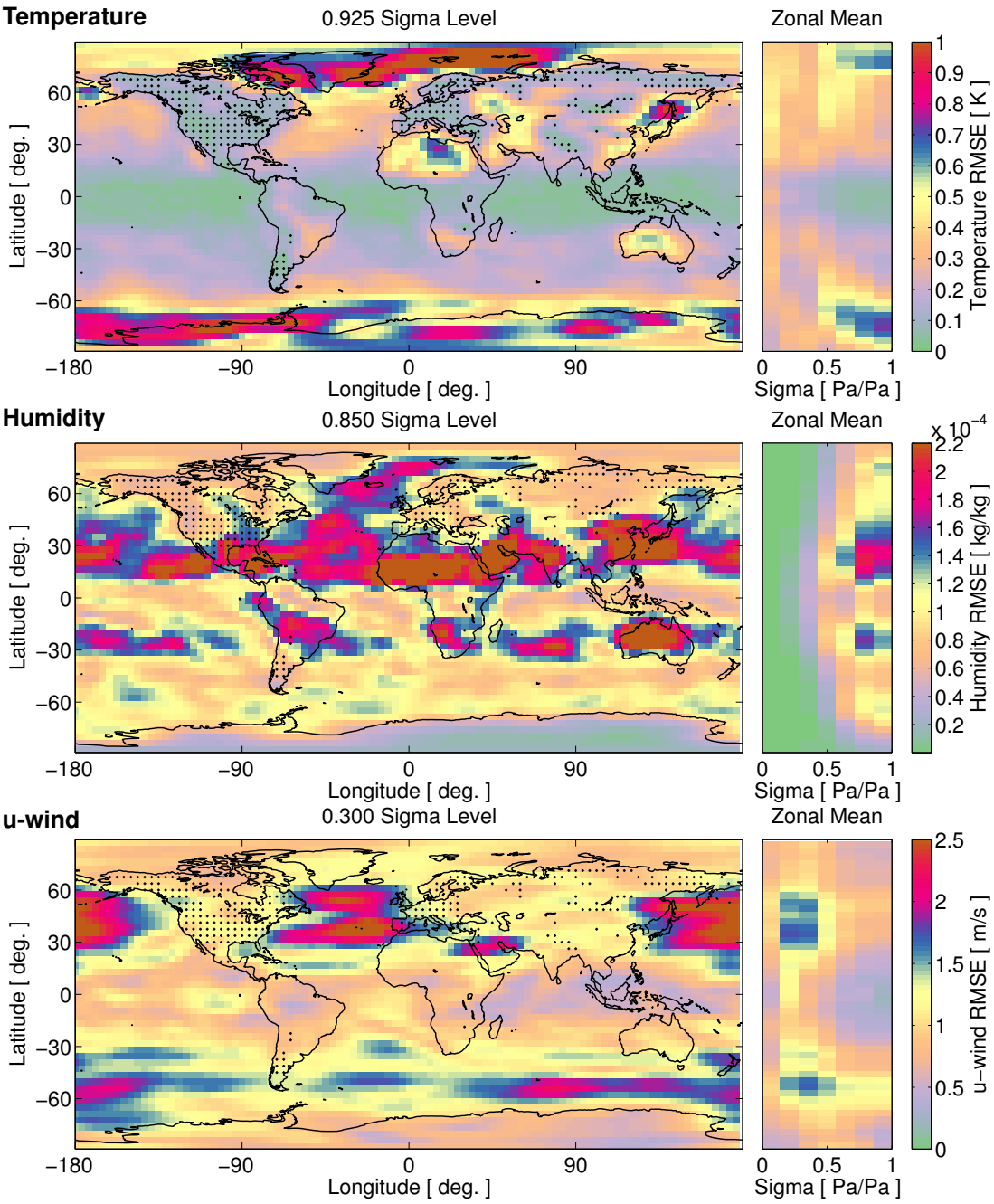

FIGURE 6.6: Analysis **RMSE** for the yearly quantities of the ensemble run constrained with TA linear observations.

An important aspect of our results concerning the DA skill when yearly averaged linear observations are assimilated, is that the error reduction regarding the free ensemble run appears modulated by the magnitude of the yearly internal variability of the particular

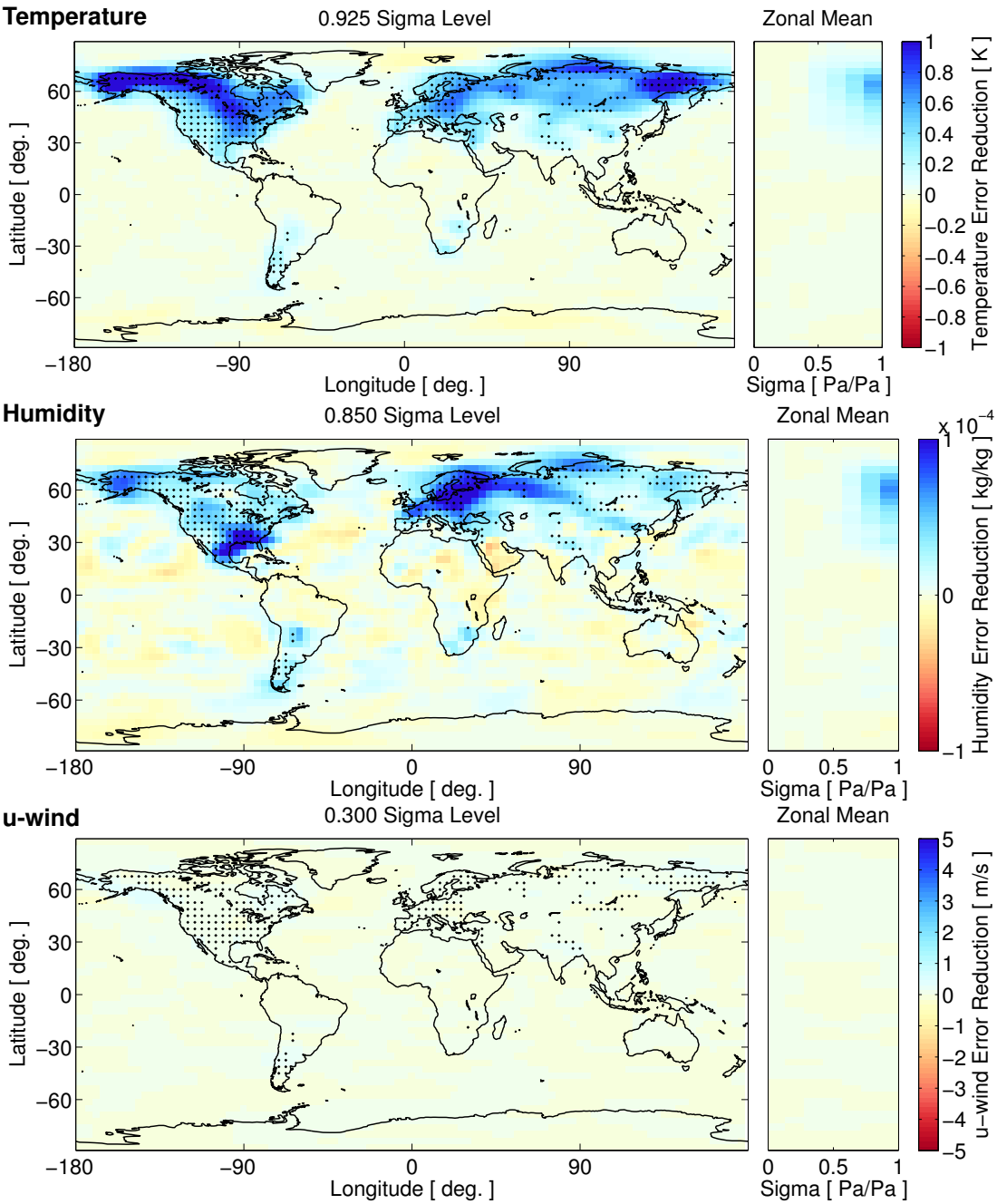

FIGURE 6.7: Analysis error reduction regarding the free ensemble run, $\mathcal{E}^{\text{FREE}}_{\text{REDUCTION}}$, for the yearly of the ensemble run constrained with TA linear observations.

variable at a specific site(compare figures 6.4 and 6.7). As a consequence, stations located in areas of strong yearly internal variability are more efficient than the others at reducing the error of the TA state estimate. An example of this are the stations located

in Alaska which constrain temperature considerably more strongly than the ones laying on south-east USA, south America or south Africa. This finding can then be utilized as guidance for the design of optimal TRW chronology networks, in particular, and proxy networks in general (see the discussion at the end of this chapter).

An additional relevant feature of figure 6.7 is that both for temperature and humidity the error reduction is strongly localized around data-rich areas. This behavior can be explained by the negligible error reduction obtained for the all the forecast variables (not shown). This complete absence of observational constraint on the forecast implies that our DA experiments are performed in an offline regime. As discussed in section 5.2.1, under this conditions the observational information is neither accumulated in time nor propagated by the model dynamics flow. Accordingly, the TA analysis skill is localized around the observational stations.

6.2.3 Assimilating pseudo-TRW observations

6.2.3.1 Original PLF representation

The use of VSL-Min as observation operator appears compatible with the EnKF-based DA technique utilized, as it is evidenced by the low **RMSE** levels observed in figure 6.8 around the observational network. Nonetheless, due to the strong nonlinear features of VSL-Min, the performance of filter is expected to be degraded with respect to the ensemble runs constrained with TA linear observations, as previously observed in the OSSEs performed with the L96 model. This behavior can be readily seen in figure 6.9, which show considerable error increases due to observation nonlinearities. Regarding temperature, $\mathcal{E}^{\text{NonLinObs}}_{\text{Increase}}$ presents particularly high values over the Labrador peninsula, central Europe and Siberia. As for humidity, there are three spots of high error increase on the northwest USA, the band extending from the gulf of Mexico to the great lakes, and the stripe connecting the Baltic with the black sea.

An interesting feature of figure 6.9 is the presence of unobserved zones with negative $\mathcal{E}^{\text{NonLinObs}}_{\text{Increase}}$ values, e.g., Antarctica for temperature and the Arabian peninsula for humidity,

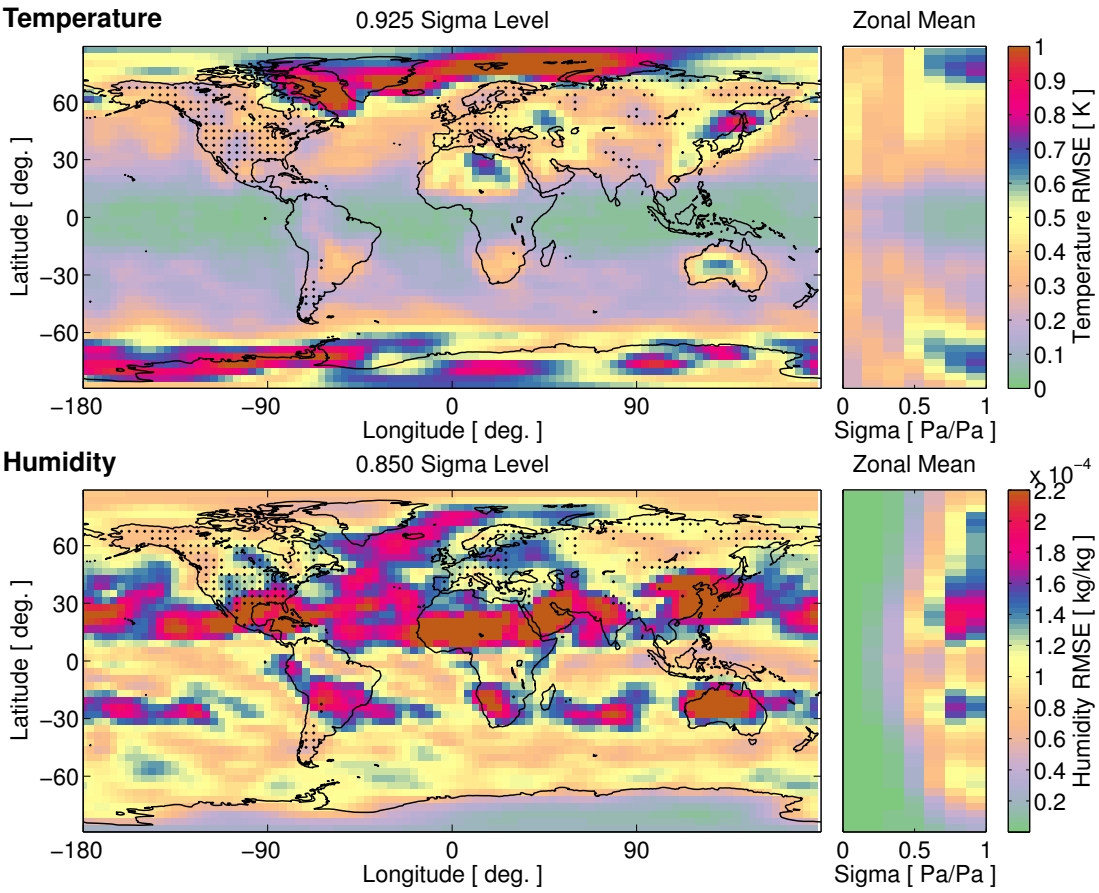

FIGURE 6.8: Analysis **RMSE** for the yearly quantities of the ensemble run constrained with VSL-Min pseudo-TRW observations.

which implies that the estimation of the TA state is not optimal over these regions. This phenomenon might be attributed to significant non-Gaussianity for these variables in this geographical areas.

6.2.3.2 Product PLF representation

The use of VSL-Prod, instead of VSL-Min, as TRW observation operator appears beneficial to the filter performance as it can be seen in figure 6.9, where the error increase becomes in general lower and more homogeneous. Notice that for humidity there remains a spot of considerably positive $\mathcal{E}^{\text{NonLinObs}}_{\text{Increase}}$ values in southeastern USA.

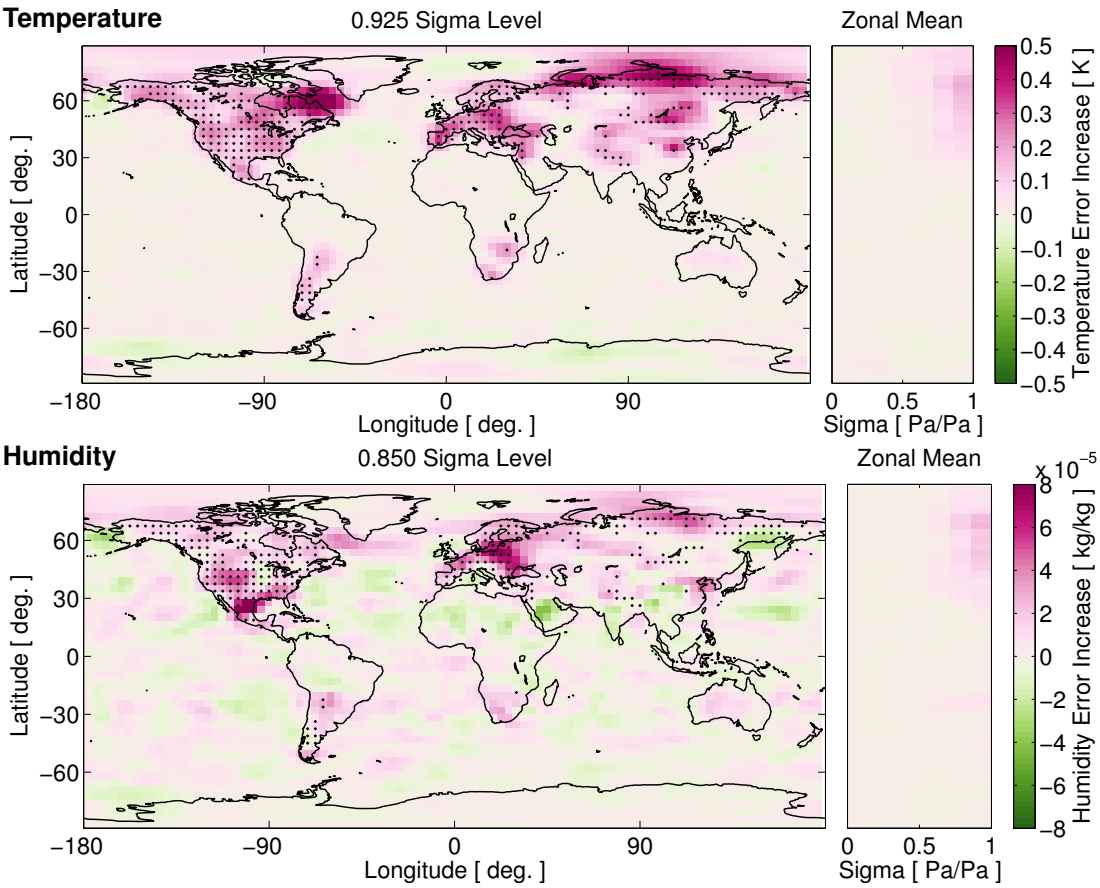

FIGURE 6.9: Analysis error increase due to observation nonlinearities, $\mathcal{E}^{\text{NonLinObs}}_{\text{Increase}}$, for the yearly quantities of the ensemble run constrained with VSL-Min pseudo-TRW observations.

An interesting behavior regarding humidity is the appearance of negative $\mathcal{E}^{\text{NonLinObs}}_{\text{Increase}}$ values over the relatively well observed area of central Siberia. This phenomenon makes again manifest the existence of non-negligible non-gausian features for certain variables at particular geographical regions, which implies lack of optimality for the TA state estimation even when TA linear observations are assimilated.

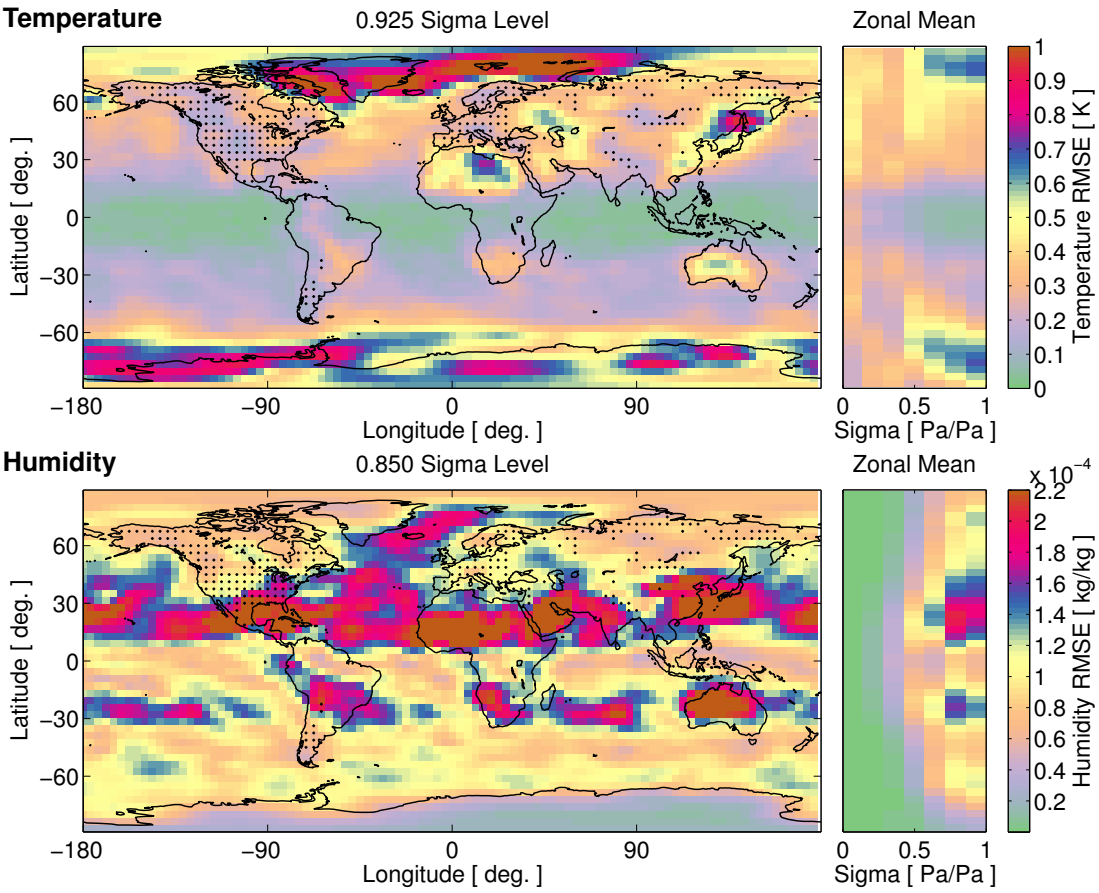

FIGURE 6.10: Analysis **RMSE** for the yearly quantities of the ensemble run constrained with VSL-Prod pseudo-TRW observations.

6.3 Discussion and Outlook

6.3.1 Error reduction efficacy of TRW chronologies

For the OSSEs studied in this chapter, it was found that the ability of a particular pseudo-TRW chronology to reduce the error of the EnKF-based estimate of the TA state appears modulated by the strength of the yearly internal variability of the model at the chronology site. This finding can in principle be employed to help the dendrochronology community to increase the effectivity of their sampling efforts by focusing on the sites with more potential to decrease reconstruction uncertainty. Furthermore, this approach can be directly applied to any proxy type with sufficiently stable time resolution.

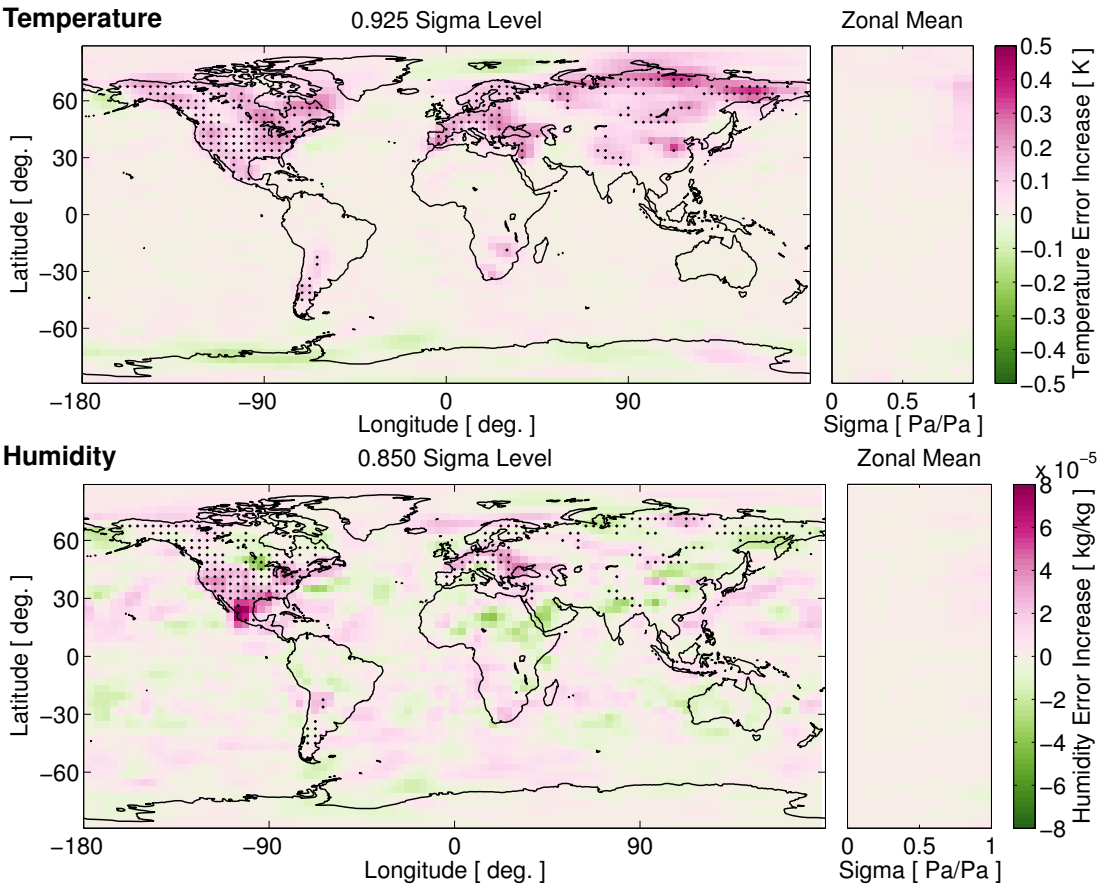

FIGURE 6.11: Analysis error increase due to observation nonlinearities, $\mathcal{E}^{\text{NonLinObs}}_{\text{Increase}}$, for the yearly quantities of the ensemble run constrained with VSL-Prod pseudo-TRW observations.

An evident caveat of the above mentioned rationale is that every model-based estimate of the climate internal variability strength for a particular time scale will necessarily exhibit the biases of the particular climate model used. We consider that this modeling subjectivity/imperfection issue can be ameliorated by means of multi-model and multi-physics approaches, which in principle should increase the robustness of the results and provide uncertainty estimates. In any case, we believe that provided the results are analyzed cautiously taking into account the weaknesses of current climate models, the huge amount of climate dynamics knowledge condensed into a earth system model can certainly be used profitably to reduce the cost of a undiscriminated proxy sampling strategy.

6.3.2 Filter operation sensitivity to the PLF representation

The results of the DA experiments conducted with SPEEDY model support in general the ones obtained for the L96 model regarding the influence of the PLF representation on the filter performance. The efficacy of the EnKF-based TA state estimation strategy appeared to be significantly sensitive to the selection of the t-norm used to calculate the growth rate, with the product t-norm clearly outperforming the minimum t-norm used in the original formulation of VSL forward model.

Tolwinski-Ward et al. [2014] described trees as fundamentally lossy[2] recorders of climate, due to the integrated nature of the information in them contained and the standardization process used to minimize the non-climatic effects on growth. In the same vein, we argue that the abrupt shifting of recorded variable –implied by the minimum function used in VSL's original formulation– might constitute an additional source of lossyness (at least within a EnKF-based DA setting used), which can be substantially reduced by resorting to alternative Fuzzy Logic (FL)-based representations of the PLF.

6.3.3 Off-line Data Assimilation

Within our simplified perfect model OSSEs, the observed situation of simultaneously having significant DA skill for analysis quantities and none for forecast quantities, currently referred to as off-line DA regime, can arise either from the dynamical model or from the DA scheme.

Regarding the dynamical model, the most obvious reason to enter into the off-line regime is that the period between consecutive observations exceeds the predictability horizon of the model. In this conditions, as already discussed in section 5.2.1, the ensemble spread reaches climatological levels before new observations are assimilated and the accumulation of observational information is essentially lost. For SPEEDY model, due to its purely atmospheric nature, it is not surprising tho enter the off-line regime for a 1-year

[2]This adjective is currently used in the information technology area to designate data encoding methods that lead to information loss from the original version for the sake of reducing the amount of data needed to store the content.

inter-observation period. This might be also the case for current operational (coupled) climate prediction systems, given their lack of useful lead times longer than one year. In this state of affairs it looks unlike to achieve effective observational constraint on the forecast using proxy records with yearly time resolution. However, there exist already evidence for the existence of potential sources of climate internal variability with time scales longer than 1 year [Smith et al., 2012]. Accordingly, it is expected to obtain actual inter-annual predictability skills in the foreseeable future.

Regarding the DA scheme, a possible culprit for the onset of the off-line regime is the Time-Averaged Update (TA-Up) strategy. It is not clear if for SPEEDY model this technique is able to properly estimate instantaneous quantities out of TA observations. Accordingly, it appears relevant to investigate the performance of the other updating techniques considered in chapter 3. Here our newly proposed Time-Averaged + Instantaneous Update (TAI-Up) technique appears particularly attractive, given that the relatively high dimensionality of SPEEDY model can easily make the Time-Augmented Update (TAug-Up) technique unaffordable.

In any case, despite its lack of accumulation of observational information over time, off-line DA has already been shown to be more robust than traditional climate field reconstruction techniques based on orthogonal empirical functions [Steiger et al., 2014]. Moreover, the implementation and running of offline DA schemes is remarkably cheaper than on-line approaches.

6.3.4 Challenges to be addressed

As a cautionary remark, we want to highlight the several important limitations of the experiments described in this chapter. The generated pseudo-TRW observations lack response saturation and their contamination with noise was performed assuming optimistically high SNR levels. Furthermore, the response thresholds were set in a completely homogeneous fashion for all the observational stations, whereas actual TRW networks are strongly heterogeneous in that sense, comprising chronologies generated under highly dissimilar growth limitation regimes. Additionally, the efficiency of EnKF technique used

relies on the Gaussianity of all the variables of the model. Nevertheless, in a climate model some variables can present strongly non-Gaussian properties –specially definite positive quantities such as humidity– and then their estimation should in principle be performed with more sophisticated strategies such a Gaussian anamorphosis [Bocquet et al., 2010; Lien et al., 2013]. Finally, it is worth mentioning the necessity of explicitly addressing model errors by conducting imperfect model OSSEs.

CHAPTER 7

Conclusions and Prospect

7.1 Filtering of Time-Averaged Observations

Our numerical results presented in chapter 3 indicate that the different Ensemble Kalman Filter (EnKF) algorithms for Time-Averaged (TA) state estimation might exhibit significantly different efficiencies in a multi-scale, strongly coupled setting. Our findings complement previous studies, which had observed equivalent performances in milder nonlinear dynamical conditions, and call for caution at the moment of selecting the filtering approach to assimilate TA observations into a multi-component climate model.

Roughly speaking, the Time-Augmented Update (TAug-Up) presents better forecasting properties given that it estimates individual instantaneous states. Accordingly, TAug-Up prevails for short averaging periods where the the fast scales are still predictable. On the other hand, the Time-Averaged Update (TA-Up) focuses on the estimate of TA state and consequently it dominates for long averaging periods where the TA observations are significantly decorrelated from the instantaneous state of the system. In this scheme of

things, TAug-Up and TA-Up appear complementary rather than redundant. Additionally, given the the wealth of time scales present in the climate system and the broad range of time resolutions offered by proxy records, favorable conditions for both updating strategies will probably appear in more realistic paleo-Data Assimilation (DA) applications.

Component-wise covariance localization appeared in general to be beneficial for the filter operation. In the weak coupling regime, the inter-scale correlations observed by the EnKF are mostly spurious and accordingly the inter-scale contamination becomes strong. In these conditions the performance of filter can be greatly improved by component localization. On the other hand, under strong coupling conditions, inter-scale correlations are no longer dominantly artificial and then the profit of component localization is less evident. Still, it appears very effective at preventing catastrophic filter divergence for the TAug-Up and Time-Averaged + Instantaneous Update (TAI-Up) updating approaches.

Finally, our experiments show that a newly proposed hybrid algorithm (TAI-Up) exhibits a remarkably similar performance as the TAug-Up methodology, but with notably superior scaling properties, given that the size of the control vector does not increase with the averaging length. Furthermore, the computational cost of our hybrid update is comparable to the one of the TA update. Accordingly, it appears as an efficient alternative option for the above mentioned conditions where the TA-Up algorithm becomes inadequate.

7.2 Fuzzy Logic approach to TRW forward modeling

From the point of view of Fuzzy Logic (FL) theory, the process-based Tree-Ring-Width (TRW) model Vaganov-Shashkin-Lite (VSL) can be understood as a rather simple fuzzy inference system, where the core of the model, i.e., the Principle of Limiting Factors (PLF), plays the role of a fuzzy AND operation that allows tree growth only if both limiting factors are simultaneously favorable to it. This new perspective on the PLF calls for a relaxation of the growth limitation policy. The exclusive single-factor limitation –implied

by the original formulation via a minimum function– is no longer necessary and multiple-factor limitation become perfectly admissible. This growth regime, currently known as co-limitation, has been widely acknowledged in ecological sciences but has been so far disregarded in the modeling community

The impact of using several PLF incarnations on VSL's forward modeling performance was assessed for a global network of TRW chronologies. VSL's skill appeared remarkably insensitive to these changes, which supports our FL reinterpretation and indicates that the skill of the model resides on its general structure and not in the particular representation of the fuzzy AND operation. Additionally, it gives freedom to select the PLF representation that best suit the application at hand.

Finally, it is worth to mention that besides shading light on the mathematical modeling strategies for tree growth limitation processes, the translation of VSL into the FL language also suggest other avenues for future research that can contribute to the further improvement of tree growth models, as well as to the development of new forward models for other proxy types. FL provides a very flexible model structure able to naturally accommodate unknown processes and expert knowledge. This outstanding feature becomes crucial for the simulation of proxies systems given the great difficulty, or even impossibility, of pursuing first-principle approaches in this highly multidisciplinary research area.

7.3 Towards the assimilation of TRW chronologies

Pseudo-TRW observations were assimilated into the two-scale nonlinear dynamical system of Lorenz [1996] and the simplified Atmospheric General Circulation Model (A-GCM) called SPEEDY. The results of these DA experiments, indicate that VSL's approach to the forward modeling of TRW chronologies appears compatible, in general terms, with EnKF-based techniques for TA state estimation.

The competitive recording of two variables, implied by the PLF, does not necessarily deteriorate the filter performance in a dramatic way. However, when the transition

between growth-limited modes occurs abruptly, as in the case of the PLF representation via the minimum t-norm, the lack of smoothness of the growth rate time series may significantly increase the optimality loss in the estimation of TA model state. This disadvantage of the original formulation of VSL can be significantly ameliorated by resorting to alternative FL-based representations of the PLF, which allow co-limitation and consequently smoother shifting between different growth limitation regimes. A particularly promising representation of the PLF was provided by the product t-norm, which increases the smoothness of the growth rate time series, with regard to the minimum t-norm, without exhibiting the additional lower response thresholding observed for other co-limitation-permitting Triangular Norms (t-norms).

Finally, a promising result of our DA experiments with SPEEDY model is that the capacity a TRW chronology to decrease the error of the EnKF-based estimate of the TA state appears controlled by the strength of the yearly internal variability at the chronology site. Based on this finding we consider that, provided climate model imperfections are properly taken into account, model-based estimates of the climate internal variability might provide guidelines for the optimization of future sampling campaigns for TRW chronologies, in particular, and proxy records in general.

7.4 Off-line Data Assimilation

The complete lack of error reduction for forecast quantities in our DA experiments with the Atmospheric General Circulation Model SPEEDY suggest at first sight that the assimilation of TRW chronologies is predestined to be performed in off-line conditions, given that the one-year time-integration period is considerably longer than the useful lead times of existent climate prediction systems. However, the very strong activity in the fields of seasonal and decadal forecasting has made evident the existence of abundant potential sources of climate internal variability with time scales longer than one year [Smith et al., 2012].

7.5 Further paleo-reanalysis challenges

Concerning the initial motivation of generating retrospective paleo-climate analyses, we deem our results promising for TRW chronologies in the sense that EnKF techniques appear robust in the face of two strong nonlinearities typically found in process-based tree-ring growth forward models, i.e., switching recording and thresholded response. Nonetheless, it is important to highlight that the Observation System Simulation Experiments (OSSEs) presented in this manuscript represent only the first steps of the long hierarchy of DA experiments needed to eventually achieve a effective assimilation of proxy records into climate models using forward proxy models. Among the many interrogations that remain to be addressed regarding the creation of a realistic paleo-reanalysis, we want to draw attention to the following:

- The use of comprehensive earth system models will certainly introduce longer time scale processes, which might bring proxy DA to the on-line regime. This would be highly beneficial given that the observational information would be accumulated and transmitted from observed areas to unobserved ones. On the other hand, the assimilation of proxy data into multi-component models would imply several complications, in particular (i) the simultaneous use of several proxy forward models to assimilate the different proxies needed to constrain the model components, and (ii) the risk of facing inter-component DA pollution, which becomes especially relevant for proxies sensing several climate components at the same time, e.g., tree rings.

- Some climate proxies are sensitive to extremely small-scale and local phenomena, e.g., the response of tree rings to soil hydrological processes and of speleothems to precipitation. This fact constitute a difficult problem given the course resolution of current climate models and their very poor representation of sub-grid scale processes. Moreover, it is common to have with the same model grid box very different, or even contradicting, proxy records. This situation evinces the need of developing spatially aggregated proxy indices able represent global scale climate quantities, such as the one proposed by Breitenmoser et al. [2014]

This multitude of stumbling blocks certainly calls for further research.

APPENDIX A

Ensemble Kalman Filter algorithms for Time-Averaged state estimation

A.1 Time-Augmented Update (TAug-Up) Algorithm

1. The instantaneous forecast ensemble states belonging to the period $[t_n - \tau_{\text{aver}}, t_n]$ are arranged into a higher dimensional vector so as to create the Time-Augmented (TAUG) forecast ensemble:

$$\mathbb{X}_f(t_n, \tau_{\text{aver}}) = [\mathbf{X}_f(t_i)], \quad t_n - \tau_{\text{aver}} > t_i > t_n \tag{A.1}$$

2. The Ensemble Kalman Filter (EnKF) update equations are applied over $\mathbb{X}_f(t_n)$ so as to find the TAUG analysis ensemble $\mathbb{X}_a(t_n)$.

3. The Time-Averaged (TA) quantities at t_n are calculated from the TAUG ensembles $\mathbb{X}_f(t_n)$ and $\mathbb{X}_a(t_n)$.

4. The instantaneous analysis ensemble $\mathbf{X}_a(t_n)$ is extracted from $\mathbb{X}_a(t_n)$.

5. $\mathbf{X}_a(t_n)$ is propagated in time until $t = t_n + \tau_{\text{obs}}$ using the model dynamics.

6. Step 1 is performed for $t = t_n + \tau_{\text{obs}}$.

A.2 Time-Averaged Update (TA-Up) Algorithm

1. The instantaneous forecast ensemble $\mathbf{X}_f$ at $t = t_n$ is decomposed according to the expression:

$$\mathbf{X}_f(t_n) = \overline{\mathbb{X}_f(t_n)}^{\tau_{\text{aver}}} + \widetilde{\mathbf{X}_f}(t_n) \tag{A.2}$$

   where $\overline{\mathbb{X}_f(t_n)}^{\tau_{\text{aver}}}$ is the Time-Averaged Time-Augmented forecast ensemble:

$$\overline{\mathbb{X}_f(t_n)}^{\tau_{\text{aver}}} = \frac{1}{\tau_{\text{aver}}} \int_{t_n - \tau_{\text{aver}}}^{t_n} \mathbf{X}_f(t')\, dt' \tag{A.3}$$

   and $\widetilde{\mathbf{X}_f}$ denotes the anomalies around it.

2. The EnKF update equations are applied solely to $\overline{\mathbf{X}^f(t_n)}$ in order to obtain the TA analysis ensemble $\overline{\mathbf{X}^a(t_n)}$.

3. The instantaneous analysis ensemble is obtained by adding the TA analysis to the unchanged forecast TA anomalies:

$$\mathbf{X}_a(t_n) = \overline{\mathbb{X}_a(t_n)}^{\tau_{\text{aver}}} + \widetilde{\mathbf{X}_f}(t_n) \tag{A.4}$$

4. $\mathbf{X}_a(t_n)$ is propagated in time using the model, so as to obtain $\mathbf{X}_f(t_n + \tau_{\text{obs}})$.

5. Perform step 1 for $t = t_n + \tau_{\text{obs}}$.

Notice that the update step only involves only the TA state and the last instantaneous one. Consequently, it is not necessary to store the whole Time-Augmented ensemble given that the TA state can be calculated by accumulating the instantaneous state at every time step of the dynamical model.

A.3 Relation between TA-Up and TAug-Up strategies

Let us introduce the Time-Averaging operator $\widehat{\mathrm{T_A}}$ and the TA anomaly operator $\widehat{\mathrm{T_P}}$, given by the following expressions:

$$\widehat{\mathrm{T_A}}\mathbb{X} = \frac{1}{\tau_{\text{aver}}} \int_{t_n - \tau_{\text{aver}}}^{t_n} \mathbf{X}(t')) \, dt', \quad \widehat{\mathrm{T_P}} = \widehat{\mathrm{I}} - \widehat{\mathrm{T_A}}, \tag{A.5}$$

where $\widehat{\mathrm{I}}$ denotes the identity operator. Using this notation the TA decomposition can be written as:

$$\mathbb{X} = \overline{\mathbb{X}}^{\tau_{\text{aver}}} + \widetilde{\mathbb{X}} = \widehat{\mathrm{T_A}}\mathbb{X} + \widehat{\mathrm{T_P}}\mathbb{X} \tag{A.6}$$

Now, assuming an standard stochastic EnKF formulation [Burgers et al., 1998], the TAUG analysis takes the form:

$$\mathbb{X}_a = \mathbb{X}^b + \mathbb{K}\left(\mathbf{y} - \mathbf{y}^e + \varepsilon\right). \tag{A.7}$$

Here $\mathbb{K}$ denotes the TAUG Kalman gain matrix:

$$\mathbb{K} = \mathbb{B}\widehat{\mathrm{H}}^{\dagger}\widehat{\mathrm{T_A}}^{\dagger}\left[\widehat{\mathrm{T_A}}\widehat{\mathrm{H}}\mathbb{B}\widehat{\mathrm{H}}^{\dagger}\widehat{\mathrm{T_A}}^{\dagger} + \mathrm{R}\right]^{-1}, \tag{A.8}$$

where $\mathbb{B}$ represents the TAUG ensemble covariance, $\mathbb{B} = cov(\mathbb{X}, \mathbb{X})$, and y^e stands for the ensemble observations, $y^e = \widehat{\mathrm{T_A}}\widehat{\mathrm{H}}\mathbb{X}^b$.

It is worth mentioning that the assumption of using a stochastic filter is made here for the sake of simplicity and the following expressions of this section can be extended to more sophisticated EnKF flavors [Huntley and Hakim, 2010]. Using equation A.6, the TAUG analysis can be written as $\mathbb{X}_a = \widehat{\mathrm{T_A}}\mathbb{X}_a + \widehat{\mathrm{T_P}}\mathbb{X}_a$, where

$$\widehat{\mathrm{T_A}}\mathbb{X}_a = \widehat{\mathrm{T_A}}\mathbb{X}^b + \widehat{\mathrm{T_A}}\mathbb{K}(\mathbf{y} - \mathbf{y}^e), \tag{A.9}$$

$$\widehat{\mathrm{T_P}}\mathbb{X}_a = \widehat{\mathrm{T_P}}\mathbb{X}^b + \widehat{\mathrm{T_P}}\mathbb{K}(\mathbf{y} - \mathbf{y}^e). \tag{A.10}$$

Assuming a linear relationship between the state and the observations, the observation operator and the time-averaging operator commute, $\widehat{\mathrm{H}}\widehat{\mathrm{T_A}} = \widehat{\mathrm{T_A}}\widehat{\mathrm{H}}$, and then

$$\widehat{\mathrm{T_A}}\mathbb{K} = \widehat{\mathrm{T_A}}\mathbb{B}\widehat{\mathrm{H}}^T\widehat{\mathrm{T_A}}^T\left[\widehat{\mathrm{T_A}}\widehat{\mathrm{H}}\mathbb{B}\widehat{\mathrm{H}}^\dagger\widehat{\mathrm{T_A}}^\dagger + \mathrm{R}\right]^{-1} \tag{A.11}$$

$$= \widehat{\mathrm{T_A}}\mathbb{B}\widehat{\mathrm{T_A}}^\dagger\widehat{\mathrm{H}}^\dagger\left[\widehat{\mathrm{H}}\widehat{\mathrm{T_A}}\mathbb{B}\widehat{\mathrm{T_A}}^\dagger\widehat{\mathrm{H}}^\dagger + \mathrm{R}\right]^{-1} \tag{A.12}$$

$$= cov(\overline{\mathbb{X}}, \mathbf{y}^e)\left[\widehat{\mathrm{H}}cov(\overline{\mathbb{X}}, \overline{\mathbb{X}})\widehat{\mathrm{H}}^\dagger + \mathrm{R}\right]^{-1} \tag{A.13}$$

$$\widehat{\mathrm{T_P}}\mathbb{K} = \widehat{\mathrm{T_P}}\mathbb{B}\widehat{\mathrm{H}}^\dagger\widehat{\mathrm{T_A}}^\dagger\left[\widehat{\mathrm{T_A}}\widehat{\mathrm{H}}\mathbb{B}\widehat{\mathrm{H}}^\dagger\widehat{\mathrm{T_A}}^\dagger + \mathrm{R}\right]^{-1} \tag{A.14}$$

$$= cov(\widetilde{\mathbb{X}}, \mathbf{y}^e)\left[\widehat{\mathrm{H}}cov(\overline{\mathbb{X}}, \overline{\mathbb{X}})\widehat{\mathrm{H}}^\dagger + \mathrm{R}\right]^{-1} \tag{A.15}$$

Finally, assuming negligible covariance between observations and the time-averaged deviations, $cov(\widetilde{\mathbb{X}}, \mathbf{y}^e) = 0$, the TAug-Up strategy reduces to the TA-Up approach [Huntley and Hakim, 2010]:

$$\overline{\mathbb{X}_a} = \overline{\mathbb{X}^b} + cov(\overline{\mathbb{X}}, \mathbf{y}^e)\left[\widehat{\mathrm{H}}cov(\overline{\mathbb{X}}, \overline{\mathbb{X}})\widehat{\mathrm{H}}^\dagger + \mathrm{R}\right]^{-1} \tag{A.16}$$

$$\widetilde{\mathbb{X}_a} = \widetilde{\mathbb{X}^b}. \tag{A.17}$$

Notice that i these conditions the TA anomalies need not be updated and the TA analysis depends only on TA quantities.

APPENDIX B

Peer reviews for paper on the assimilation of pseudo-Tree-Ring-Width (TRW) chronologies

The Fuzzy Logic (FL) reinterpretation of Vaganov-Shashkin-Lite (VSL) model as well as the results on the assimilation of pseudo-TRW observations into the two-scale Lorenz [1996] model (L96) were used as material for a paper submitted to Climate Dynamics [Acevedo et al., 2015]. The decision letter from the editor Sussana Corti is to be found below (in italics).

Ref.: Ms. No. CLDY-D-14-00387 Towards the assimilation of tree-ring-width records using Ensemble Kalman Filtering techniques Climate Dynamics

Dear Mr Acevedo,

The reviewers have now commented on your manuscript. You will see that they are advising that you revise your manuscript. Therefore, the manuscript is returned for minor revision.

The reviewers' comments can be found at the end of this email or can be accessed by following the provided link.

If you are prepared to undertake the work required, I would be pleased to continue with the review process.

If you decide to revise the manuscript, please submit a revised version taking the reviewers' comments into account. Please also submit a point-by-point listing of your response/action for each of the reviewers' comments/suggestions.

Your revision is due by 31/10/2014 (dd-mm-yyyy).

Please note: When uploading your revised files, please make sure only to submit your editable source files (i. E. Word, tex).

To submit a revision, go to http://cldy.edmgr.com/ and log in as an Author. You will see a menu item call Submission Needing Revision. You will find your submission record there.

Yours sincerely,

Susanna Corti Executive Editor Climate Dynamics

Reviewers' comments:

Reviewer 1: Review of the manuscript "Towards the Assimilation of Tree-Ring-Width Records using Ensemble Kalman Filtering Techniques" by Walter Acevedo, Sebastian Reich, and Ulrich Cubasch

This paper explores the possibility to assimilate tree-ring width (TRW) information into climate models to achieve a "paleo-reanalysis" in the near future. A major challenge in this assimilation process is that proxies record climate information in complex and not linear ways. Thus, a model is required to translate the proxy units (here TRW) to simulated variables of the climate system such as a mix of growth limiting temperatures and precipitation. This translation can be achieved with so-called forward models. Acevedo et al. explore the potential and error risks of a model which could be used for assimilation of TRW into a climate model. They find increasing errors which arise in case a tree-growth

limiting factor is changing, e.g. from temperature to moisture. To resolve this, the authors develop a new fuzzy logic based version of the most commonly used tree-ring model which is better suited for data assimilation with Kalman-filtering techniques.

This work will move the very new field of paleo-data assimilation a little but important step ahead. Hence the title "Towards the assimilation . . . " is well chosen. The idea of translating the forward model to fuzzy logic is a very innovative idea and may help if forward models for other proxies will be developed in the future.

Furthermore, the paper is mostly well written, clearly structured and has an appropriate amount of figures. Thus, I recommend publication after minor revisions.

General comments: After reading the paper, I understand the abstract very well but reading it the first time, I found it extremely complicated. Thus I suggest to rewrite the abstract in shorter sentences and using easier words. Most readers will for instance not know the meaning of expressions like "coupled toy model", "switching recording", "optimality loss" or "fuzzy logic reincarnations of . . . limiting factors".

A special focus is put on "improvements concerning the abrupt shifting of recorded variables in the forward model as it is found that this introduces problems in Kalman based assimilation"? In how many

Can you add a little explanation why you analyze the slow and fast components separately?

I would suggest to add some more information about the applied Kalman Filtering technique and Kalman filtering in general, as not all readers be comfortable with this method (line 267ff).

A clearer structure would help the reader in the discussion . One option would be 3 subsections for the three features: (i) time averaging, (ii) "switching recording" and (iii) bounded response windows leading to "threshold response". Another option would be stating in places like line 431 something along the lines: Concerning factor iii) the "response threshold". Bye the way, the order of these 3 features in not consistent throughout the paper.

Detailed comments:

Sect. 1 Line 18: Optimality loss needs an explanation. Line 54: I would say "The formation of proxy records CAN/MIGHT . . . " as not all all mechanisms have to be involved in all proxies. Line 60: Maybe explain the term "forward model" in a few words; e.g. "... forward model, which translates time integrated temperature and precipitation information into tree-ring width". Line 66: I would use a simple comma instead of brackets. That makes it easier to read. Line 68: What do you mean with "stable"? Line 74: skilLfully Line 81: I would add an examples like ". . . abrupt shifting of recorded variable, e.g. from temperature to precipitation" and "threshold response, e.g. no growth below 5°C" (at least for me that would be clearer than "finite size response span") and "time averaging , e.g. integrating climate conditions over the entire growth season" Line 86: Make rather shorter sentences. ". . . VS-Lite model. THIS can be improved . . . " Line 89ff: Maybe explain the idea behind fuzzy logic in a sentence like "similar to Boolean logic (0=false, 1=true) but fuzzy logic allows for values in between 0 and 1 if something is partially true" Line 101: assesS

Section 2.2 I would suggest to rewriting the first paragraph in a more easy and clear way for people who are not familiar with the concept of fuzzy logic at all

Section 2.5 Line 213: Maybe change title to "Crude climate model" Line 213: "Applying the dynamical system described above we perform . . . " Line 237: "an ensemble run" How many members, how many grid cells/resolution, . . . Please give more detail about the simulations you conducted. Line 239ff: Maybe better say that you use VS-Lite to generate pseudo proxies using T and M simulated with your dynamical system / crude model. Line 246: Signal to noise ratio of 10? Why don't you use a ratio that is closer to ratios found in real proxy data? Line 247: explained symbols are not in equation above. Some latex formatting error? Line 271: What is "B-localization"? Add citation for Gaspari-Cohn function. What is your grid spacing?

Sect. 3.1 Line 297ff: you present the forecasting skill tau=1 as a result and compare it with other studies. This is a circular argument as you yes in Sect. 2.4 that your model is tuned to reach these values

Sect. 3.2.3 Line 354: "in which" -¿ "how"

Sect. 4 Line 425 to 430: I would only mention that this is a question of future research. Line 438: Should it be M^L instead of T^U ? Line 463: scales scales

Reviewer 2: Summary:

A simple, well known, model having fast and slow variability is used to test revisions to the logic of the VS-Lite tree-ring-width forward model. The ultimate goal, beyond the scope of this paper, is to use VS-Lite as the forward model for data assimilation experiments with real proxy data. Three challenges are addressed concerning the assimilation of tree-ring width with VS-Lite: time averaging, a response that depends nonlinearly on two variables (temperature and soil moisture), and threshold responses due to cutoffs in the VS-Lite model. The general problem of forward models for proxy data has emerged as a key barrier to using data assimilation on proxy data and comparing GCM simulations to proxy data, so the paper is both timely and important.

The main novelty here is the framing of aspects of VS-Lite's logic in fuzzy logic terms, which are then modified to accomodate tests of several fuzzy logic functions. I am not an expert on fuzzy logic, but I trust that the authors have presented and tested mainstream concepts for the logic they introduce to VS-Lite. Results show that smoothness of response depends sensitively on the logic function, and that for the model considered a product function performs best.

The paper is well presented, although if I made one major comment it would be that the model chosen is a bit simplistic for the identified challenges, and it is unclear if the product function will remain the best option for more complete models. Therefore, a model hierarchy would be a better approach. However, I view such revision as outside the scope of the present manuscript, and presumably something the authors will take up in future work. I recommend minor revision.

Comments:

line 15-16: I do not know what this means

l 54: I suggest spending some time here explaining what a proxy system model is (i.e., describe the "forward" mapping from traditional climate variables to proxy measurement)

l 68: What does "most stable" mean?

l 81: Please provide more information for the reader on what this means

l 113: In what sense is it "intermediate" (between VS and simple linear regression on a set of parameters?)

l 271: You should say a bit more about what this means

l 276: I may have missed it, but if not, the reader needs more details on how observations are defined

Bibliography

Acevedo, W., Cubasch, U., Reich, S., and Matthes, K. (2013). Forward modelling of tree-ring width chronologies from the spanish pyrenees using vs-lite model. *TRACE - Tree Rings in Archaeology, Climatology and Ecology*, 11:56–59.

Acevedo, W., Reich, S., and Cubasch, U. (2015). Towards the assimilation of tree-ring-width records using ensemble kalman filtering techniques. *Accepted by Climate Dynamics under minor revisions*.

Amezcua, J., Ide, K., Kalnay, E., and Reich, S. (2014). Ensemble transform kalman-bucy filters. *Q.J.R. Meteorol. Soc.*, 140(680):995–1004.

Annan, J. D. and Hargreaves, J. C. (2012). Identification of climatic state with limited proxy data. *Clim. Past*, 8(4):1141–1151.

Baker, A., Bradley, C., Phipps, S. J., Fischer, M., Fairchild, I. J., Fuller, L., Spötl, C., and Azcurra, C. (2012). Millennial-length forward models and pseudoproxies of stalagmite δ^{18}O: an example from nw scotland. *Clim. Past*, 8(4):1153–1167.

Barkmeijer, J., Iversen, T., and Palmer, T. N. (2003). Forcing singular vectors and other sensitive model structures. *Quarterly Journal of the Royal Meteorological Society*, 129(592):2401–2423.

Bengtsson, L. and Shukla, J. (1988). Integration of space and in situ observations to study global climate change. *Bull. Amer. Meteor. Soc.*, 69(10):1130–1143.

Bengtsson, T., Bickel, P., and Li, B. (2008). Curse-of-dimensionality revisited: Collapse of the particle filter in very large scale systems. In *IMS collections: probability and statistics: essays in Honor of David A. Freedman*, volume 2, pages 316–334. IMS.

Bhend, J., Franke, J., Folini, D., Wild, M., and Brönnimann, S. (2012). An ensemble-based approach to climate reconstructions. *Climate of the Past*, 8(3):963–976.

Blackman, F. F. (1905). Optima and limiting factors. *Ann. Bot.*, 19:281–295.

Bocquet, M., Pires, C. A., and Wu, L. (2010). Beyond gaussian statistical modeling in geophysical data assimilation. *Mon. Wea. Rev.*, 138(8):2997–3023.

Bosilovich, M. G., Chaudhuri, A. H., and Rixen, M. (2013). Earth system reanalysis: Progress, challenges, and opportunities. *Bull. Amer. Meteor. Soc.*, 94(8):ES110–ES113.

Boucher, E., Guiot, J., Hatté, C., Daux, V., Danis, P.-A., and Dussouillez, P. (2014). An inverse modeling approach for tree-ring-based climate reconstructions under changing atmospheric co2 concentrations. *Biogeosciences*, 11(12):3245–3258.

Bourke, W. (1974). A multi-level spectral model. i. formulation and hemispheric integrations. *Mon. Wea. Rev.*, 102(10):687–701.

Breitenmoser, P., Brönnimann, S., and Frank, D. (2014). Forward modelling of tree-ring width and comparison with a global network of tree-ring chronologies. *Climate of the Past*, 10(2):437–449.

Brönnimann, S. (2011). Towards a paleoreanalysis? *ProClim-Flash*, 1(51):16.

Burgers, G., van Leeuwen, P. J., and Evensen, G. (1998). Analysis scheme in the ensemble Kalman filter. *Monthly Weather Review*, 126:1719–1724.

Compo, G. P., Whitaker, J. S., and Sardeshmukh, P. D. (2006). Feasibility of a 100-year reanalysis using only surface pressure data. *Bull. Amer. Meteor. Soc.*, 87(2):175–190.

Compo, G. P., Whitaker, J. S., Sardeshmukh, P. D., Matsui, N., Allan, R. J., Yin, X., Gleason, B. E., Vose, R. S., Rutledge, G., Bessemoulin, P., Brönnimann, S., Brunet, M., Crouthamel, R. I., Grant, A. N., Groisman, P. Y., Jones, P. D., Kruk, M. C., Kruger, A. C., Marshall, G. J., Maugeri, M., Mok, H. Y., Nordli, O., Ross, T. F., Trigo, R. M., Wang, X. L., Woodruff, S. D., and Worley, S. J. (2011). The twentieth century reanalysis project. *Q.J.R. Meteorol. Soc.*, 137(654):1–28.

Cook, E. R. (1985). *A time series approach to tree-ring standardization*. PhD thesis, University of Arizona.

Cook, E. R., Meko, D. M., Stahle, D. W., and Cleaveland, M. K. (1999). Drought reconstructions for the continental united states. *J. Climate*, 12(4):1145–1162.

Danis, P.-A., Hatté, C., Misson, L., and Guiot, J. (2012). Maideniso: a multiproxy biophysical model of tree-ring width and oxygen and carbon isotopes. *Can. J. For. Res.*, 42(9):1697–1713.

Dee, D. P., Balmaseda, M., Balsamo, G., Engelen, R., Simmons, A. J., and Thépaut, J.-N. (2013). Toward a consistent reanalysis of the climate system. *Bull. Amer. Meteor. Soc.*, 95(8):1235–1248.

Deza, J. I., Masoller, C., and Barreiro, M. (2014). Distinguishing the effects of internal and forced atmospheric variability in climate networks. *Nonlin. Processes Geophys.*, 21(3):617–631.

Dirren, S. and Hakim, G. J. (2005). Toward the assimilation of time-averaged observations. *Geophysical Research Letters*, 32(4):L04804.

Dubinkina, S. and Goosse, H. (2013). An assessment of particle filtering methods and nudging for climate state reconstructions. *Climate of the Past*, 9(3):1141–1152.

Evans, M., Reichert, B., Kaplan, A., Anchukaitis, K., Vaganov, E., and Cane, M. (2006). A forward modeling approach to paleoclimatic interpretation of tree-ring data. *Journal of Geophysical Research*, 111:G03008.

Evans, M., Tolwinski-Ward, S., Thompson, D., and Anchukaitis, K. (2013). Applications of proxy system modeling in high resolution paleoclimatology. *Quaternary Science Reviews*, 76(0):16 – 28.

Evans, M. N. (2007). Toward forward modeling for paleoclimatic proxy signal calibration: A case study with oxygen isotopic composition of tropical woods. *Geochem. Geophys. Geosyst.*, 8(7):Q07008–.

Evensen, G. (1994). Sequential data assimilation with a nonlinear quasi-geostrophic model using monte carlo methods to forecast error statistics. *Journal of Geophysical Research: Oceans*, 99(C5):10143–10162.

Fritts, H. C. (1976). *Tree rings and climate*. Academic Press, New York.

Fritts, H. C., Shashkin, A., Downes, G. M., Wimmer, R., and Vetter, R. (1999). A simulation model of conifer ring growth and cell structure. *Tree-ring analysis: biological, methodological and environmental aspects.*, pages 3–32.

Gaspari, G. and Cohn, S. E. (1999). Construction of correlation functions in two and three dimensions. *Q.J.R. Meteorol. Soc.*, 125(554):723–757.

Gibson, J. K., Kållberg, P., Uppala, S., Nomura, A., Hernandez, A., and Serrano, E. (1997). Era description. In *ECMWF ERA-15 Project Report Series, No. 1*. European Centre for Medium-Range Weather Forecasts, Shinfield, Reading, UK.

Goosse, H., Crespin, E., de Montety, A., Mann, M. E., Renssen, H., and Timmermann, A. (2010). Reconstructing surface temperature changes over the past 600 years using climate model simulations with data assimilation. *J. Geophys. Res.*, 115(D9):D09108–.

Gottwald, G. A. and Majda, A. J. (2013). A mechanism for catastrophic filter divergence in data assimilation for sparse observation networks. *Nonlinear Processes in Geophysics*, 20(5):705–712.

Guiot, J., Wu, H. B., Garreta, V., Hatté, C., and Magny, M. (2009). A few prospective ideas on climate reconstruction: from a statistical single proxy approach towards a multi-proxy and dynamical approach. *Climate of the Past*, 5(4):571–583.

Hamill, T. M. (2006). Ensemble-based atmospheric data assimilation. In Palmer, T. and Hagedorn, R., editors, *Predictability of Weather and Climate*. Cambridge University Press. Web: http://dx.doi.org/10.1017/CBO9780511617652.007.

Hamill, T. M., Whitaker, J. S., and Snyder, C. (2001). Distance-dependent filtering of background error covariance estimates in an ensemble kalman filter. *Mon. Wea. Rev.*, 129(11):2776–2790.

Harpole, W. S., Ngai, J. T., Cleland, E. E., Seabloom, E. W., Borer, E. T., Bracken, M. E., Elser, J. J., Gruner, D. S., Hillebrand, H., Shurin, J. B., and Smith, J. E. (2011). Nutrient co-limitation of primary producer communities. *Ecology Letters*, 14(9):852–862.

Harris, I., Jones, P., Osborn, T., and Lister, D. (2014). Updated high-resolution grids of monthly climatic observations - the cru ts3.10 dataset. *Int. J. Climatol.*, 34(3):623–642.

Heinze, C. (2001). Towards the time dependent modeling of sediment core data on a global basis. *Geophys. Res. Lett.*, 28(22):4211–4214.

Holton, J. (1992). *An Introduction to Dynamic Meteorology*. Academic Press.

Huang, J., van den Dool, H. M., and Georgarakos, K. P. (1996). Analysis of model-calculated soil moisture over the united states (1931–1993) and applications to long-range temperature forecasts. *J. Climate*, 9(6):1350–1362.

Hughes, M. and Ammann, C. (2009). The future of the past – an earth system framework for high resolution paleoclimatology: editorial essay. *Climatic Change*, 94(3-4):247–259.

Hughes, M., Guiot, J., and Ammann, C. (2010). An emerging paradigm: Process-based climate reconstructions. *PAGES news*, 18(2):87–89.

Hunt, B. R., Kostelich, E. J., and Szunyogh, I. (2007). Efficient data assimilation for spatiotemporal chaos: A local ensemble transform kalman filter. *Physica D: Nonlinear Phenomena*, 230(1–2):112–126.

Huntley, H. and Hakim, G. (2010). Assimilation of time-averaged observations in a quasi-geostrophic atmospheric jet model. *Climate Dynamics*, 35(6):995–1009.

Jones, P., Briffa, K., Osborn, T., Lough, J., van Ommen, T., Vinther, B., Luterbacher, J., Wahl, E., Zwiers, F., Mann, M., Schmidt, G., Ammann, C., Buckley, B., Cobb, K., Esper, J., Goosse, H., Graham, N., Jansen, E., Kiefer, T., Kull, C., Küttel, M., Mosley-Thompson, E., Overpeck, J., Riedwyl, N., Schulz, M., Tudhope, A., Villalba, R., Wanner, H., Wolff, E., and Xoplaki, E. (2009). High-resolution palaeoclimatology of the last millennium: a review of current status and future prospects. *The Holocene*, 19(1):3–49.

Jones, P. D. and Mann, M. E. (2004). Climate over past millennia. *Rev. Geophys.*, 42(2):RG2002.

Kalman, R. E. (1960). A new approach to linear filtering and prediction problems. *Transactions of the ASME–Journal of Basic Engineering*, 82(Series D):35–45.

Kalnay, E. (2003). *Atmospheric modeling, data assimilation, and predictability*. Cambridge university press.

Kalnay, E., Kanamitsu, M., Kistler, R., Collins, W., Deaven, D., Gandin, L., Iredell, M., Saha, S., White, G., Woollen, J., Zhu, Y., Leetmaa, A., Reynolds, R., Chelliah, M., Ebisuzaki, W., Higgins, W., Janowiak, J., Mo, K. C., Ropelewski, C., Wang, J., Jenne, R., and Joseph, D. (1996). The NCEP/NCAR 40-year reanalysis project. *Bull. Amer. Meteor. Soc.*, 77(3):437–471.

Kurahashi-Nakamura, T., Losch, M., and Paul, A. (2014). Can sparse proxy data constrain the strength of the atlantic meridional overturning circulation? *Geoscientific Model Development*, 7(1):419–432.

Lahoz, W., Khattatov, B., and Menard, R. (2010). *Data Assimilation: Making Sense of Observations*. Springer.

Li, H., Kalnay, E., Miyoshi, T., and Danforth, C. M. (2009). Accounting for model errors in ensemble data assimilation. *Mon. Wea. Rev.*, 137(10):3407–3419.

Lien, G.-Y., Kalnay, E., and Miyoshi, T. (2013). Effective assimilation of global precipitation: simulation experiments. *2013*, 65.

Lorenc, A. C. (1986). Analysis methods for numerical weather prediction. *Q.J.R. Meteorol. Soc.*, 112(474):1177–1194.

Lorenz, E. N. (1963). Deterministic nonperiodic flow. *J. Atmos. Sci.*, 20(2):130–141.

Lorenz, E. N. (1996). Predictability, a problem partly solved. In *Proceedings of ECMWF seminar on Predictability*, pages 1–19, Reading, UK. ECMWF.

Luhandjula, M. and Gupta, M. (1996). On fuzzy stochastic optimization. *Fuzzy Sets and Systems*, 81(1):47–55.

MacMynowski, D. G. and Tziperman, E. (2008). Factors affecting enso's period. *J. Atmos. Sci.*, 65(5):1570–1586.

Mann, M. E., Zhang, Z., Hughes, M. K., Bradley, R. S., Miller, S. K., Rutherford, S., and Ni, F. (2008). Proxy-based reconstructions of hemispheric and global surface temperature variations over the past two millennia. *Proceedings of the National Academy of Sciences*.

Marchini, A. (2011). Modelling ecological processes with fuzzy logic approaches. In Jopp, F., Reuter, H., and Breckling, B., editors, *Modelling Complex Ecological Dynamics*, pages 133–145. Springer Berlin Heidelberg.

Mathiot, P., Goosse, H., Crosta, X., Stenni, B., Braida, M., Renssen, H., Van Meerbeeck, C. J., Masson-Delmotte, V., Mairesse, A., and Dubinkina, S. (2013). Using data assimilation to investigate the causes of southern hemisphere high latitude cooling from 10 to 8 ka bp. *Climate of the Past*, 9(2):887–901.

McCarroll, D. and Loader, N. J. (2004). Stable isotopes in tree rings. *Quaternary Science Reviews*, 23:771–801.

Misson, L., Rathgeber, C., and Guiot, J. (2004). Dendroecological analysis of climatic effects on quercus petraea and pinus halepensis radial growth using the process-based maiden model. *Can. J. For. Res.*, 34(4):888–898.

Miyoshi, T. (2005). *Ensemble Kalman filter experiments with a primitive-equation global model*. PhD thesis, University of Maryland, College Park. 197pp.

Miyoshi, T. (2010). The gaussian approach to adaptive covariance inflation and its implementation with the local ensemble transform kalman filter. *Mon. Wea. Rev.*, 139(5):1519–1535.

Molteni, F. (2003). Atmospheric simulations using a gcm with simplified physical parametrizations. i: model climatology and variability in multi-decadal experiments. *Climate Dynamics*, 20(2-3):175–191.

Nguyen, H. T., Prasad, N. R., Walker, C. L., and Walker, E. A. (2002). *A First Course in Fuzzy and Neural Control*. Chapman and Hall/CRC, 1 edition.

Nichols, N. (2010). Mathematical concepts of data assimilation. In Lahoz, W., Khattatov, B., and Menard, R., editors, *Data Assimilation*, pages 13–39–. Springer Berlin Heidelberg.

Niinemets, U. and Kull, K. (2005). Co-limitation of plant primary productivity by nitrogen and phosphorus in a species-rich wooded meadow on calcareous soils. *Acta Oecologica*, 28(3):345–356.

Paul, A. and Schäfer-Neth, C. (2005). How to combine sparse proxy data and coupled climate models. *Quaternary Science Reviews*, 24:1095–1107.

Peña, M. and Kalnay, E. (2004). Separating fast and slow modes in coupled chaotic systems. *Nonlinear Processes in Geophysics*, 11(3):319–327.

Pendergrass, A., Hakim, G., Battisti, D., and Roe, G. (2012). Coupled air-mixed layer temperature predictability for climate reconstruction. *Journal of Climate*, 25(2):459–472.

Robert, A. (1966). The integration of a low order spectral form of the primitive meteorological equations. *Journal of the Meteorological Society of Japan*, 44:237–245.

Roden, J. S., Lin, G., and Ehleringer, J. R. (2000). A mechanistic model for interpretation of hydrogen and oxygen isotope ratios in tree-ring cellulose. *Geochimica et Cosmochimica Acta*, 64(1):21–35.

Rood, R. and Bosilovich, M. (2010). Reanalysis: Data assimilation for scientific investigation of climate. In Lahoz, W., Khattatov, B., and Menard, R., editors, *Data Assimilation*, pages 623–646–. Springer Berlin Heidelberg.

Ruiz, J. J., Pulido, M., and Miyoshi, T. (2013). Estimating model parameters with ensemble-based data assimilation: A review. *Journal of the Meteorological Society of Japan. Ser. II*, 91(2):79–99.

Saito, M. A., Goepfert, T. J., and Ritt, J. T. (2008). Some thoughts on the concept of colimitation: three definitions and the importance of bioavailability. *Limnology and Oceanography*, 53(1):276.

Salski, A. (2006). Ecological applications of fuzzy logic. In Recknagel, F., editor, *Ecological Informatics*, pages 3–14. Springer Berlin Heidelberg.

Schmidt, G. A. (1999). Forward modeling of carbonate proxy data from planktonic foraminifera using oxygen isotope tracers in a global ocean model. *Paleoceanography*, 14(4):482–497.

Schneider, T., Bischoff, T., and Haug, G. H. (2014). Migrations and dynamics of the intertropical convergence zone. *Nature*, 513(7516):45–53.

Se, Z. (2009). *Fuzzy Logic and Hydrological Modeling*. CRC Press.

Singh, B. N. and Lal, K. N. (1935). Limitations of blackman's law of limiting factors and harder's concept of relative minimum as applied to photosynthesis. *Plant Physiology*, 10(2):245–268.

Smerdon, J. E. (2012). Climate models as a test bed for climate reconstruction methods: pseudoproxy experiments. *Wiley Interdisciplinary Reviews: Climate Change*, 3(1):63–77.

Smerdon, J. E., Kaplan, A., Zorita, E., Gonzalez-Rouco, J. F., and Evans, M. N. (2011). Spatial performance of four climate field reconstruction methods targeting the common era. *Geophysical Research Letters*, 38(11):n/a–n/a.

Smith, D. M., Scaife, A. A., and Kirtman, B. P. (2012). What is the current state of scientific knowledge with regard to seasonal and decadal forecasting? *Environmental Research Letters*, 7(1):015602.

Smith, T. M., Reynolds, R. W., Livezey, R. E., and Stokes, D. C. (1996). Reconstruction of historical sea surface temperatures using empirical orthogonal functions. *J. Climate*, 9(6):1403–1420.

Steiger, N., Hakim, G., Steig, E., Battisti, D., and Roe, G. (2014). Assimilation of time-averaged pseudoproxies for climate reconstruction. *Journal of Climate*, 27(1):426–441.

Sturm, C., Zhang, Q., and Noone, D. (2010). An introduction to stable water isotopes in climate models: benefits of forward proxy modelling for paleoclimatology. *Clim. Past*, 6(1):115–129.

Sugeno, M. (1985). *Industrial Applications of Fuzzy Control*. Elsevier Science Inc., New York, NY, USA.

Talagrand, O. (1997). Assimilation of observations, an introduction. *Journal-Meteorological Society of Japan Series 2*, 75:81–99.

Thompson, D. M., Ault, T. R., Evans, M. N., Cole, J. E., and Emile-Geay, J. (2011). Comparison of observed and simulated tropical climate trends using a forward model of coral $d^{18}O$. *Geophys. Res. Lett.*, 38(14):L14706–.

Thompson, D. W. J. and Wallace, J. M. (2000). Annular modes in the extratropical circulation. part i: Month-to-month variability. *J. Climate*, 13(5):1000–1016.

Tippett, M. K., Anderson, J. L., Bishop, C. H., Hamill, T. M., and Whitaker, J. S. (2003). Ensemble square root filters*. *Mon. Wea. Rev.*, 131(7):1485–1490.

Tolwinski-Ward, S., Tingley, M., Evans, M., Hughes, M., and Nychka, D. (2014). Probabilistic reconstructions of local temperature and soil moisture from tree-ring data with potentially time-varying climatic response. *Climate Dynamics*, pages 1–16.

Tolwinski-Ward, S. E. (2012). *Inference on Tree-Ring Width and Paleoclimate Using a Proxy Model of Intermediate Complexity*. PhD thesis, The University of Arizona.

Tolwinski-Ward, S. E., Anchukaitis, K. J., and Evans, M. N. (2013). Bayesian parameter estimation and interpretation for an intermediate model of tree-ring width. *Climate of the Past*, 9(4):1481–1493.

Tolwinski-Ward, S. E., Evans, M. N., Hughes, M., and Anchukaitis, K. J. (2011). An efficient forward model of the climate controls on interannual variation in tree-ring width. *Climate Dynamics*, 36(11-12):2419–2439.

Trenberth, K. E. and Olson, J. G. (1988). An evaluation and intercomparison of global analyses from the national meteorological center and the european centre for medium range weather forecasts. *Bull. Amer. Meteor. Soc.*, 69(9):1047–1057.

Vaganov, E., Hughes, M., and Shashkin, A. (2006). *Growth Dynamics of Conifer Tree Rings: Images of Past and Future Environments*, volume 183 of *Ecological studies*. Springer, New York.

van der Schrier, G. and Barkmeijer, J. (2005). Bjerknes' hypothesis on the coldness during ad 1790-1820 revisited. *Climate Dynamics*, 25(5):537–553–.

van Leeuwen, P. J. (2010). Nonlinear data assimilation in geosciences: an extremely efficient particle filter. *Q.J.R. Meteorol. Soc.*, 136(653):1991–1999.

von Storch, H., Cubasch, U., González-Ruoco, J., Jones, J., Widmann, M., and Zorita, E. (2000). Combining paleoclimatic evidence and GCMs by means of data assimilation through upscaling and nudging (datun). *Proceedings 28-31. 11th Symposium on global change studies, AMS, Long Beach, CA, USA.9-14/1*, pages 2119–2128.

Wanru, W. and Dickinson, R. (2004). Time scales of layered soil moisture memory in the context of land-atmosphere interaction. *Journal of Climate*, 17:2752–2764.

Whitaker, J. S., Compo, G. P., and Thépaut, J.-N. (2009). A comparison of variational and ensemble-based data assimilation systems for reanalysis of sparse observations. *Mon. Wea. Rev.*, 137(6):1991–1999.

Widmann, M., Goosse, H., van der Schrier, G., Schnur, R., and Barkmeijer, J. (2010). Using data assimilation to study extratropical northern hemisphere climate over the last millennium. *Climate of the Past*, 6(5):627–644.

Woollings, T., Pinto, J. G., and Santos, J. A. (2011). Dynamical evolution of north atlantic ridges and poleward jet stream displacements. *J. Atmos. Sci.*, 68(5):954–963.

Wu, C., Chen, J. M., Black, T. A., Price, D. T., Kurz, W. A., Desai, A. R., Gonsamo, A., Jassal, R. S., Gough, C. M., Bohrer, G., Dragoni, D., Herbst, M., Gielen, B., Berninger, F., Vesala, T., Mammarella, I., Pilegaard, K., and Blanken, P. D. (2013). Interannual variability of net ecosystem productivity in forests is explained by carbon flux phenology in autumn. *Global Ecology and Biogeography*, 22(8):994–1006.

Yin, X. and Struik, P. (2009). C3 and C4 photosynthesis models: An overview from the perspective of crop modelling. *NJAS - Wageningen Journal of Life Sciences*, 57(1):27–38.

Zadeh, L. (1965). Fuzzy sets. *Information and Control*, 8(3):338 – 353.

Zadeh, L. A. (1975). Fuzzy logic and approximate reasoning. *Synthese*, 30(3-4):407–428.

List of Abbreviations

20CR	20th Century Reanalysis
3D-Var	3-Dimensional Variational Analysis
4D-Var	4-Dimensional Variational Analysis
A-GCM	Atmospheric General Circulation Model
CPC-LBM	USA's Climate Prediction Center Leaky Bucket Model
CRU-TS	Climatic Research Unit (University of East Anglia) Time Series
DA	Data Assimilation
ECMWF	European Centre for Medium-Range Weather Forecasts
EnKF	Ensemble Kalman Filter
ENSO	El Niño Southern Oscillation
EOF	Empirical Orthogonal Functions
FL	Fuzzy Logic
hPa	hectopascal
ICTP	International Center for Theoretical Physics
ITCZ	Inter-Tropical Convergence Zone
KF	Kalman Filter
L63	Lorenz [1963] model
L96	two-scale Lorenz [1996] model
LETKF	Local Ensemble Transform Kalman Filter
MCMC	Markov Chain Monte Carlo method

NCEP	National Centers for Environmental Prediction
NCAR	National Center for Atmospheric Research
ODE	Ordinary Differential Equation
OSSE	Observation System Simulation Experiment
PDF	Probability Density Function
PDSI	Palmer Drought Severity Index
PLF	Principle of Limiting Factors
PK2004	Peña and Kalnay [2004] model
PPE	Pseudo-Proxy Experiment
RMS	Root-Mean-Square (quantity)
RMSE	Root Mean Square Error
SNR	Signal-To-Noise ratio
SPEEDY	Simplified Parametrizations, primitivE-Equation Dynamics model
SPEEDY-LETKF	LETKF framework for SPEEDY model
SST	Sea Surface Temperature
TA	Time-Averaged (quantity)
TAUG	Time-Augmented (quantity)
TA-Up	Time-Averaged Update
TAug-Up	Time-Augmented Update
TAI-Up	Time-Averaged + Instantaneous Update
t-norm	Triangular Norm
TRW	Tree-Ring-Width
u-wind	Zonal Wind
VS	Vaganov-Shashkin model
VSL	Vaganov-Shashkin-Lite model
VSL-Min	VSL model with PLF represented by the Minimum t-norm
VSL-Prod	VSL model with PLF represented by the Product t-norm
VSL-Yager	VSL model with PLF represented by the Yager t-norm
VSL-Luka	VSL model with PLF represented by the Lukasiewcz t-norm
v-wind	Meridional Wind

List of Figures